NOVEL MULTICHROMOPHORIC ENERGY TRANSFER CASSETTES BASED ON FUNCTIONALIZED BODIPY DYES

A THESIS

SUBMITTED TO THE MATERIALS SCIENCE AND NANOTECHNOLOGY PROGRAM OF THE GRADUATE SCHOOL OF ENGINEERING AND SCIENCE OF BİLKENT UNIVERSITY

IN PARTIAL FULFILLMENT OF THE REQUIREMENTS

FOR THE DEGREE OF

MASTER OF SCIENCE

By

GİZEM ÇELTEK

September 2012

I certify that I have read this thesis and that in my opinion it is fully adequate, in scope and in quality, as a thesis of the degree of Master of Science.

…….

Prof. Dr. Engin U. Akkaya (Principal Advisor)

I certify that I have read this thesis and that in my opinion it is fully adequate, in scope and in quality, as a thesis of the degree of Master of Science.

…….

Asst. Prof. Dr. Turgay Tekinay

I certify that I have read this thesis and that in my opinion it is fully adequate, in scope and in quality, as a thesis of the degree of Master of Science.

…….

Asst. Prof. Dr. Serdar Atılgan

Approved for the Graduate School of Engineering and Science:

…….

Prof. Dr. Levent Onural

Director of the Graduate School of Engineering and Science

ABSTRACT

NOVEL MULTICHROMOPHORIC ENERGY TRANSFER CASSETTES BASED ON FUNCTIONALIZED BODIPY DYES

Gizem ÇELTEK

M.S. in Material Science and Nanotechnology
Supervisor: Prof. Dr. Engin U. Akkaya
September, 2012

Energy necessity is one of the leading problems in the world due to the developing technologies and strategies. There are many energy sources, which are being used for years, however; conversion and transfer of the energy is a problem in many fields due to energy loss. In this manner, the efficiency of energy transfer is very crucial. For this purpose, we have designed multichromophoric molecules, which can absorb the light with donor parts, then transfer the energy to the acceptor site. During this process, energy loss is tried to be prevented by lowering the distance between the donor and acceptor Boradiazaindacene (BODIPY) molecules. Three different energy transfer cassettes are synthesized and characterized. The design of the supramolecule, in means of spectral overlap and distance between the donor and the acceptor site are observed to affect the energy transfer efficiency. Through functional design, these molecules absorb and emit light in different wavelengths. Substation of distyryl and tetrastyryl groups to the acceptor BODIPY core changes the emission and absorption maxima. Increasing number of styryl groups attached to the molecule shifts the spectrum to the red part of the visible region. Through rational design, these molecules can be used in applications of energy transfer and broad spectrum absorber purposes.

Keywords: Boradiazaindacene (BODIPY), dye, supramoleculer chemistry, multichromophore, energy transfer, Sonogashira coupling.

ÖZET

FONKSİYONLANDIRILMIŞ BODİPY BOYALARINA DAYANAN YENİ MULTİKROMOFORLU ENERJİ AKTARIM KASETLERİ

Gizem ÇELTEK

Yüksek Lisans, Malzeme Bilimi ve Nanoteknoloji Programı
Tez Yöneticisi: Prof. Dr. Engin U. Akkaya
Eylül, 2012

Gelişen teknoloji ve strateji yüzünden, enerji gereksinimi dünyada belli başlı sorunlardan biri haline gelmiştir. Yıllardır kullanılan birçok enerji kaynağı olmasına rağmen, enerji dönüşümü ve transferi, oluşan enerji kaybı nedeniyle bir çok alanda problem olmuştur. Bu bağlamda, enerji transferinin verimi önemli bir rol oynamaktadır. Bu nedenle, ışığı donör kısımları ile absorblayıp, bu enerjiyi akseptör kısma transfer edebilen multikromoforlu moleküller dizayn edilmiştir. Transfer sırasındaki enerji kaybını önlemek için, donör ve akseptör Boradiazaindasen (BODIPY) molekülleri arasındaki uzaklık mümkün olduğunca kısaltılmıştır. Üç farklı yapıda enerji transfer kaseti sentezlenmiş ve analizleri başarıyla gerçekleştirilmiştir. Süpramolekülün dizaynının, donör ve akseptör molekülün arasındaki spektral çakışma ve uzaklık bakımından, enerji transferinin verimini etkilediği gözlemlenmiştir. Fonksiyonel dizaynı sayesinde bu moleküller ışığı farklı dalga boylarında absorblamakta ve yaymaktadırlar. Akseptör BODİPY çekirdeğine substite edilen di-stiril ve tetra-stiril grupları, absorbsiyon ve ışıma en üst değerlerini değiştirmektedir. Moleküle substite edilen stiril gruplarının artması, spektrumu görünür bölgenin kırmızı kısmına kaydırmaktadır. Bu moleküller rasyonel dizayn yapılması durumunda, enerji transferi uygulamalarında ve geniş spektrumda absorbansı olan boya gereksinimi olan amaçlarda kullanılabilirler.

Anahtar Kelimeler: Boradiazaindasen (BODIPY), boya, süpramoleküer kimya, multikromofor, enerji aktarımı, Sonogashira bağlaması.

Dedicated to my Parents

ACKNOWLEDGEMENT

I would like to express my gratitude to my supervisor Prof. Dr. Engin U. Akkaya for his guidance, support and patience during the course of this research. I am also grateful to him for being lead and teaching how to become a good scientist I will never forget his support throughout my life.

I owe a special thank to Yusuf Çakmak for his generous help in Time-resolved Fluorescence analysis. I would like to thank Fazlı Sözmen, for his partnership in this research.

I want to thank our group members Sündüs Erbaş Çakmak, Murat Işık, Esra Eçik Tanrıverdi, Ayşegül Gümüş, Ruslan Guliyev, Bilal Kılıç, Safacan Kölemen, Seda Demirel, Onur Büyükçakır, İlke Şimşek Turan, Nisa Yeşilgül, Ziya Köstereli, Tuğba Özdemir Kütük, Şeyma Öztürk, Fatma Pir Çakmak, Tuğçe Durgut, Fatma Tuba Yaşar, Muhammed Büyüktemiz, Taha Bilal Uyar, Ahmet Atılgan, Yiğit Altay and rest of the SCL (Supramolecular Chemistry Laboratory) members for valuable friendships, wonderful collaborations, and great ambiance in the laboratory. It was wonderful to work with them.

I would like to thank to TÜBİTAK (The Scientific and Technological Research Council of Turkey) for financial support.

I would like to express my special thanks to my valuable friends Ateş Derviş, İrem Sak, Elif Ertem, Kutay Yıldız, Damla Şenol, Hatice Turgut, Hami Tural and Mehmet Uğur Öney for adding joy to my time during the course of this research.

Finally, I want to express my gratitude to my family for their encouragement, love, support, and understanding. I owe them a lot.

LIST OF ABBREVIATIONS

BODIPY:	Boradiazaindacene
DNP:	Dinitrophenyl hydrazine
TFA:	Trifluoroacetic acid
DCM:	Dichloromethane
THF:	Tetrahydrofuran
DIPA:	Diisopropyl amine
DMF:	Dimethylformamide
NBS:	N-Bromosuccinimide
FRET:	Förster Resonance Energy Transfer
TLC:	Thin layer chromatography
NMR:	Nuclear magnetic resonance
$CHCl_3$:	Chloroform
RT:	Room Temperature
MeOH:	Methanol
EtOH:	Ethanol
AcOH:	Acetic Acid
HOMO:	Highest occupied molecular orbital
LUMO:	Lowest unoccupied molecular orbital

TABLE OF CONTENTS

LIST OF FIGURES

LIST OF TABLES

CHAPTER 1

INTRODUCTION

1.1. BODIPY Dyes

Boradiazaindacene (BODIPY) dyes were first synthesized in 1968, about half century ago, by Kreuzer and Treibs[1]. Due to the ease of synthesis, high quantum yield and tunability of spectrum by functionalization, BODIPY dyes accomplished great interest among many research groups. In addition, these dyes are relatively stable and can dissolve in both organic and inorganic solvents through rational design. After the initial synthesis, these colorful molecules make use in biological imaging[2], chemosensors[3] and light harvesting systems[4].

BODIPY molecule has many advantageous properties. For instance, these molecules can easily be functionalized by using coupling and condensation reactions. In recent years, BODIPY chemistry becomes a main interest of many research groups, demonstrating the rich chemistry[5]. Possible chemical modifications of different positions of the core, makes it easier to functionalize the molecule for structural and photophysical purposes. Substitution of 1^{st}, 3^{rd}, 5^{th} and 7^{th} position with suitable groups using condensation reactions generally yields with long wavelength absorbing and emitting dyes[6]. Naked BODIPY molecule has an absorption value around 500 nm. Incorporation of aromatic rings and groups from *meso* position does not cause a significant change in the photophysical properties of the molecule[7].

Position numbering for BODIPY molecules can sometimes be confusing, however; α and β signatures make it easier to indicate the positions. In addition, 8^{th} position of the core has a special name called *meso* position. (Figure 1)

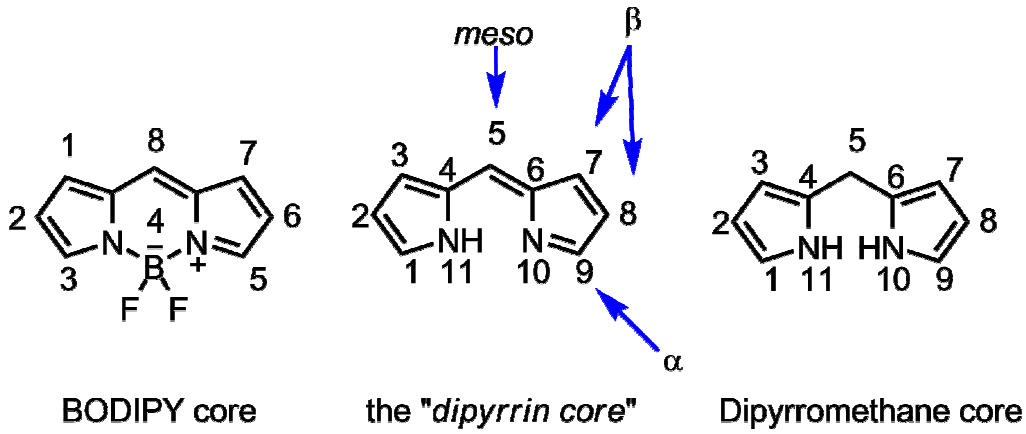

Figure 1: Position Numbering of BODIPY core.

Halogenation of 2nd and 6th position of the core has an important role in successful metal coupling reactions like Sonogashira and Suzuki coupling. Since these positions have the relatively least positive charge than other positions, electrophilic attacks are possible. Halogenations generally implemented with excess use of halogen in organic solvents for both 2nd and 6th positions. Mono-halogenation is also possible with suitable reaction conditions. However, halogenation generally has a disadvantage: it reduces the quantum yield by quenching the fluorescence, due to heavy atom effect. The spectrum generally shifts to red region and molecule gains deep pinkish color[7].

When treated with clorosulphonic acid, 2nd and 6th positions of BODIPY molecule gives electrophilic substation reaction[8]. After the treatment, BODIPY core becomes soluble in water, which can be used for biological purposes. This process also provides stability to the BODIPY core.

3rd and 5th positions of the core are also be functionalized by Knoevenagel condensation reaction. Since methyl groups on this position are acidic, condensation with an aldehyde is applied to the molecule. The reaction generally gives high yields with the naked BODIPY core and functionalized

2nd, 6th and *meso* position. Here are some BODIPY dyes in the literature, which are functionalized by this condensation reaction[9].

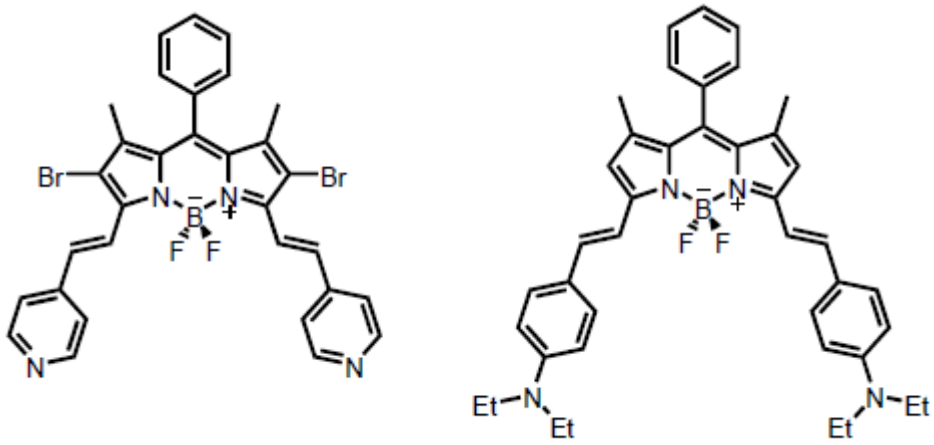

Figure 2: Knoevenagel Condensation From 3rd and 5th position

1.1.2. Applications of BODIPY dyes in Literature

There are many possible modifications and application areas of BODIPY dyes due to excellent properties explained before. Since they have high quantum yields and tunable spectrum properties, BODIPY structure is used in energy transfer cassettes and solar cells[10]. Large Stokes' shift generally needed for biological applications for preventing the self-absorption and intervention of biological components inside of the cell. For that reason, energy transfer systems are widely used[11]. For usage in fluorescent labeling, both through-bond (Dexter type) and through-space (Förster type) energy transfer cassettes are designed[12].

In 2003, energy transfer cassettes, which are formed by anthracene-BODIPY acceptor and donor sites, are synthesized and analyzed[10a]. Ten differently conjugated donor-acceptor systems are designed for fluorescent

labeling and molecular imaging purposes in the work of Kevin Burgess and coworkers[10a].

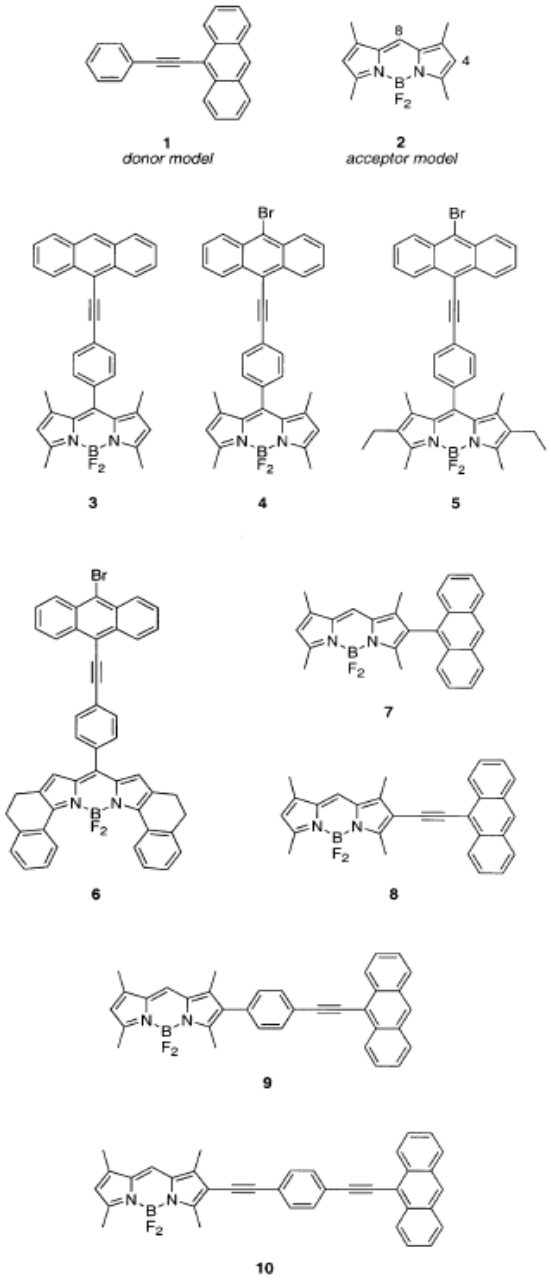

Figure 3: Energy transfer cassettes based on BODIPY dyes prepared by Sonogashira coupling[10a]. Copyright © 2003 Wiley-VCH Verlag GmbH&Co. KGaA, Weinheim. Adapted with permission.

Generally, two mechanisms used for the energy transfer process: Förster Resonance energy transfer (FRET) and Dexter electron transfer. Detailed information will be provided about the mechanism and usage area of these processes in the next sessions. FRET mechanism generally involves a spacer between two conjugated dyes. In order to FRET to occur, there must be a spectral overlap between the emission wavelength of the donor molecule and absorption of the acceptor molecule. Spacer can consists of non-conjugated chemical structure and it should not have any π-conjugation. The main purpose of the spacer is that it stops the conjugation between the donor and acceptor molecule. Due to the spectral overlap, non-emissive energy transfer occurs between the donor and acceptor dye. The distance is also very crucial; it is supposed to be less than 10 nm[13]. R. Ziessel and his coworkers worked on through-bond energy transfer systems in 2006. These molecules also capable of showing FRET, since spectral overlap between the donor and acceptor is modest[14].

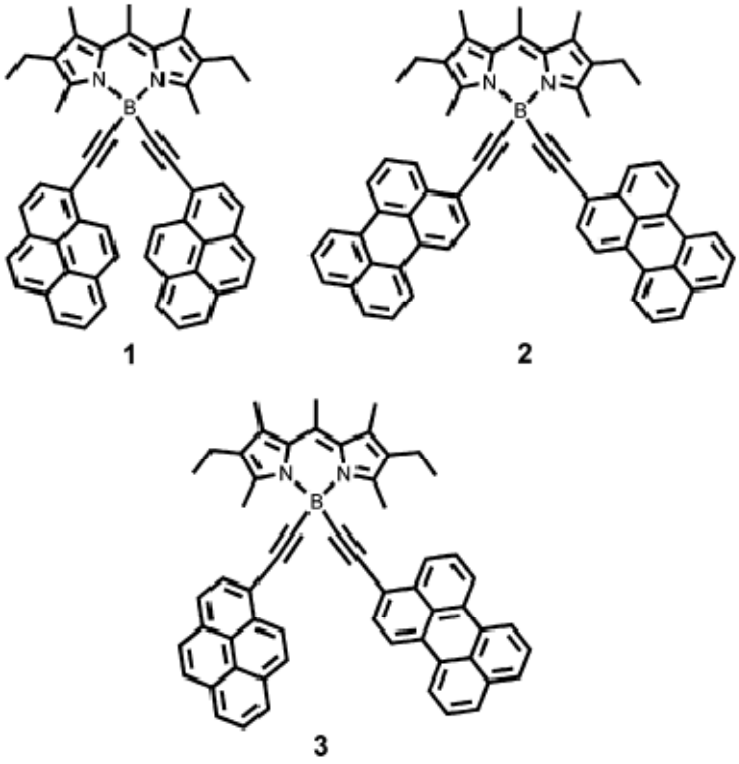

Figure 4: BODIPY-based cascade type dyes studied by R. Ziessel and his team[12].

Dexter type energy or electron transfer is more advantageous to some extent. Since the transfer occurs via electron transfer through π-conjugation, there is no necessity for the spectral overlap among donor and acceptor sites. Therefore, this property enables large Stokes' shifts and tunable photophysical advantages. In addition, the energy transfer is said to be more efficient than FRET[15]. In 2006, E .U. Akkaya and his team accomplished efficient energy transfer assembled on light harvesting systems with perylenediimide derivatives[16]. This molecule bears a spacer for the use of FRET. Light harvesting molecule promises a large cross-sectional area of the visible spectrum. The molecular design is dendrimer-based. The core of the dendrimer bears the acceptor BODIPY; while 2nd generation of dendrimer occupies the donor perylenediimide functionalized groups. This study is a promising study for energy transfer systems based on dendrimer structures.

Since three decades, BODIPY functionalized molecules have found usage in different research areas. In the last decade, BODIPY became very popular and attract attention of many scientists.

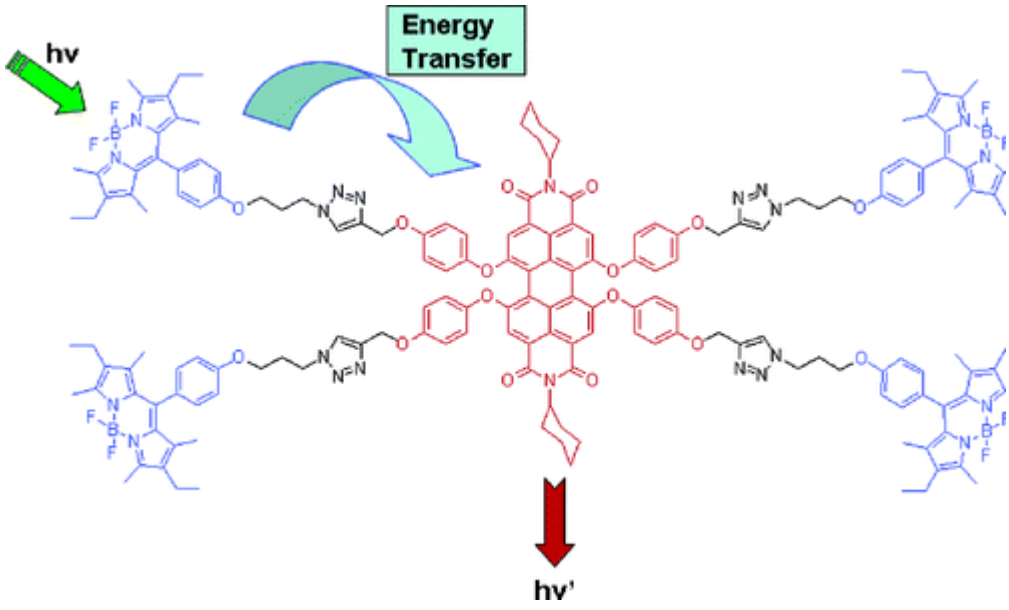

Figure 5: Light harvesting molecule with perylenediimide groups reported by E. U. Akkaya and his team[13]. Copyright © 2006 American Chemical Society. Adapted with permission.

BODIPY dyes have enormous application areas, even in the solar cell field[17]. In recent years, efficient and effective utilization of solar energy is an important target for make use as energy source for many field[18]. Dye synthesized solar cells (DSSc) are promising materials, which give an alternative opportunity towards expensive technologies. In this manner, a convergent dendrimer is designed, which can collect the solar energy and transfer to the core molecule.

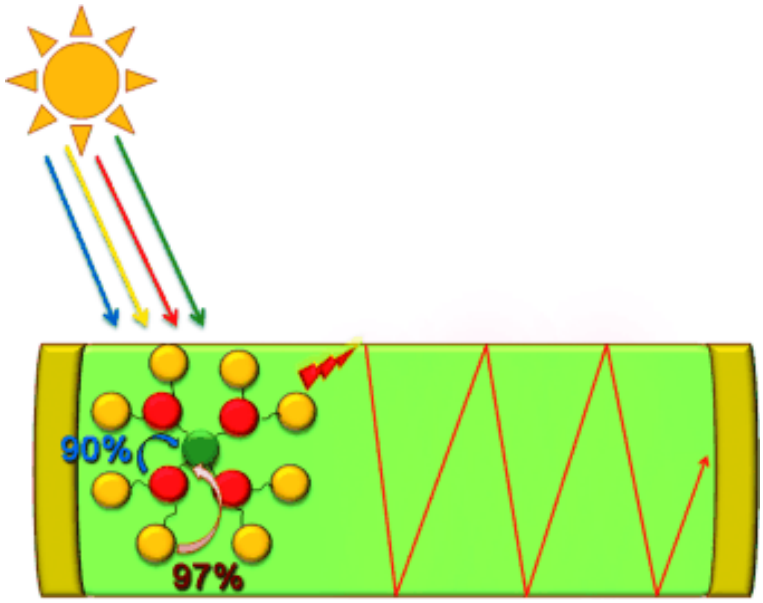

Figure 6: Schematic Representation of solar concentration in a waveguide.

Other application area of BODIPY dyes is photodynamic therapy, which is a novel alternative cancer treatment. In this therapy, a photodynamic reagent and near-IR visible light is used. Generally 650-800 nm of light is used, since the tolerated part of the skin is between this region of light. The treatment begins with placement of photo dynamic reagent to cancer tissue and exposure of light. The reagent is designed to synthesize singlet oxygen species

from the molecular oxygen inside of the cell. Singlet oxygen species ($^1O_2$) are very fatal to cancer cells and damage them. The result is even apoptosis of the cell.

In this application area, Akkaya et al. designed a photodynamic molecule, which can synthesize singlet oxygen when treated with 660 nm[19]. In addition, the molecule can detect the acidity and concentration of Na^+ inside of the cell and target the cancer cells. Cancer cells have more acidic environment than normal cells[20]. In acidic media, pyridine groups attached to molecule are protonated and absorbance shifts. Sodium concentration also encourages the process and photoinduced electron transfer is prevented. Therefore, molecule absorbs the light and begins producing singlet oxygen species to kill cancer cells. The work is published in 2008 as a AND logic gate with the inputs of cancer cells.

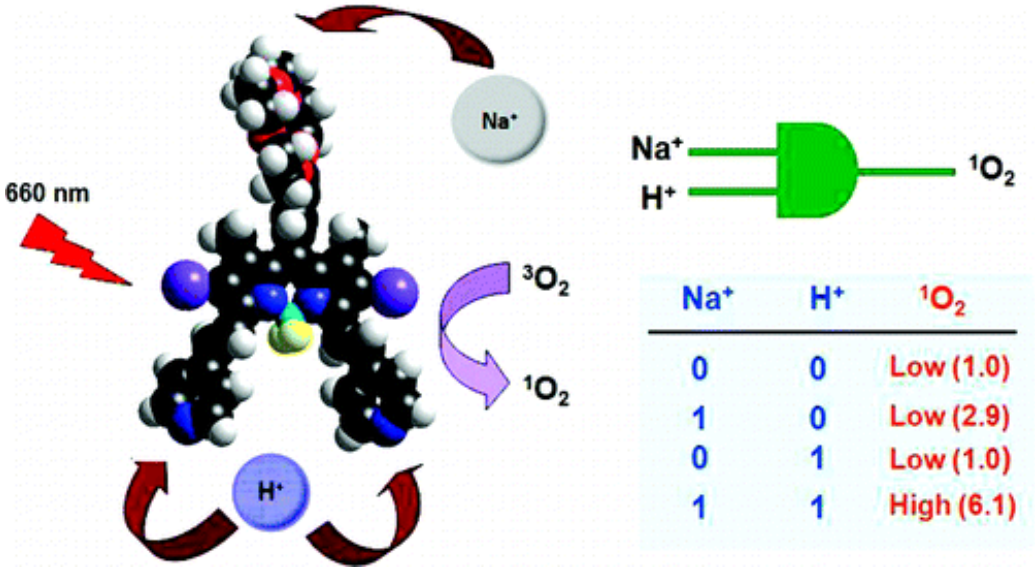

Figure 7: A proof of principle of photodynamic therapy reagent for cancer treatment. Copyright © 2008 American Chemical Society. Adapted with permission.

1.2. Cross Coupling Reactions

Coupling reactions aim to form carbon-carbon bonds between two hydrocarbons with an assistant of metal catalyst, generally Pd, Ni or Cu. Cross coupling reactions occur between two different hydrocarbons, one being organic halide and other being the organometallic compound[21]. These reactions are important tool in organic chemistry to form carbon-carbon bonds, and gain incredible growth over a century[22]. In BODIPY chemistry, coupling reactions are generally performed with halogenated BODIPY core and alkyne-functionalized reagent. Alkyne groups are suitable for cross coupling purposes, since they are electron-rich, they have rigid structure and unsaturated nature. The crucial reactant for the coupling reactions is the catalyst. Metal catalyst for the reaction is Pd catalyst, sometimes with the aid of Cu. One of the most common coupling reactions among all is Sonogashira Coupling, in which a terminal alkyne and a haloarene gives reaction in the presence of Pd catalyst with the aid of Cu and mildly-strong base[23]. Many coupling reactions have found their way in different areas like pharmaceuticals[24], chemical sensors and wires[25]. For instance, in 2009, cross coupling reactions are used in biological systems; for reactions of proteins, successfully[26].

Figure 8: Aqueous Suzuki–Miyaura cross coupling for proteins. Copyright © 2009 American Chemical Society. Adapted with permission.

1.2.1. Sonogashira Coupling

Sonogashira coupling reaction and mechanism first discovered by Kenkichi Sonogashira, Yasuo Tohda, and Nobue Hagihara and published in 1975[27]. This coupling type also uses Pd as the metal catalyst, generally in the assistance with Cu presence, which increases the reactivity of reaction and reduces the harsh conditions. The reaction is still being optimized in the means of synthetic capabilities[28]. Not all the reactions require additional Cu metal. Usages of mild bases, room temperature and even aqueous media have made this coupling reaction useful in many wide areas using carbon-carbon bond formation[29]. These mild conditions also come in handy in many complex structure formations. High temperature and strong base addition in other coupling reactions can react with the reagents and damage their structure, even the target molecule. Harsh conditions can also lower the yield.

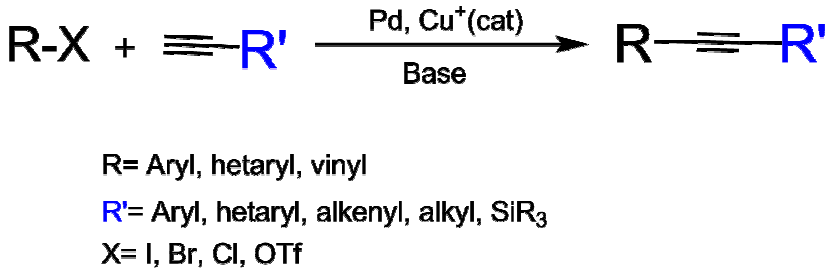

Figure 9: Sonogashira Coupling reaction conditions

Addition of Cu salts can sometimes bring some drawbacks, however; all copper free methods involve the use of excess amine, which changes the friendly conditions of the medium. It also affects the environmental and economical advantages of the methodology[30].

1.2.2. Sonogashira Coupling Mechanism

Although the real mechanism behind the Sonogashira Coupling reaction cannot be thoroughly understood, the widely accepted one is very similar in the publication of Sonigashira, 1975[13]. According to the report, there is a Pd cycle and Cu cycle, which are not independent from each other. Pd cycle has several steps and provides the formation of final product, while Cu helps the mechanism by formation of copper halide. The presence of anions and halides in the medium are believed to cause the formation of anionic species, which can be the real catalyst of the reaction[14].

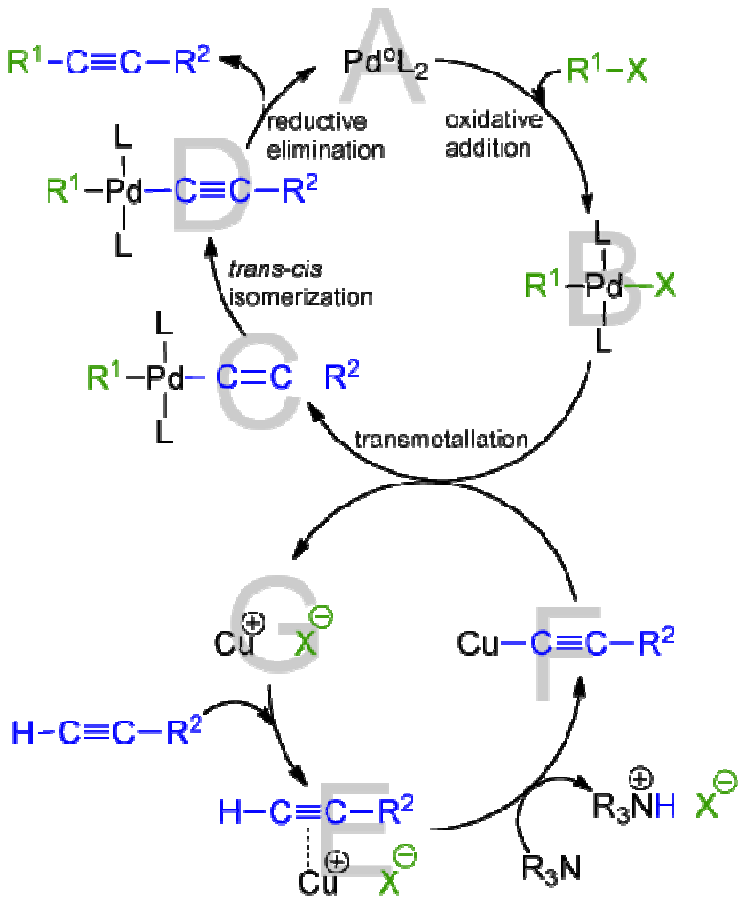

Figure 10: Cu-cocatalyzed Sonogashira Coupling Mechanism[14]

The mechanism of the reaction is not well understood. However, there is an optimum mechanism suggestion for both Pd and Cu cycle[31]. In this suggestion of Pd cycle, active Pd catalyst reacts with the aryl or vinyl halide in an oxidative addition reaction. Intermediate then reacts with Cu co-catalyst, which is produced in the Cu cycle. Cis-trans isomerization occurs within the Pd intermediate and alkyne is produced with reductive elimination reaction[25]. The Cu cycle on the other hand, is easier to understand and predict. Presence of the base in the medium assists in the formation of alkyne complex. This complex is made more acidic by the base used in the reaction and copper acetylide intermediate is formed. When copper intermediate reacts with the Pd intermediate, Cu cycle is completed and Cu is formed again.

Generally a catalyst and co-catalyst is needed for the reaction: zerovalent Pd complex (Pd^0) and halide of copper(I) salt. Commonly used Pd catalyst are integrated with phosphine complexes. Sometimes derivatives of $[Pd(PPh_3)_4]$, like $[Pd(PPh_3)_2]Cl_2$ can be used. However in this position, Pd is not zerovalent. In the reactions with no copper addition, tetrakis (triphenylphosphine)Pd^0 is used directly. This catalyst is very sensitive to O_2, therefore it is preferred over phosphine derivatives. Copper(I) salts, especially copper iodide can react with terminal alkyne group[32]. Iodine atom can leave Cu atom easier in basic conditions, due to its large atomic radii.

Sonogashira coupling reaction is done under argon or nitrogen gas, since catalysts are very sensitive to O_2. %2-6 mol of Pd catalyst is added with 2 times mole of Cu co-catalyst[33]. Sometimes, addition of triphenylphosphine is necessary, especially when the phosphine derivative of Pd catalyst is used. Triethylamine or DIPA is generally used as the base source, since they are not very strong bases. If the base creates a harsh environment, then the reagents may be damaged or decompose before the coupling reaction happens. Coupling reaction is typically run under very mild conditions; therefore it is preferable in biological applications. As solvent, DMF, THF and even ether groups can be used[34].

1.2.3. Applications of Sonogashira coupling in literature

Sonogashira coupling has large number of applications in both natural and non-natural process. Typical Sonogashira reaction, which uses aryl halides, has been employed in large list of conditions. There are so many examples of coupling with Pd^0 catalyst, however; significant cases are difficult to find. A bioanalytical application is prepared with iodinated phenylalanine and d-biotin, which is functionalized with terminal alkyne group[35]. This methodology is used with the formation of Pd^0 catalyst in situ, with the aid of 2 times CuI and phosphine source.

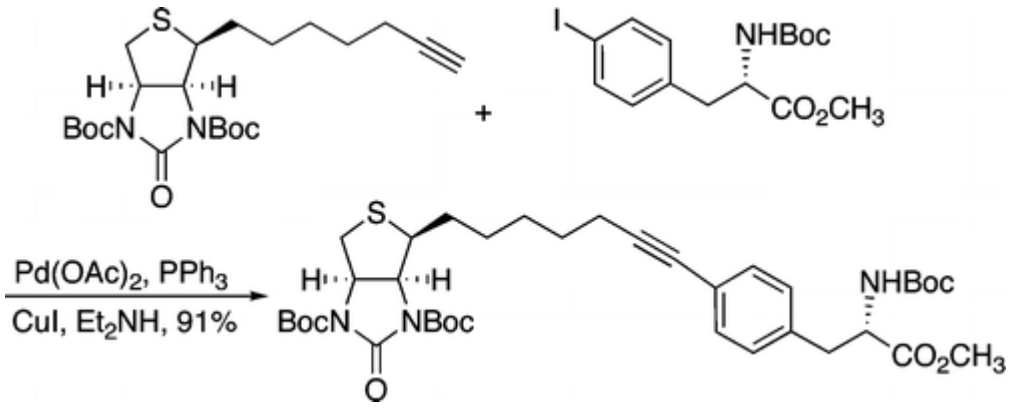

Figure 11: Synthesis of a Biotin-Derived Alkyne[29]

Sonogashira coupling can also be seen in natural processes, since many metabolism in the nature contain alkyne or alkyne-derivative structures[36]. There is a recent example of formation of natural product benzylisoquinoline, which is synthesized by the reaction of aryl iodide cyclization. The alkaloids of the reagent give (+)-(S)-laudanosine and (–)-(S)-xylopinine[37]. This natural products help to decrease the seizure threshold, inducing them at sufficient concentrations[38].

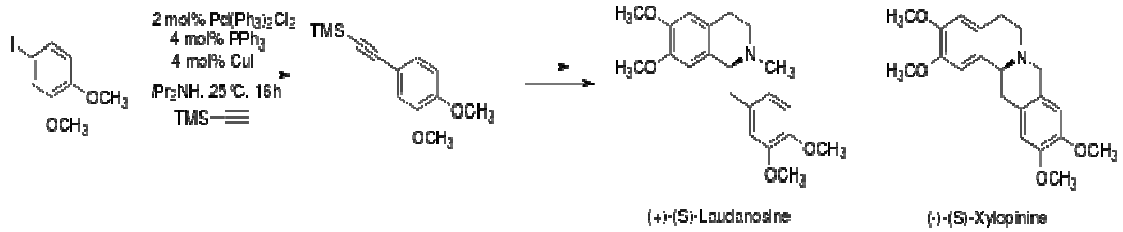

Figure 12: Synthesis of natural products (+)-(S)-laudanosine and (–)-(S)-xylopinine[31].

Another research links the porphyrin units for formation of large molecular assemblies like molecular rods[39]. These supramolecules are planned to make use in light harvesting purposes, due to its structure of four porphyrin molecules which are connected to methane core as acceptor.

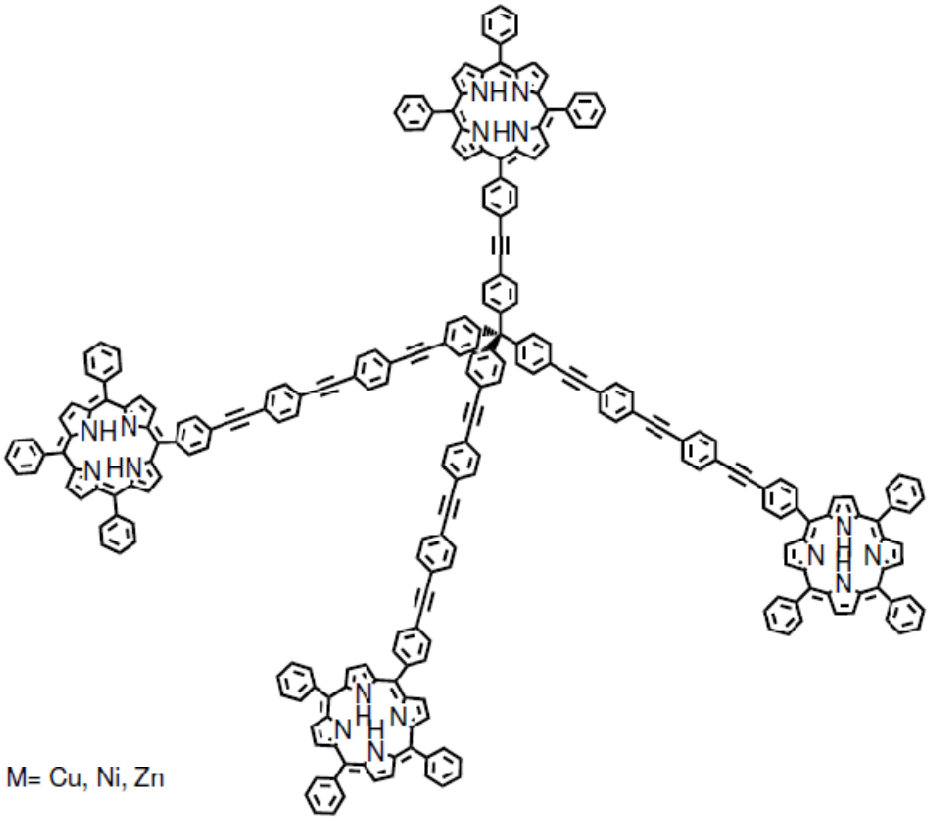

Figure 13: Light harvesting assembly with four porphyrin units[33].

1.3. Transfer mechanisms of electronic excitation

Energy transfer mechanism is very important in biological imaging purposes, solar cells and energy transfer cassettes. Typically, non-radiative energy or electron transfer is preferred for developing emission intensity. In this kind of systems, donor molecule or molecules absorb energy at relatively short wavelength, whereas acceptor molecule, which is attached to the donor parts, emits the transferred energy at relatively longer wavelength. This process happens in two pathways: through-space (FRET) or through bond (dexter type energy transfer).

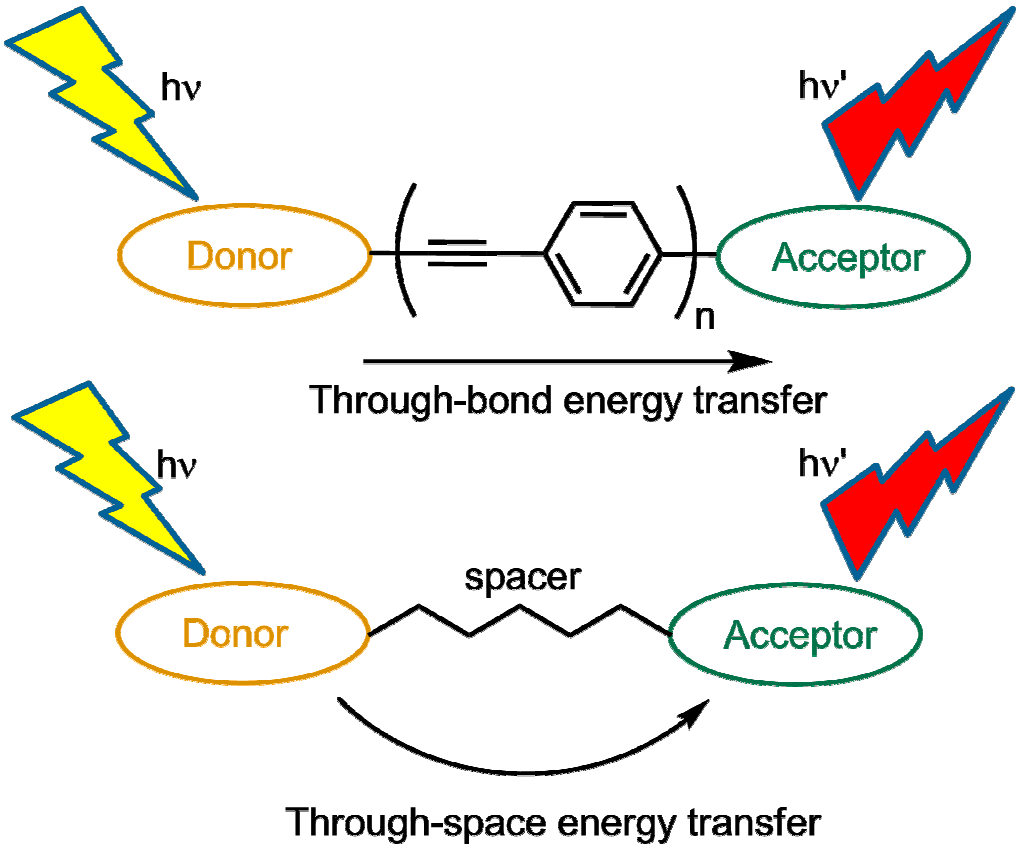

Figure 14: Through-bond (Dexter) and Through-space (FRET) energy transfer

1.3.1. Through-space Energy Transfer

Fluorescence resonance energy transfer is a non-radiative process, in which excited state donor molecule transfer its energy to ground state acceptor. Spectral overlap between these parts has no importance in this type mechanism. Distance between the donor and acceptor therefore, does not prevent to achieve the energy transfer[40]. For many applications, Stokes' shift of a single molecule is not sufficient. Especially in biological applications, large Stokes' shift is needed to prevent self-absorption and organelle intervention. For that purpose, multichromophoric molecules are frequently used, since emission occurs in longer wavelengths. For the energy transfer to happen, acceptor molecule and donor parts are held together with a spacer between them. Spacer, works for non-conjugated part of the molecule and it prevents through-bond energy transfer mechanism.

FRET mechanism is known for decades[41]. An electron of acceptor molecule in its HOMO level, is excited by the energy of donor molecule coming from an electron in its LUMO state. During this relaxation, energy is lost between the vibrational and rotational levels of the donor molecule. The energy can also be lost by the heat energy. The rate of the transfer depends on some factors. These factors are commonly the distance between donor and acceptor molecule, the relative orientation of the transition dipoles, availability of spectral overlap[42]. FRET mechanism occurs distances between 10-100 Å.

An example illustrated in 2010, a chemosensor for polyphosphates like ATP or ADP is designed[43]. This sensor is based on the binding-supported FRET process due to spectral overlap. Illustrations inside of the cell are also shown in the work.

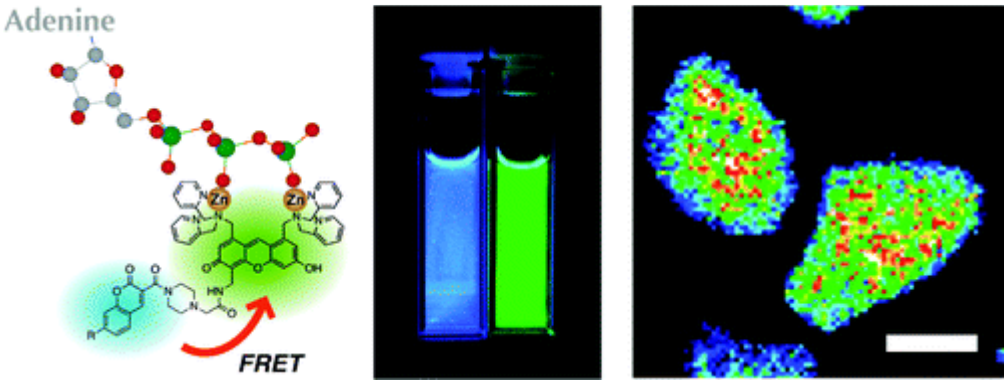

Figure 15: FRET based energy transfer cassttes used for biological chemosensors[37]. Copyright © 2010 American Chemical Society. Adapted with permission.

In another nice work, dendrimer containing four coumarin derivatives are analyzed[44]. The results showed that 99% of the UV light absorbed by the system and transferred energy is the sent to core molecule by FRET.

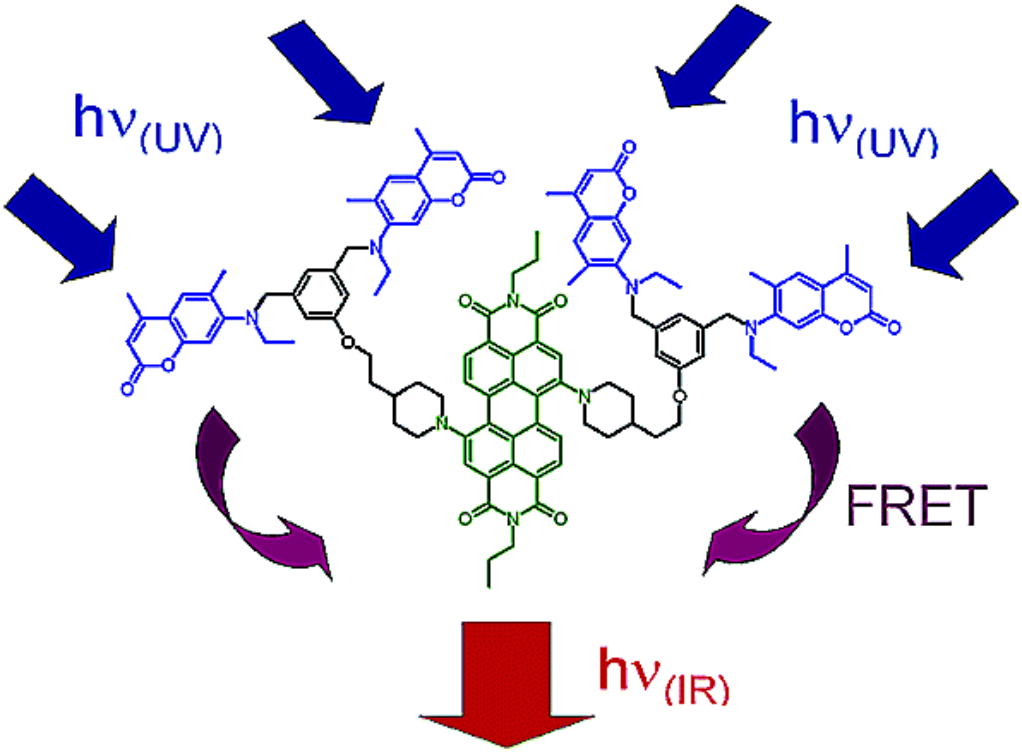

Figure 16: FRET based energy transfer cassettes in dendrimeric structure[38]. Copyright © 2002 American Chemical Society. Adapted with permission.

An example of FRET using pH dependent medium is published in 2002[45]. The donor and acceptor distance is adjusted by pH change. In acidic conditions, FRET is blocked and only donor emission is seen at 542 nm. In more basic conditions, the distance gets smaller and energy transfer is observed effectively.

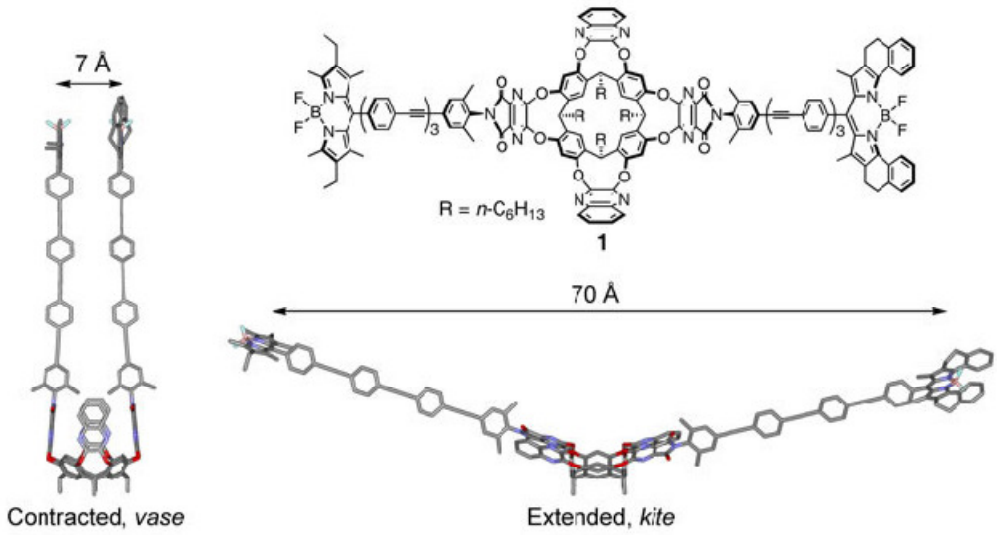

Figure 17: pH-dependent FRET[39].

FRET has many other usage areas in the literature. It is commonly used in protein labeling and biological processes, as explained before.

1.3.2. Through-bond Energy Transfer

When the donor and acceptor molecule are connected to each other with a conjugated system, the energy transfer may occur with an electron through bonds. Through-bond energy transfer mechanism on the other hand, does not

require spectral overlap between the excited donor chromophore and acceptor core. The dependency of transfer to orbital interactions restricts the process in relatively shorter distanced than FRET. The distance therefore, should be less than 10 Å. Since orbital interaction is unnecessary, this type of transfer has also many applications[46]. The acceptor and donor molecules are generally connected to each other with coupling reactions of terminal alkyne and halide groups. To some extent, dexter type energy transfer is more efficient due to direct interaction of the donor chromophore and acceptor molecule.

One interesting example of through-bond energy transfer is published in 2008 by E. U. Akkaya and his coworker[47]. In this work, oligomers which are attached to each other with phenylethynyl groups are presented. The BODIPY groups are attached to each other with Sonogashira coupling reaction. Figure below shows the structure of the molecule:

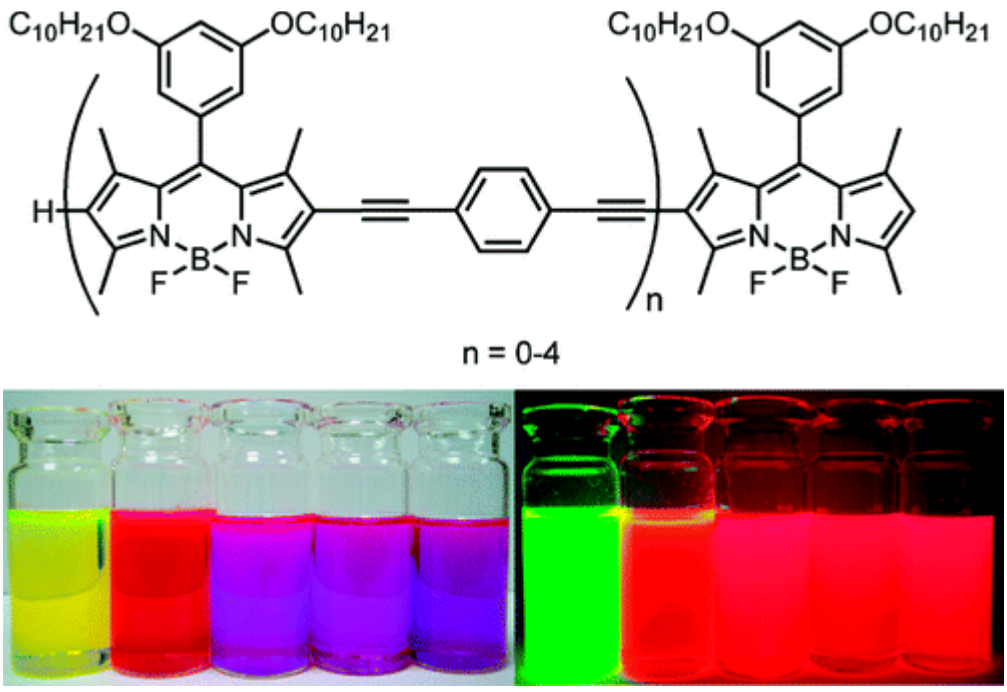

Figure 18: Through-bond energy transfer oligomers ad their colors under ambient light (left) and under UV irradiation (right). Copyright © 2008 American Chemical Society. Adapted with permission.

Another work on this mechanism is based on water soluble molecules for molecular imaging purposes[48]. Donor part of the molecule consists of fluorescein functionalized component. It transfers the energy through ethynyl groups to the acceptor molecule, which is based on rhodamine. This part emits the energy in significantly longer wavelength, creating large Stokes'shift.

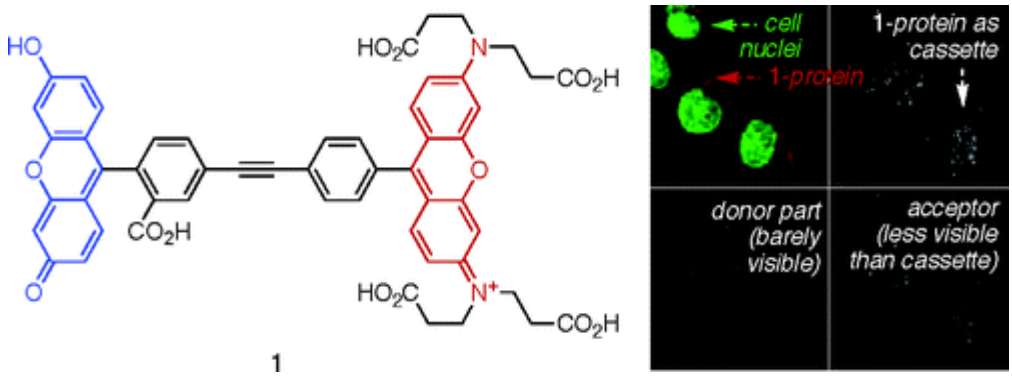

Figure 19: Water-soluble through bond energy transfer cassettes. Copyright © 2006 American Chemical Society. Adapted with permission.

Symmetrical energy transfer cassettes are also exist in the literature[49]. This study uses di, tri and tetra substitution to acceptor BODIPY core. Analysis and results showed that more substitute BODIPY chromophore has longer absorption and emission wavelengths. Therefore, the spectral tunability is provided.

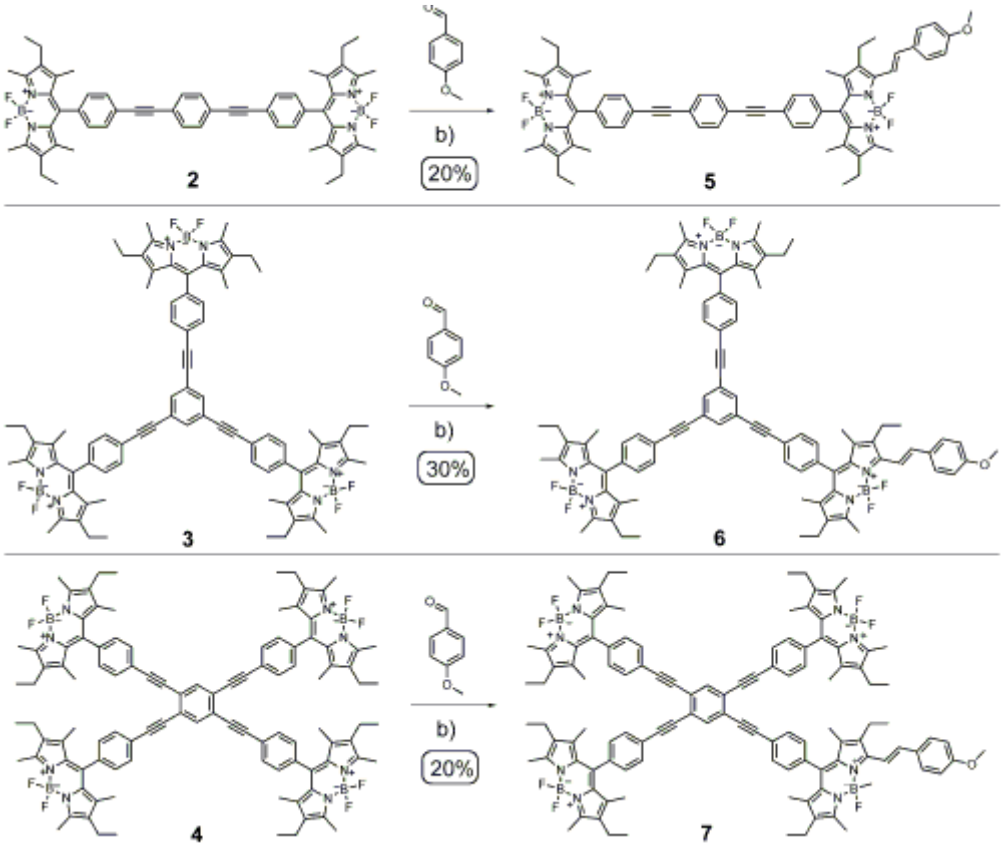

Figure 20: Selected examples of symmetrical Through-bond energy transfer cassettes[43].

Literature examples of through-bond energy transfer can vary, due to high efficiency of energy transfer and tenability of spectrum. In addition, no spectral interaction between the donor and acceptor chromophore is needed. Therefore, these molecules make use in biological applications, solar cells, sensors and many other application areas.

CHAPTER 2

EXPERIMENTAL

2.1. General

All chemical compounds and solvents obtained from Sigma-Aldrich were used without further purification. Column chromatography purification on silica gel was performed over Merck Silica gel 60 (particle size: 0.040-0.063 mm, 230-400 mesh ASTM). Reactions were monitored by thin layer chromatography technique using Merck TLC Silica gel 60 F_{254}.

^{1}H NMR and ^{13}C NMR spectra were recorded at room temperature on Bruker DPX-400 (operating at 400 MHz for ^{1}H NMR and 100 MHz for ^{13}C NMR) in $CDCl_3$ with tetramethylsilane (TMS) as internal standard. Chemical shifts are reported in parts per million (ppm) and coupling constants (*J values*) are given in Hz Splitting patterns are designated as s (singlet), d (doublet), t (triplet), q (quartet), m (multiplet), and p (pentet).

Absorption spectra in solution were acquired using a Varian Cary-100 spectrophotometer. Varian Eclipse spectrofluorometer was used to determine and record the fluorescence spectra of target compounds. Measurements were conducted at 25 ^{o}C using a 1x0.5 cm-sized quartz cuvettes. Mass spectra were recorded on Agilent Technologies 6530 Accurate-Mass Q-TOF LC/MS in Bilkent University, UNAM. The fluorescence decay measurements are carried out with the TM-3 Laserstrobe Time-Resolved Fluorometer utilizing a pulsed nitrogen/dye laser excitation and stroboscopic detection system. The laser dye excitation is at 492 nm and 526 nm. The instrument response is measured with an aqueous Ludox solution. The decays are calculated with a multiexponential fitting functionby iterative reconvolution and chi-square minimization. Quantum yield calculations are carried out with Cresyl Violet (λ_{exc}=610 nm) in

methanol and Rhodamine 6G (λ_{exc}=488 nm) in water as reference chromophores. Their calculated quantum yield values are 0.66 and 0.95 respectively. All absorption values are kept below 0.1 for avoiding self-quenching. The following formula is used for calculations[50]:

$$\mathbf{Q = Q_R\ (I/I_R)*(A_R/A)*(n^2/n_R^2)} \qquad (1)$$

where Q_R stands for quantum yield of reference, I and I_R for integrated area of emission spectrum for specific wavelength for sample and for standard respectively, A and A_R represents absorbance of corresponding wavelength for sample and standard, n and n_R refer to refractive indices of solvents in which sample and standard compounds were dissolved respectively. Refractive index values were taken to be 1.333 for water and 1.329 for methanol. All samples except standards were dissolved in chloroform with an n value of 1.49.

2.2. Syntheses

BODIPY based dyes and derivatives are synthesized according to literature. Other aromatic compounds and catalysts are gathered from Sigma-Aldrich and equivalent suppliers. Inorganic compounds are gathered from local Turkish suppliers.

2.2.1. Synthesis of Compound 3

To a 250 mL round-bottomed flask, 1 equivalent 3,5-Dihydroxybenzyl alcohol **(1)** (2 g, 14.27 mmol) and 3 equivalent K_2CO_3 (9.86 g, 71.35 mmol) is added. 150 mL acetone is degassed under argon for 20 minutes. Degassed acetone is added to the reagents which are put in 250 mL round-bottomed

flask. 18-crown-6 (0.4 g, catalytic amount) and KI (1.18 g, 7.13 mmol) are added respectively. Finally, 1-Bromodecane **(2)** (8.84 mL, 42.81 mmol) is added and mixture is refluxed for 12h under argon atmosphere using septum. After 12h stirring, solvent is evaporated. Crude is partitioned with water and ethyl acetate. Organic layer is gathered and washed with brine. Crude is dried with Na_2SO_4. Solvent is evaporated and purified over silica gel column using (EtOAc: Hexane 40:60) as eluent. White solid (6 g, 95%).

^{1}H-NMR (400 MHz, $CDCl_3$) δ_H: 6.38 (2H, s ArH), 6.25 (1H, s, ArH), 4.45 (2H,s, CH_2OH), 3.80 (4H, t, J = 6.6 Hz, OCH_2), 2.36 (1H,s, OH), 1.65 (4H, m,CH_2), 1.1-1.4 (28H,m, CH2), 0.8 (6H, t, J = 6.5 Hz, CH3).

^{13}C-NMR (100 MHz, $CDCl_3$) δ_C: 160.49, 143.21, 105.02, 100.52, 68.05, 65.35, 33.98, 32.85, 31.91, 29.60, 28.79, 26.06, 24.80, 22.69, 14.11 ppm.

MS (TOF- ESI): m/z: Calcd: 421.3697 $[M]^+$, Found: 421.3745 $[M]^+$, Δ=11.4 ppm.

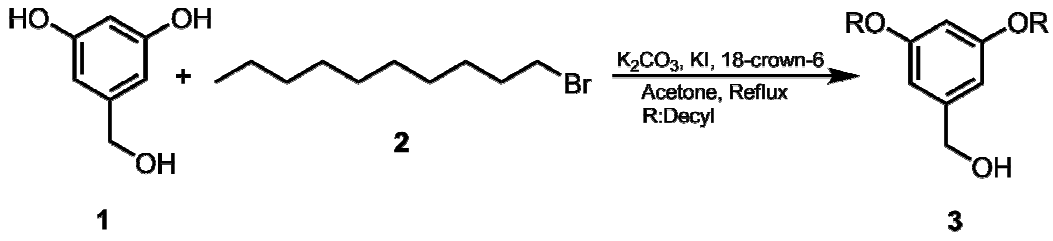

Figure 21. Synthesis of Compound **3**

2.2.2. Synthesis of Compound 4

To a 250 mL round-bottomed flask, 120 mL of dichloromethane is added and degassed for 20 minutes. **3** (6.00 g, 14.26 mmol) is added to the

flask and stirred for a while. Pyridinium chlorochromate (3.87 g, 17.97 mmol) is added to the mixture and stirred for further 3 h in RT. During stirring TLC control is applied and aldehyde dye (DNP in ethanol) is used for reaction monitoring. Extraction is applied with water and CH_2Cl_2. Organic layer is gathered and dried over Na_2SO_4. Solvent is evaporated and crude is purified with silica gel column as %12-25 EtOAc in hexane is eluent. Yellowish liquid (4.54 g, 75.7%).

^{1}H NMR (400 MHz, $CDCl_3$) δ_H: 9.91 (1H, s), 7.00 (2H, s, ArH), 6.72 (1H, s, ArH), 4.01 (4H, t, *J* = 13.04 Hz, OCH_2), 1.79 (4H, m, CH_2), 1.45 (4H, m, CH_2), 1.30 (24H, s, CH_2), 0.90 (6H, t, *J* = 7.32 Hz, CH_3).

^{13}C NMR (100 MHz, CDCl3) δ_C: 192.0, 160.8, 138.4, 108.1, 107.1, 68.5, 31.9, 29.6, 29.5, 29.3, 29.1, 26.0, 22.7, 14.1.

MS (TOF- ESI): m/z: Calcd: 419.3515 $[M]^+$, Found: 419.3585 $[M]^+$. Δ=16.7 ppm

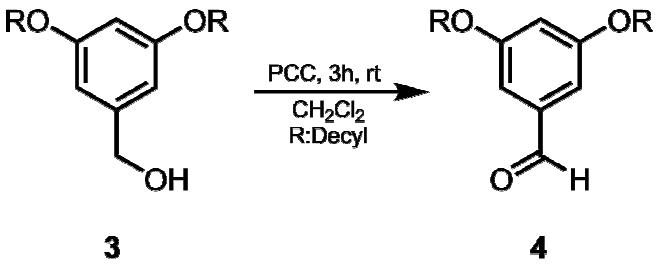

Figure 22. Synthesis of Compound **4**

2.2.3. Synthesis of Compound 5

PART I: To a two-necked 2000 mL round-bottomed flask, 190 mL ethyl acetoacetate (1.49 mmol) and 450 mL glacial acetic acid are added. 52 g

of $NaNO_2$ (0.754 mol) is dissolved in 100 mL water in a beaker, separately. The latter solution is added to a dropper and added to the previous mixture drop wise in 30 minutes, while the mixture is cooled to 5 ^{0}C by ice bath. The final mixture is stirred for extra 4 h at RT. During stirring, dropping funnel is replaced with a condenser. 100 g of zinc dust (1.53 mol) is added to the mixture with small portions. Then the mixture is refluxed at 125 ^{0}C for further 5h. Crude is poured in to 5 L of water immediately, while it is still hot. Precipitation is waited overnight. Then the crude product is filtered using suction filtration with Büchner funnel. Remaining zinc is washed and removed with acetic acid portions. Filtrate is also washed with acetic acid. The product is left for drying for a few days. Orange solid (125 g, 70.12%).

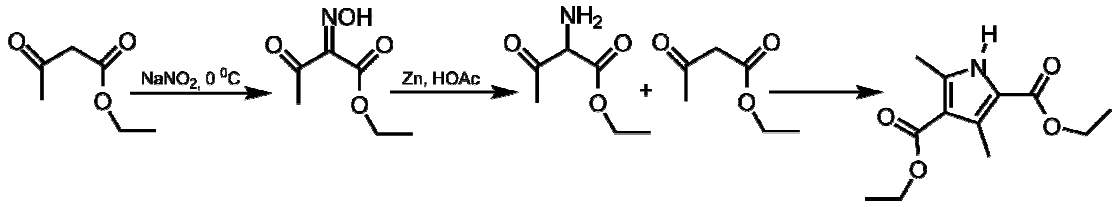

Figure 23. Synthesis of Compound **5-1**

PART II: A solution of 225 g (4 mol) KOH in 126 mL of water is prepared in 1 L round-bottomed flask. 100 g of crude (0.42 mol), 2,4-Dimethyl-3,5-Dicarboxy-pyrrole is added to the mixture and stirred for 3-4 h with reflux condenser at around 130 ^{0}C, until the crude liquidifies due to the formation of 2,4-Dimethyl-pyrrole (**5**). Then condenser is replaced with distillation apparatus, temperature is raised to 160 ^{0}C. Pyrrole is collected with Clevenger apparatus. The mixture is extracted with diethyl ether and water. Organic layer is dried with K_2CO_3. Solvent is dried under vacuum. Orange liquid (23 g, 60.43%).

^{1}H NMR (400 MHz, $CDCl_3$) δ_H: 7.61 (s, 1H), 6.54 (s, 1H), 5.94 (s, 1H), 2.37 (s, 3H), 2.26 (s, 3H).

MS (TOF- ESI): m/z: Calcd: 96.0769 $[M]^+$, Found: 96.0816 $[M]^+$. Δ=49.02 ppm

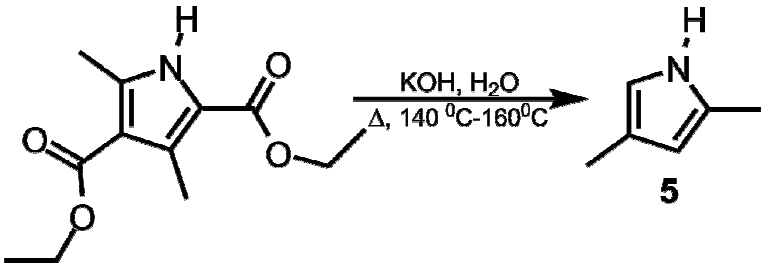

Figure 24. Synthesis of Compound **5**

2.2.4. Synthesis of Compound 6

250 mL round-bottomed flask is dried in oven for about 20 minutes. 150-200 mL of CH_2Cl_2 is bubbled with argon for about 15 minutes. **4** (1 g, 2.59 mmol) is added to the solvent and continued bubbling. 2 equivalent of **5** (585.9 µL, 5.70 mmol) is then added. Reaction mixture is bubbled for 10 more minutes and 3 drops of TFA is added. Reaction is stirred for overnight at RT. 1 equivalent of p-chloranil (636.80 mg, 2.59 mmol) is added and the mixture is stirred for 2 hours. Et_3N (5 equivalent, 1.8 mL) is then added and mixture is stirred for 20 minutes. Finally, $BF_3.OEt_2$ (8.5 equivalent, 3.5 mL) is added and stirred for 1 hour. Extraction is applied with water and CH_2Cl_2. Organic layer is gathered and dried over Na_2SO_4. Solvent is evaporated and crude is purified with silica gel column as CH_2Cl_2: Hexane (2:1) is eluent. Orange waxy liquid (360 mg, 23.6%).

^{1}H NMR (400 MHz, $CDCl_3$) δ_H: 6.56 (1H, s, ArH), 6.45 (2H, s, ArH), 6.01 (2H, s, H2, H6), 3.95 (4H, t, J = 13.24 Hz, OCH_2), 2.58 (6H, s, CH_3), 1.79

(4H, m, CH_2), 1.59 (6H, s, CH_3), 1.46 (4H, m, CH_2), 1.30 (24H, s, CH_2), 0.91 (6H, t, J = 13.64 Hz, CH_3).

^{13}C NMR (100 MHz, $CDCl_3$) δ_C: 161.2, 155.4, 143.2, 136.4, 131.2, 121.0, 106.4, 102.3, 68.4, 31.9, 29.6, 29.5, 29.3, 29.2, 26.0, 22.7, 14.6, 14.2, 14.0.

MS (TOF- ESI): m/z: Calcd: 638.4767 $[M+H]^+$, Found: 638.4816 $[M+H]^+$. Δ=7.67 ppm

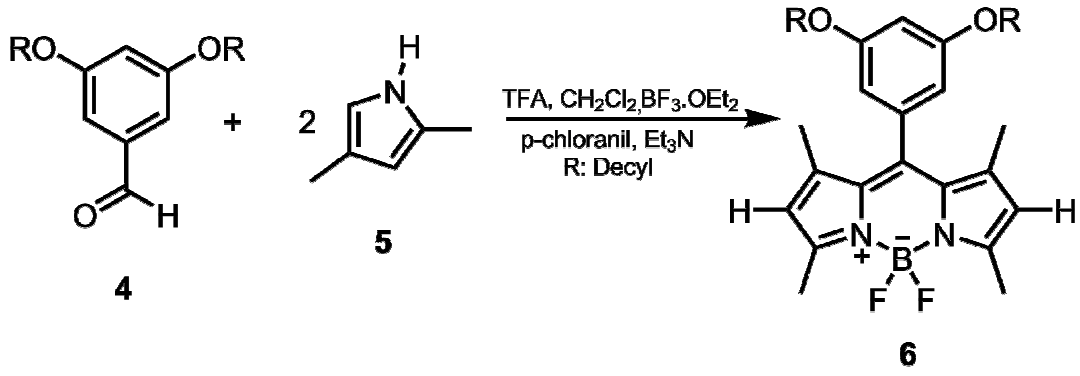

Figure 25. Synthesis of Compound **6**

2.2.5. Synthesis of Compound 7

Compound **6** (250 mg, 0.39 mmol) is taken to a 250 mL round bottomed flask and dissolved in 120 mL EtOH. 2.5 equivalent iodine (248 mg, 0.98 mmol) is added to the mixture. Iodic acid (137.2 mg, 0.78 mmol) is dissolved in 2 mL of water. Iodic acid solution is added to mixture of **6** and iodine. The reaction temperature is raised to 60^oC and is monitored by TLC ($CHCl_3$). When all the starting material is consumed, 50 mL saturated $Na_2S_2O_3$ solution in water is added and stirred for 15 minutes until all excess iodine is consumed. The product is extracted into CH_2Cl_2 with water and dried over

Na_2SO_4. Solvent is evaporated and crude is purified with silca gel column DCM: Hexane (1:1). Red waxy liquid (320 mg, 92%).

^{1}H-NMR (400 MHz, $CDCl_3$) δ_H: 6.57 (1H, s, ArH), 6.38 (2H, s, ArH), 3.94 (4H, t, *J* = 13.20 Hz, OCH_2), 2.64 (6H, s, CH_3), 1.77 (4H, m, CH_2), 1.58 (6H, s, CH_3), 1.45 (4H, m, CH_2), 1.28 (24H, s, CH_2), 0.88 (6H, t, *J* = 13.57 Hz, CH_3).

^{13}C-NMR (100 MHz, $CDCl_3$) δ_C: 161.4, 156.7, 145.4, 141.4, 136.1, 131.0, 106.1, 102.7, 85.5, 68.5, 31.9, 29.6, 29.5, 29.4, 29.3, 29.1, 26.0, 22.7, 16.9, 16.0, 14.1.

MS (TOF- ESI): m/z: Calcd: 869.2698 $[M-F]^+$, Found: 869.2705 $[M-F]^+$. Δ=0.8 ppm

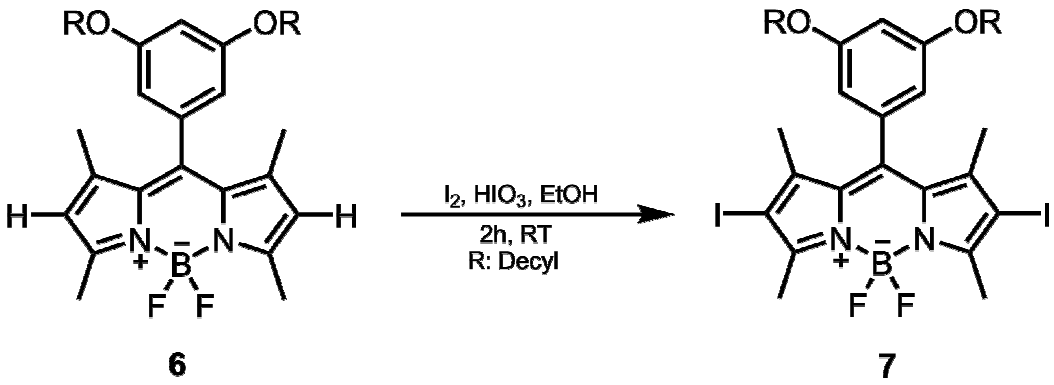

6 7

Figure 26. Synthesis of Compound **7**

2.2.6. Synthesis of Compound 10

100 mL round-bottomed flask is dried in oven and p-iodobenzoyl chloride **(8)** (560 mg, 2.1 mmol) is added with a magnetic bar. 40 mL of 1,2-dichloroethane is added to the flask and solid is dissolved. **5** (425 µL, 4.2

mmol) is then added to the flask dropwise and color change is observed. Themixture is refluxed about 13 hours at 92 ^{0}C. After 13 hours, the mixture is cooled to room temperature and 1.5 mL (5 equivalent) of Et_3N is added by syringe and stirred for 20 minutes. Then, 8.5 equivalent of $BF_3.OEt_2$ (2.25 mL) is added and reaction is stirred for 10 more minutes. Reaction mixture is refluxed again for 2 hours at 92^{0}C. Then it is cooled to room temperature and solvent is evaporated under vacuum. The product is extracted into CH_2Cl_2 with water and dried over Na_2SO_4. Solvent is evaporated and crude is purified with silca gel column DCM: Hexane (1:1). Red solid (340 mg, 37%).

^{1}H-NMR (400 MHz, $CDCl_3$) δ_H: 7.86 (2H, d, *J* = 8.32 Hz, ArH), 7.07 (2H, d, *J* = 8.36 Hz, ArH), 2.53 (6H, s, CH_3), 2.32 (4H, m, CH_2), 1.33 (6H, s, CH_3), 0.99 (6H, t, *J* = 15.13 Hz, CH_3)

^{13}C NMR (100 MHz, CDCl3) δ_C: 154.16, 138.14, 135.41, 133.06, 130.50, 94.46, 17.07, 14.59, 12.55, 12.53, 12.50, 11.95.

MS (TOF- ESI): m/z: Calcd: 507.1235 $[M]^+$, Found: 507.1349 $[M]^+$. Δ=22.4 ppm

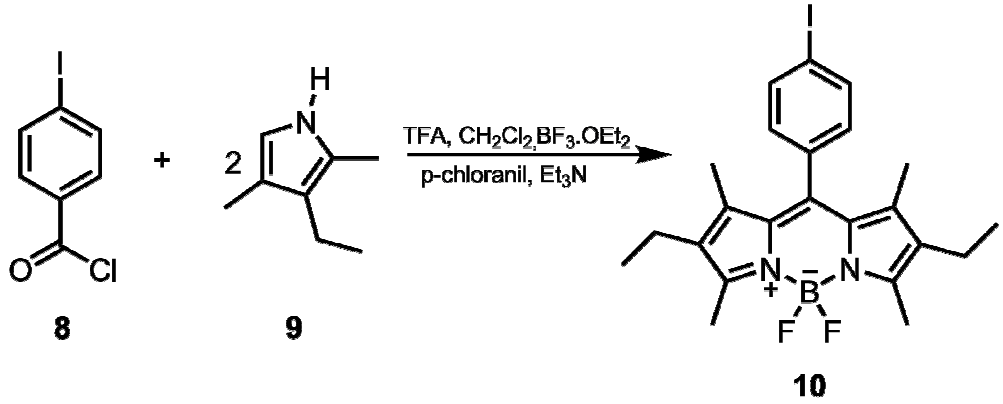

Figure 27. Synthesis of Compound **10**

2.2.7. Synthesis of Compound 12

THF is distilled in the set-up for about 4 hours. Then it is degassed for 15 minutes. Compound **10** (250 mg, 0.49 mmol) is dissolved in freshly distilled THF and degassed for 10 minutes more. $Pd(PPh_3)_2Cl_2$ (18 mg, 0.03 mmol) and CuI (10 mg, 0.06 mmol) are added to the reaction mixture while bubbling. Then, PPH_3 (7 mg, 0.03 mmol) is introduced. DIPA is added and mixture is degassed for additional 5 minutes. Finally, TMS (**11**) (100 µL, 0.75 mmol) is introduced and argon is removed. The reaction is proceed for overnight at 62°C. Reaction is cooled down and solvent is evaporated under vacuum. Crude is extracted with CH_2Cl_2 and water. Organic layer is gathered and dried over Na_2SO_4. Solvent is evaporated and purified over silica gel column DCM: Hexane (2: 3) as the eluent. Product is dark orange solid (190 mg, 79.8%).

^{1}H-NMR (400 MHz, $CDCl_3$) δ_H: 7.63 (2H, d, *J* = 8.00 Hz, ArH), 7.20 (2H, d, *J* = 8.36 Hz, ArH), 2.55 (6H, s, CH_3), 2.33 (4H, m, CH_2), 1.32 (6H, s, CH_3), 0.99 (6H, t, *J* = 15.13 Hz, CH_3), 0.31 (s, TMS)

^{13}C NMR (100 MHz, CDCl3) δ_c: 154.02, 139.21, 138.21, 133.06, 132.15, 131.94, 130.50, 128.56, 123.67, 104.36, 95.61, 29.69, 17.06, 14.58, 12.51, 11.88, 1.01.

MS (TOF- ESI): m/z: Calcd: 476.2631 $[M]^-$, Found: 419.3585 $[M]^-$. Δ=16.7 ppm

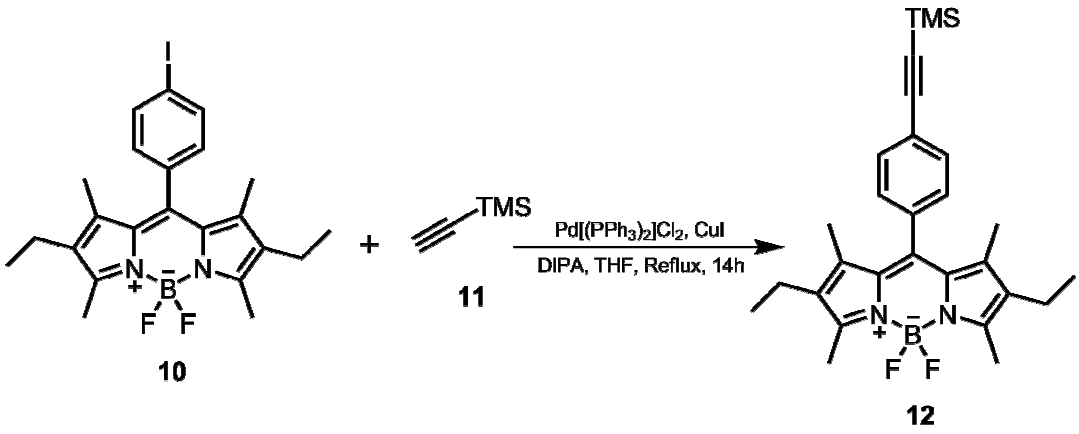

Figure 28. Synthesis of Compound **12**

2.2.8. Synthesis of Compound 13

Compound **12** (150 mg, 0.31 mmol) is dissolved in MeOH: THF (3:8) mixture and stirred for a while. 7 equivalent KF (207 mg, 2.20 mmol) is added and reaction is kept stirring for 5 hours at RT. TLC control is applied during stirring. For work-up, mixture is dissolved in $CHCl_3$ and extracted with brine. Organic layer is gathered and dried over Na_2SO_4. Solvent is evaporated under vacuum. Orange solid (97 mg, %77.8).

^{1}H-NMR (400 MHz, $CDCl_3$) δ_H: 7.63 (2H, d, *J* = 8.20 Hz, ArH), 7.28 (2H, d, *J* = 8.20 Hz, ArH), 3.20 (1H, s, Alkin), 2.55 (6H, s, CH_3), 2.31 (4H, m, CH_2), 1.32 (6H, s, CH_3), 1.00 (6H, t, *J* = 15.10 Hz, CH_3)

^{13}C NMR (100 MHz, $CDCl_3$) δ_C: 154.10, 139.02, 138.17, 136.16, 132.95, 128.30, 122.71, 83.02, 78.39, 17.06, 14.57, 12.51, 11.85.

MS (TOF- ESI): m/z: Calcd: 403.2235 $[M]^-$, Found: 403.3506 $[M]^-$. Δ=31.5 ppm

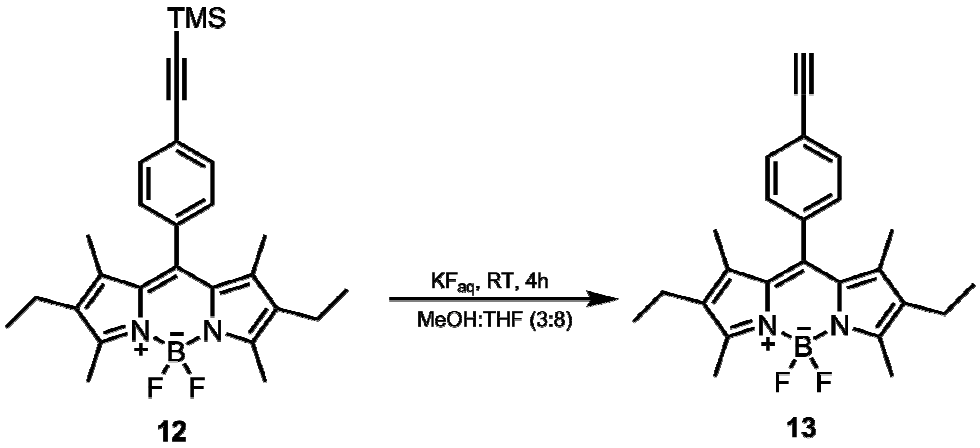

Figure 29. Synthesis of Compound **13**

2.2.9. Synthesis of Compound 14

THF is distilled in the set-up for about 4 hours. Then it is degassed for 15 minutes. Compound **7** (100 mg, 0.11 mmol) is dissolved in freshly distilled THF and degassed for 10 minutes more. $Pd(PPh_3)_2Cl_2$ (5.12 mg, 6% equivalent) and CuI (2.57 mg, 12% equivalent) are added to the reaction mixture while bubbling. Then, PPH_3 (1.78 mg, 6% equivalent) is introduced. DIPA is added and mixture is degassed for additional 5 minutes. Finally, 2.2 equivalent of compound **13** (101 mg, 0.25 mmol) is introduced and argon is removed. Flask is secured with septum and filled with argon by syringe. Reaction mixture is proceed for 72 hours at 62°C. Reaction is cooled down and solvent is evaporated under vacuum. Crude is extracted with CH_2Cl_2 and water. Organic layer is gathered and dried over Na_2SO_4. Solvent is evaporated and purified over silica gel column DCM: Hexane (1: 1) as the eluent. Product is bright pink solid (27 mg, 7.55%).

^{1}H NMR (400 MHz, $CDCl_3$) δ_H: 7.52 (d, J = 7.9 Hz, 4H), 7.21 (d, J = 5.9 Hz, 4H), 6.54 (s, 1H), 6.39 (s, 2H), 2.70 (s, 6H), 2.47 (s, 12H), 2.24 (q, J = 7.5 Hz, 6H), 1.70 (s, 6H), 1.48 (s, 8H), 1.27 (s, 18H), 1.25 – 1.12 (m, 42H), 0.92 (t, J = 7.5 Hz, 12H).

^{13}C NMR (100 MHz, $CDCl_3$) δ_C: 161.4, 156.2, 155.9, 149.3, 149.1, 141.0, 137.7, 136.9, 132.1, 132.0, 131.9, 131.6, 131.1, 128,6, 128.4, 127.2, 124.2, 123.9, 121.4, 118.6, 106.2, 96.4, 83.0, 68.5, 31.9, 29.6, 29.4, 29.3, 29.2, 26.0, 22.7, 14.1. 13.9.

MS (TOF- ESI): m/z: Calcd: 1440.8795 $[M]^-$, Found: 1440.1946 $[M]^-$. Δ=47.5 ppm

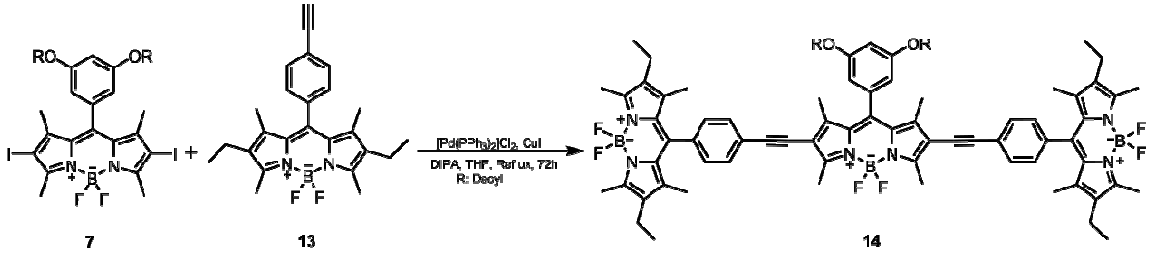

Figure 30. Synthesis of Compound **14**

2.2.10. Synthesis of Compound 16

Compound **7** (100 mg, 0.11 mmol) is dissolved in 20 mL benzene in a two-necked round bottomed flask. 2.4 equivalent of compound **15** (33 µL, 0.27 mmol) is added to the flask. 0.4 mL piperidine and 0.4 mL glacial AcOH is added and mixture is refluxed for about 2 hours at 104 ^{0}C by using Dean-Stark apparatus. Reaction is monitored with TLC control. When all the starting material is consumed, reaction is cooled down and extracted with CH_2Cl_2 and water. Organic layer is gathered and dried over Na_2SO_4. Solvent is evaporated and purified over silica gel column DCM: Hexane (1: 1) as the eluent. Product is green solid (120 mg, 94.8%).

^{1}H NMR (400 MHz, $CDCl_3$) δ_H: 8.07 (d, *J* = 16.3 Hz, 2H), 7.58 – 7.41 (m, *J* = 11.9 Hz, 6H), 6.89 (d, *J* = 8.7 Hz, 4H), 6.51 (s, 1H), 6.34 (s, 2H), 3.80 (s, 6H), 1.57 (s, 6H), 1.47 (s, 12H), 1.30 – 1.06 (m, 30H).

^{13}C NMR (101 MHz, $CDCl_3$) δ_C: 160.42 (d, *J* = 17.4 Hz), 159.87, 149.63, 144.87, 138.20, 137.53, 135.81, 131.69, 128.77, 128.50, 128.24, 115.93, 113.45, 105.78, 101.77, 81.72, 67.63, 54.54, 31.04, 30.57, 29.34, 29.28 – 28.10, 25.11, 21.82, 16.52, 13.26, 0.15.

MS (TOF- ESI): m/z: Calcd: 1124.7621 $[M]^-$, Found: 1124.5532 $[M]^-$. Δ=18.5 ppm

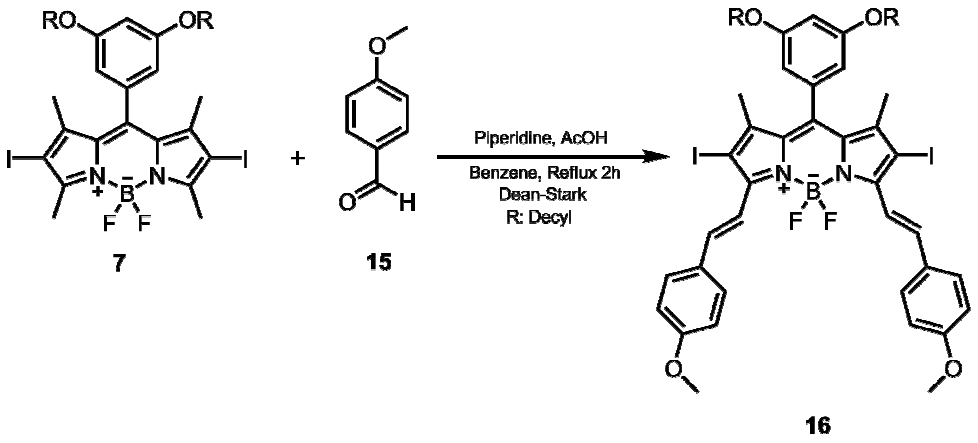

Figure 31. Synthesis of Compound **16**

2.2.11. Synthesis of Compound 17

THF is distilled in the set-up for about 4 hours. Then it is degassed for 15 minutes. Compound **16** (120 mg, 0.10 mmol) is dissolved in freshly distilled THF and degassed for 10 minutes more. $Pd(PPh_3)_2Cl_2$ (5.2 mg, 6% equivalent) and CuI (2.7 mg, 12% equivalent) are added to the reaction mixture while bubbling. Then, PPH_3 (1.9 mg, 6% equivalent) is introduced. DIPA is added and mixture is degassed for additional 5 minutes. Finally, 2.2 equivalent of compound **13** (100 mg, 0.24 mmol) is introduced and argon is removed. Flask is secured with septum and filled with argon by syringe. Reaction mixture is proceed for 72 hours at 62°C. Reaction is cooled down and solvent is evaporated under vacuum. Crude is extracted with CH_2Cl_2 and water. Organic layer is gathered and dried over Na_2SO_4. Solvent is evaporated and purified over silica gel column DCM: Hexane (2: 1) as the eluent. Product is dark green solid (48 mg, 32.2%).

^{1}H NMR (400 MHz, $CDCl_3$) δ_H: 8.37 (d, *J* = 16.7 Hz, 2H), 7.69 (d, *J* = 16.3 Hz, 2H), 7.62 – 7.43 (m, 8H), 7.23 (d, 4H), 6.89 (d, *J* = 18.6, 7.2 Hz, 4H), 6.54 (s, 1H), 6.43 (s, 2H), 3.90 (t, *J* = 6.5 Hz, 4H), 3.81 (s, 6H), 2.47 (s, 12H), 2.24 (q, *J* = 7.3 Hz, 8H), 1.74 (s, 6H), 1.27 (s, 12H), 1.27 – 1.03 (m, 42H), 0.92 (t, *J* = 7.5 Hz, 12H), 0.80 (t, *J* = 8.1, 5.2 Hz, 6H).

^{13}C NMR (101 MHz, $CDCl_3$) δ_C: 161.34, 160.91, 154.09, 152.70, 145.09, 139.37 – 138.88, 138.20, 136.23, 135.82, 132.98, 132.54, 131.51, 130.58, 129.75, 129.30, 128.77, 128.05, 124.14, 116.79, 114.46, 113.23, 106.68, 102.64, 97.53, 85.46, 77.33, 77.02, 76.70, 68.54, 55.43, 31.89, 30.07 – 29.08, 26.00, 22.67, 17.09, 14.60, 14.11, 13.25, 12.54, 11.95, 1.38, 1.02, 0.65.

MS (TOF- ESI): m/z: Calcd: 1677.1989 $[M]^-$, Found: 1677.9671 $[M]^-$. Δ=45.8 ppm

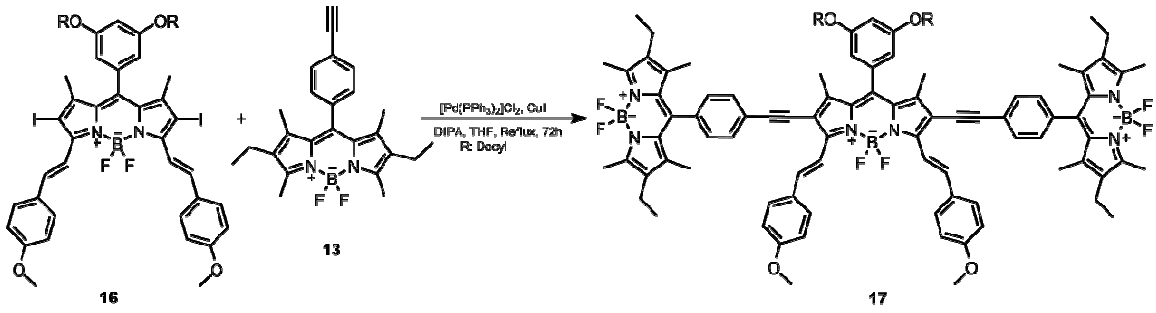

Figure 32. Synthesis of Compound **17**

2.2.12. Synthesis of Compound 18

Compound **6** (100 mg, 0.16 mmol) is dissolved in 40 mL of DCM: DMF (1:1) mixture in a 100 mL round-bottomed flask. 2.3 equivalent NBS (63.9 mg, 0.36 mmol) is dissolved in 15 mL DCM and added to the mixture dropwise. This step is very critical and addition is done by dropping funnel and TLC control is applied. After the formation of desired compound, mixture is extracted with CH_2Cl_2 and water and organic layer is dried with Na_2SO_4. Solvent is evaporated and product is purified with silica gel column using DCM: hexane (3:2) as eluent. Product is pink solid (120 mg, 96.1%).

^{1}H NMR (400 MHz, $CDCl_3$) δ_H: 6.47 (s, 1H), 6.31 (s, 2H), 3.83 (t, 4H), 2.51 (s, 6H), 1.68 (q, 4H), 1.45 (s, 6H), 1.29 – 1.08 (m, 42H), 0.79 (t, J = 6.8 Hz, 6H).

^{13}C NMR (101 MHz, $CDCl_3$) δ_C: 161.45, 153.85 , 142.09 , 140.68 , 135.72 , 130.11 , 111.65 , 106.07 , 105.77 , 102.61 , 68.48 , 31.88 , 30.09 – 28.92, 25.94 , 22.67 , 14.04, 13.61 , 1.38 , 1.01 , 0.64 .

MS (TOF- ESI): m/z: Calcd: 793.4979 $[M]^-$, Found: 793.4611 $[M]^-$. Δ=4.6 ppm

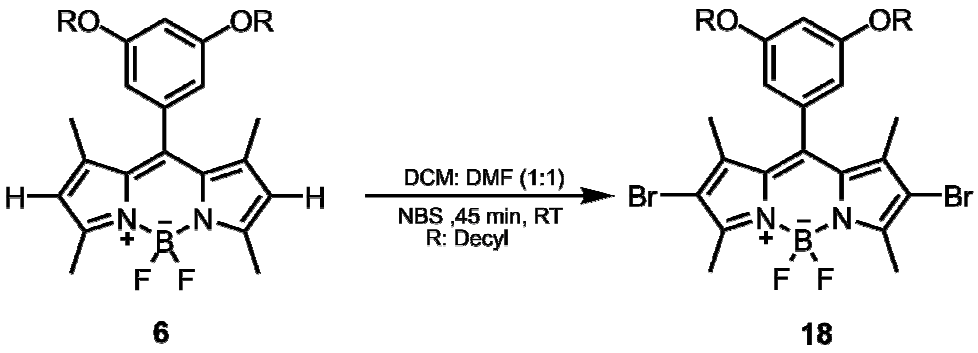

Figure 33. Synthesis of Compound **18**

2.2.13. Synthesis of Compound 19

Compound 1**7** (450 mg, 0.58 mmol) is dissolved in 15 mL benzene in a two-necked round bottomed flask. 10 equivalent of compound **15** (600 µL, 5.77 mmol) is added to the flask. 0.8 mL piperidine and 0.8 mL glacial AcOH is added and mixture is refluxed for about 5 hours at 104 ^{0}C by using Dean-Stark apparatus. Benzene is added when evaporated. Reaction is monitored with TLC control. When all the starting material is consumed, reaction is cooled down and extracted with CH_2Cl_2 and water. Organic layer is gathered and dried over Na_2SO_4. Solvent is evaporated and purified over silica gel column DCM: Hexane (3: 1) as the eluent. Product is dark green solid (145 mg, 20%).

^{1}H NMR (400 MHz, $CDCl_3$) δ_H: 8.18 (d, *J* = 16.5, 5.9 Hz, 2H), 7.66 (d, 8H), 7.07 (d, *J* = 16.5 Hz, 4H), 7.02 (d, 4H), 6.99 (d, *J* = 8.9, 1.8 Hz, 4H), 6.79 (d, *J* = 8.8 Hz, 4H), 6.52 (s, 2H), 5.88 (d, *J* = 16.5, 5.7 Hz, 2H), 3.89 (s, 16H), 3.84 (s, 6H), 3.71 (t, *J* = 6.6 Hz, 4H), 1.38 – 1.17 (m, 42H), 0.92 (t, *J* = 6.9 Hz, 6H).

^{13}C NMR (101 MHz, $CDCl_3$) δ_C: 160.40 , 159.77 , 158.75 , 148.37 , 139.81 – 139.41, 138.68 , 136.94 , 134.93 , 134.25 , 133.72 , 131.36 , 129.44, 128.91 , 128.54, 126.99 , 117.29 , 116.28 , 115.11 , 113.31 , 112.68, 107.13 , 104.83 , 102.00 , 67.48 , 54.30 , 30.89 , 28.49, 28.22, 24.87 , 21.68 , 13.11 .

MS (TOF- ESI): m/z: Calcd: 1266.4502 $[M]^+$, Found: 1266.4476 $[M]^+$. Δ=2.05 ppm

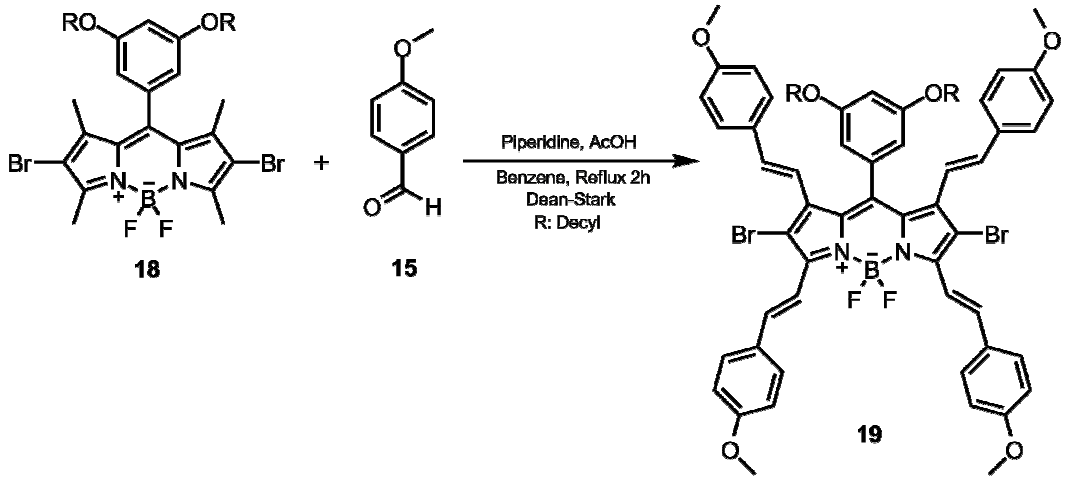

Figure 34. Synthesis of Compound **19**

2.2.14. Synthesis of Compound 20

THF is distilled in the set-up for about 4 hours. Then it is degassed for 15 minutes. Compound **19** (95 mg, 0.076 mmol) is dissolved in freshly distilled THF and degassed for 10 minutes more. $Pd(PPh_3)_2Cl_2$ (4.4 mg, 6% equivalent) and CuI (3.2 mg, 12% equivalent) are added to the reaction mixture while bubbling. Then, PPH_3 (1.5 mg, 6% equivalent) is introduced. DIPA is added and mixture is degassed for additional 5 minutes. Finally, 2.4 equivalent of compound **13** (75 mg, 0.19 mmol) is introduced and argon is removed. Flask is secured with septum and filled with argon by syringe. Reaction mixture is proceed for 96 hours at 62°C. Reaction is cooled down and solvent is evaporated under vacuum. Crude is extracted with CH_2Cl_2 and water. Organic layer is gathered and dried over Na_2SO_4. Solvent is evaporated and purified over silica gel column DCM: Hexane (2: 1) as the eluent. Product is dark green solid (48 mg, 32.2%).

^{1}H NMR (400 MHz, $CDCl_3$) δ_H: 7.66 (d, *J* = 8.7 Hz, 4H), 7.58 (d, *J* = 7.0 Hz, 2H), 7.51 (d, *J* = 5.1 Hz, 2H), 7.03 (d, 4H), 7.00 (d, *J* = 5.9, 2.5 Hz, 4H), 6.98 (d, 4H), 6.81 (d, 2H), 6.79 (d, 2H), 6.59 (s, 2H), 6.51 (s, 1H), 5.87 (d, *J* = 16.4, 8.8 Hz, 2H), 3.91 (s, 6H), 3.84 (s, 6H), 3.82 (s, 6H), 2.52 (s, 12H), 2.41 (q, 8H), 2.18 (s, 6H), 1.39 – 1.16 (m, 42H), 1.09 (t, 12H), 0.92 – 0.90 (m, *J* = 5.5, 2.8 Hz, 6H).

^{13}C NMR (101 MHz, $CDCl_3$) δ_C: 161.32 , 160.48 , 159.75 , 137.69 , 136.63 , 134.07 , 132.11, 130.12 , 129.81 , 129.78 – 128.95, 128.58 , 128.49 – 127.42, 118.56 , 115.12 – 114.55, 114.55 – 113.39, 108.35 , 103.04 , 68.58 , 55.34, 37.10 , 32.76 , 31.90 , 31.73 – 30.65, 30.65 – 30.26, 29.76, 30.65 – 28.26, 27.09 , 25.90 , 22.69 , 19.73 , 17.19, 14.89 , 14.57 , 14.36 , 14.11 , 12.53 , 9.37 , 1.38 , 1.16 , 0.83.

MS (TOF- ESI): m/z: Calcd: 1904.0504 $[M]^+$, Found: 1904.0847 $[M]^+$. Δ=1.8 ppm

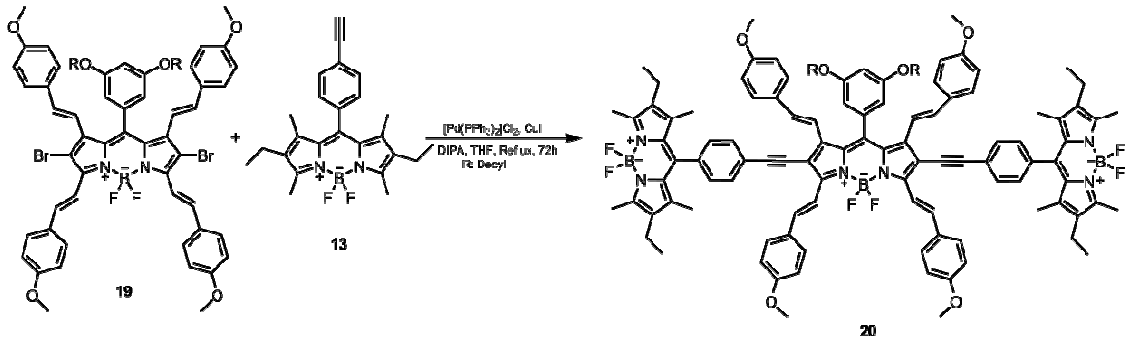

Figure 35. Synthesis of Compound **20**

CHAPTER 3

RESULTS and DISCUSSION

3.1. General Perspective

In this study, we have synthesized three different target molecules, having different acceptor cores and donor parts. These molecules have different physical and spectroscopic properties due to their acceptor parts. Having methoxy groups attached to the BODIPY core makes these dyes shift to red region of the spectrum. Acceptor and donor parts of the target molecules are connected to each other by acetylene groups. Sonogashira coupling reaction procedures are applied to put these parts together. 8th position of the BODIPY dyes, also named as *meso* position, can be functionalized by choosing the appropriate aldehyde. In this case, we choose an aldehyde with decyl groups at the 3rd and 5th position, in order not to interfere in to the conjugation. In addition these decyl groups provide mobility to the naked BODIPY. The possible positions of BODIPY dyes which can be modified are illustrated below:

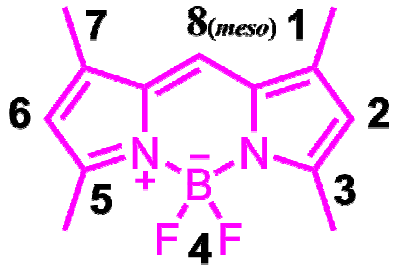

Figure 36. Possible modification positions of BODIPY core

8th (*meso*) position of these dyes are functionalized in the basic synthesis procedure, aldehyde is modified and proceed in to reaction with Pyrrole. 1st, 3rd, 5th, and 7th position can be functionalized by again using aldehyde in Knovenagel Condensation reactions. Coupling reactions like Suzuki coupling or Sonogashira coupling are used to modify 2nd and 6th position. For Sonogashira coupling at these sites, Bromination or iodination reactions are applied to make these positions electrophilic centers, which makes them available for this coupling reaction. Acetylene groups are nucleophilic centers, which are used for coupling reactions to form carbon-carbon bonds. A BODIPY dye with modified sites with different functional groups can show different physical and spectroscopic properties. Fluorescence and absorption spectrum of these dyes can be changed by addition of electron-withdrawing and electron-donating groups to the conjugation. Functionalized target compounds for the formation of energy transfer cassettes are pictured in Figure 37:

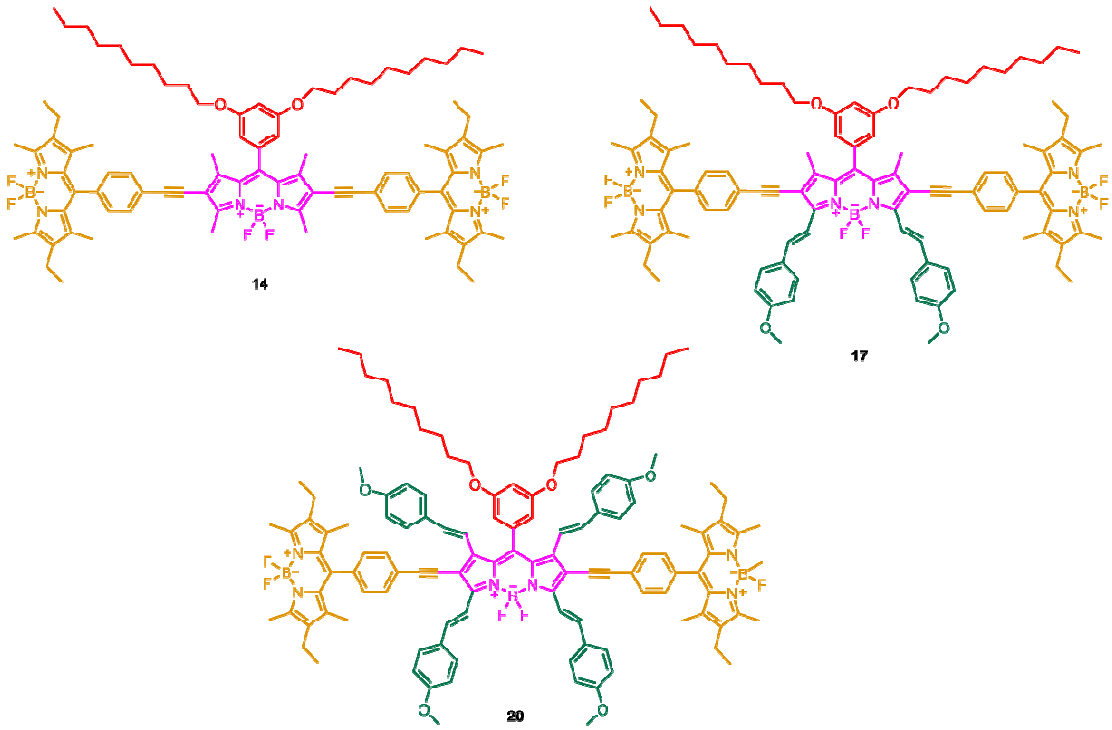

Figure 37. Possible modification positions of BODIPY core

3.2. Design and Working Principle of Target Compounds

Herein, differently functionalized two BODIPY cores are used and electronically connected to each other with acetylene groups. BODIPY dyes are preferred for the synthesis, due to easily functionalized sites and easy synthesis steps with high yield. In addition, these dyes have relatively high quantum yields, they are photostable and their spectroscopic properties in the UV-Vis region of the spectrum can be tuned easily with functional groups. Acetylene groups connect two different BODIPY cores to each other and they contribute to the conjugation of the system.

Energy transfer in conjugated systems occur in two different phenomena: Dexter type energy transfer and Förster type energy transfer. As mentioned before, dexter type electron transfer occurs between donor and acceptor chromophores. It requires short distances and spectral overlap between donor and acceptor molecule. This type of electron transfer is sometimes called as through-bond energy transfer, since it occurs in short distances. Wavefunction overlap provides electron exchange between two chromophores. Herein, we designed compound 14 with two chromophores having nearest spectral properties and therefore overlap. We expect a better through-bond energy transfer in this compound than other target molecules.

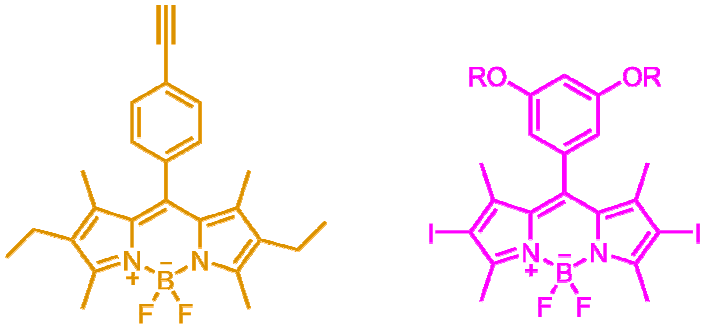

13 λ_{max}=528 **7** λ_{max}=535

Figure 38. Donor (**13**) and Acceptor (**7**) components of Compound **14**

Förster resonance energy transfer on the other hand, donor chromophore transfers its energy to acceptor molecule by the assistant of dipole-dipole coupling. In this process, again distance is an crucial measurement. Compound **17** and Compound **20** are designed with the same donor BODIPY molecules, however; different acceptor parts used for comparison of energy transfer efficiency. Compound **17** consists of distyryl BODIPY with electron donating methoxy groups, making the target compound less acidic. These groups also cause a red shift in the spectrum. Compound **20** has the same design, with a tetrastyryl BODIPY as the acceptor core; therefore, this compound has more electron-donating groups. However, the distance between the acceptor and donor part of the molecule is the longest among target compounds.

3.3. Spectroscopic Properties

After the synthesis of target compounds and characterization, photophysical properties are analyzed. The results indicate that increase in the electron-donating groups and π conjugation shifts the spectrum to longer wavelength. Absorption and emission maxima of the target compounds undergo red shift and therefore, spectral overlap between the donor and acceptor molecule decreases. According to this overlap, through-bond energy transfer (Dexter type) or Förster type energy transfer occurs between the donor groups and acceptor groups. The efficiency of the energy transfer shows the success of spectral overlap and conjugation. Efficiency of energy transfer is also calculated by using the excitation and emission data of the target compounds. Normalized absorption and emission graphics of target compounds with donor and acceptor molecules are shown below:

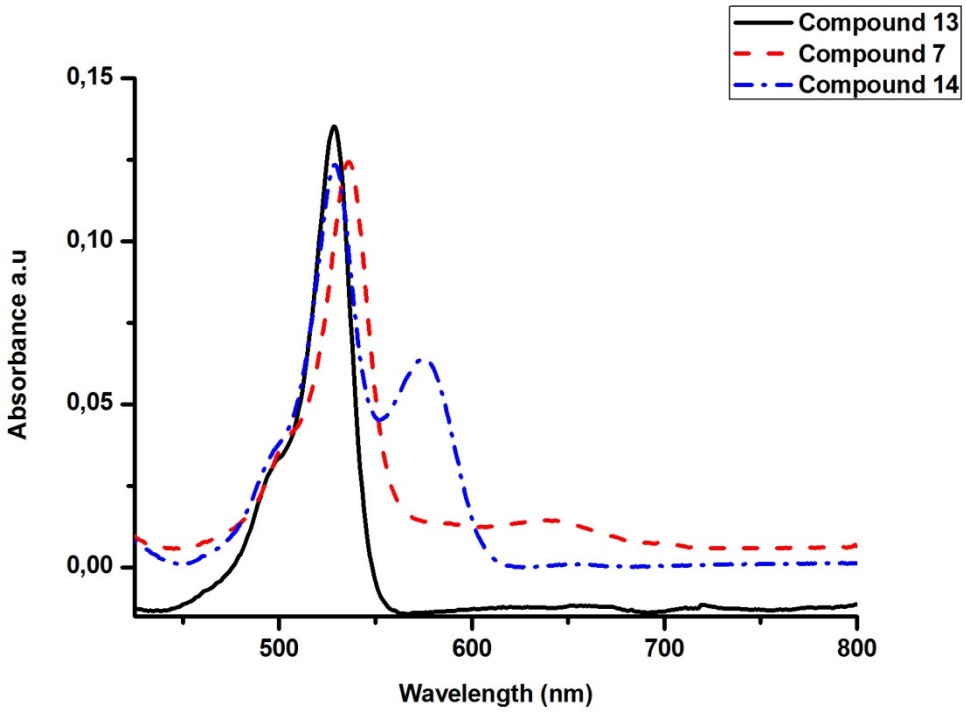

Figure 39. Normalized Absorbance Spectra of Donor (**13**), Acceptor (**7**) and Target (**14**)

As concluded from the absorption spectrum, the absorption maximum of acceptor compound undergoes red shift due to energy loss during electron transfer. This shift is more distinct at the target compound. In addition, target compound absorbs more intense from donor wavelength of absorbance than acceptor wavelength. Normalized emission spectrum has also the same trend. When excited from 525 nm, which correspond to the λ_{abs} maximum of the donor, target compound shows dramatic decrease in intensity at the donor wavelength maximum. The decrease is shown in the emission spectrum with arrows. Expectedly, there is an increase of intensity in the λ_{abs} range of acceptor. This increase is also shown with arrows. Decrease in the intensity of donor and dramatic increase in the intensity of acceptor molecule shows a distinct energy transfer between the donor and acceptor molecule.

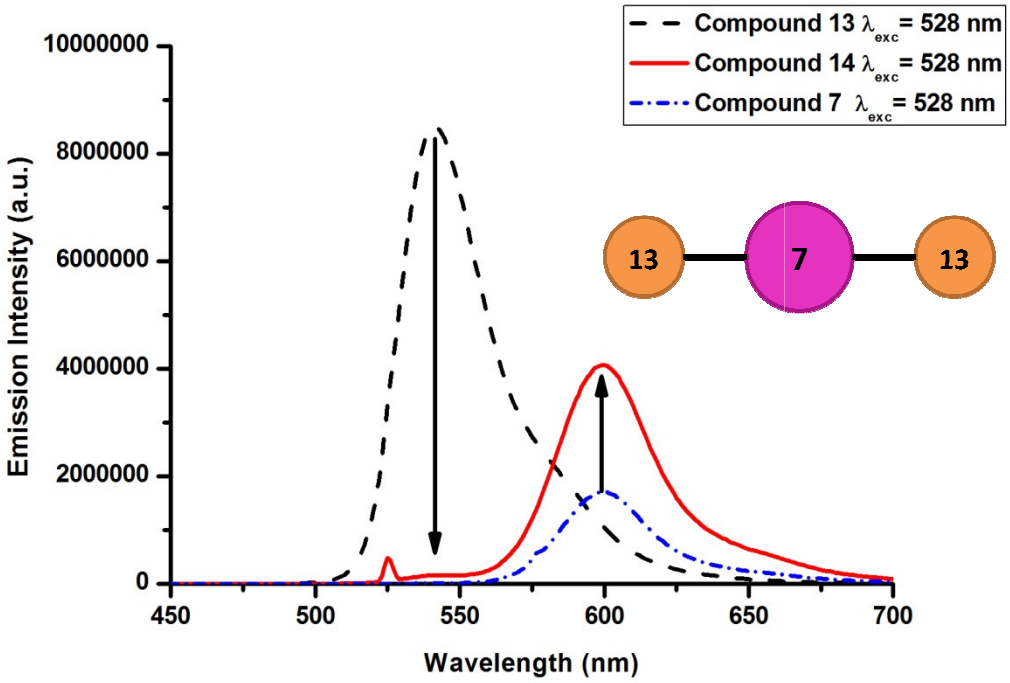

Figure 40. Normalized Emission Spectra of Donor (**13**), Acceptor (**7**) and Target (**14**)

The energy transfer between these molecules is expectedly Dexter electron transfer, since the distance between the donor and acceptor molecule is very short. FRET is also possible, but since the efficiency of energy transfer is very high, it can be concluded that through-bond energy transfer is dominant in this case. The energy transfer efficiency is calculated by normalization of donor absorbance wavelength and by proportion of excitation and emission spectrum of **14**. Generally, the energy transfer efficiency between the donor and acceptor molecule in FRET case cannot be more than 50%, due to energy loss during the energy transfer. Not all the energy is transferred through conjugation. Remarkable amount of energy is lost during vibration, internal conversion and between the energy levels.

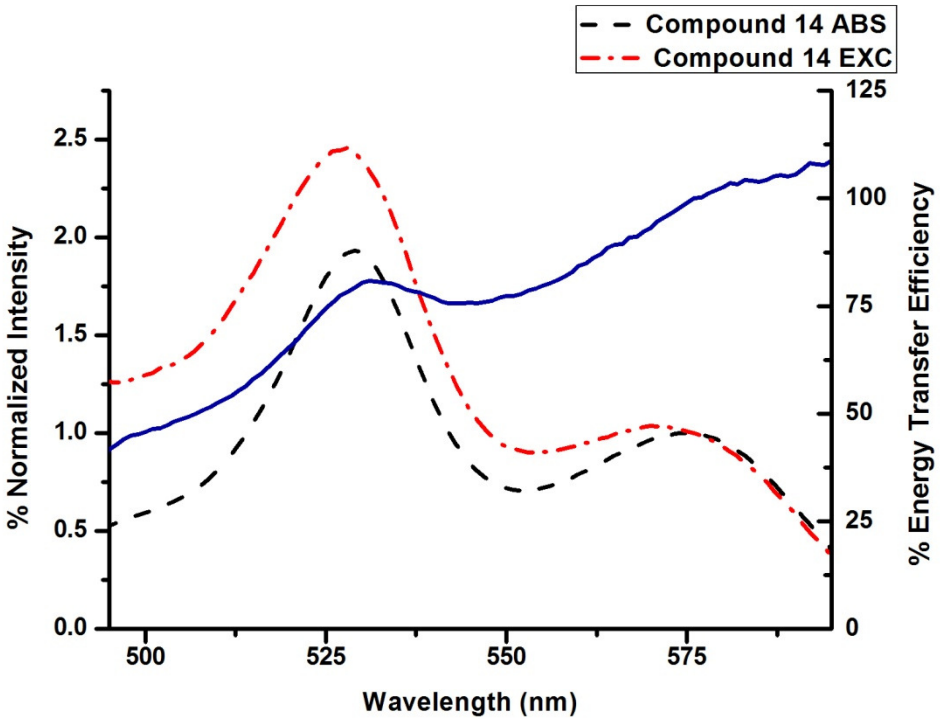

Figure 41. Percent Energy Transfer Efficiency of Compound **14**

At the point of λ_{ems}= 528 nm, which corresponds to the emission wavelength of donor molecule; energy transfer efficiency is more than 75%. When the λ_{ems} maximum of acceptor molecule is normalized, excitation and absorbance ratio shows the difference of the intensity between the excitation and absorbance spectrum. In the case of Compound **14**, about 80% of photons which are absorbed by the donor molecule are transferred to acceptor molecule. The calculation can also be implemented by normalization of emission wavelength of the target compound at the donor wavelength. In this case, we again expect to observe around 80% efficiency of energy transfer between the donor and acceptor molecules.

Compound **17** also has the same trend with **14**, however; the performance of the transfer is less. This result indicates that the spectral overlap in **17** is poorer than that of **14**. Due to styryl structure of the acceptor molecule in target **17**, the acceptor core and donor parts are far from each other

and therefore the efficiency decreases. Figure 42 shows the absorbance spectrum of donor and acceptor part of compound **17**:

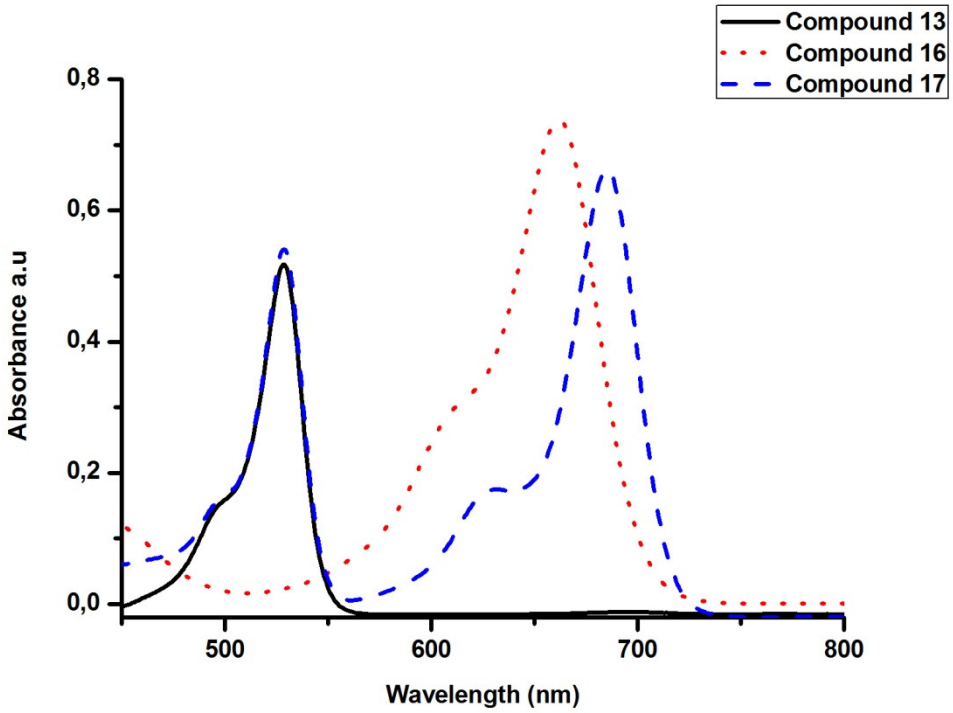

Figure 42. Normalized Absorbance Spectra of Donor (**13**), Acceptor (**16**) and Target (**17**)

In the emission spectrum of **17**, we observe dramatic decrease in the wavelength spectrum of the donor molecule, whereas acceptor intensity increases slightly. This result again proves that there is an energy transfer among the donor molecules and the acceptor, since emission intensity of the donor molecule decreases and nearly approaches to 0. Intensity of the target molecule at the acceptor emission wavelength increases approximately 2.5 times. In addition, there becomes a red shift in the spectrum of the target **17**, due to energy loss during transfer. This energy loss is caused by the energy levels in the excitation spectrum and vibrational-rotational movements of the molecule.

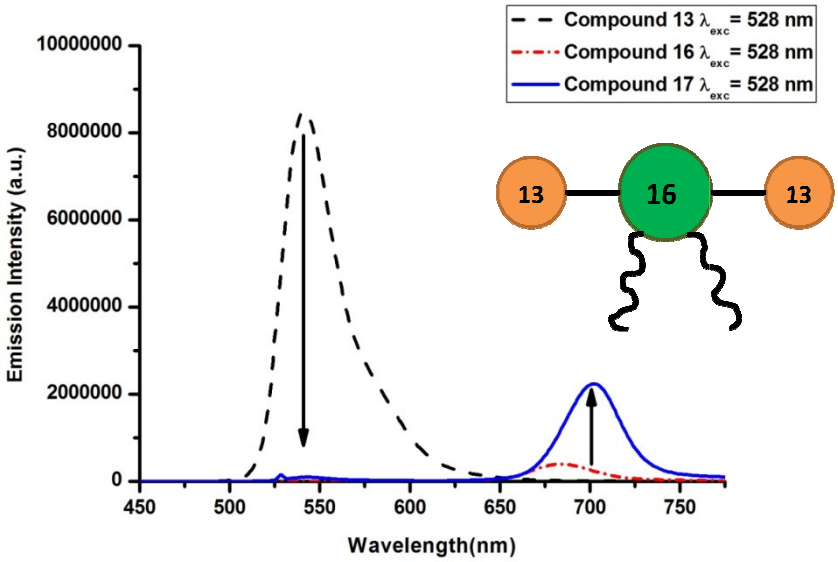

Figure 43. Normalized Emission Spectra of Donor (**13**), Acceptor (**16**) and Target (**17**)

The efficiency of the energy transfer is calculated and graph is designed. The graph shows that energy transfer efficiency is less than that of target **14**, indicating that the spectral overlap is poorer. In addition, acceptor sites of Compound **17** are far from donor molecule, than that of target **14**.

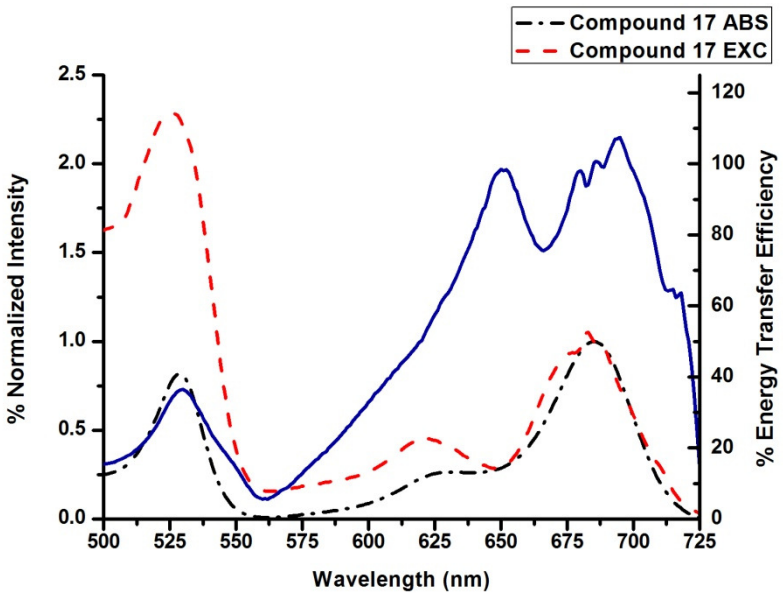

Figure 44. Percent Energy Transfer Efficiency of Compound **17**

Target **20** has the largest acceptor of all. Acceptor core has the longest wavelength absorption and emission values compared to **14** and **17**. Therefore, we expect weaker energy transfer in this compound, due to poorer spectral overlap. The larger the difference between absorption and emission wavelength of donor and acceptor molecule, the weaker the spectral overlap. Besides, the distance between the acceptor and donor sites of the target **20** are the most distant of all.

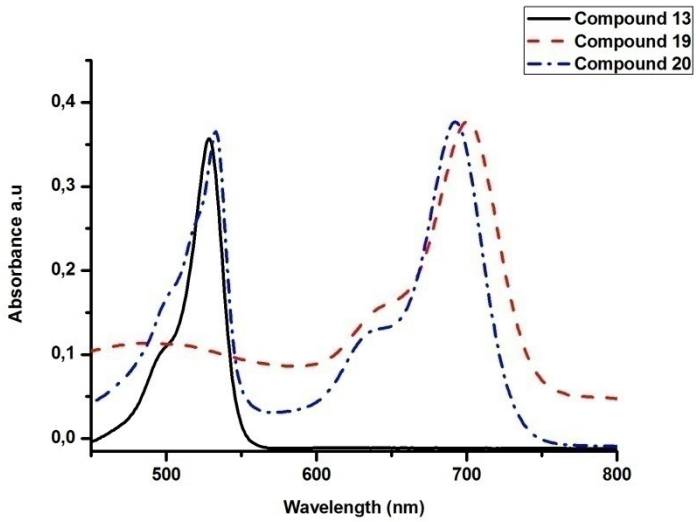

Figure 45. Normalized Absorbance Spectra of Donor (**13**), Acceptor (**19**) and Target (**20)**

Although absorption spectrum gives predictable spectrum, compound **20** does not show significant energy transfer in the emission spectrum. The reason is as explained above, mismatch in the spectral overlap and distance. The distance is so large that, the energy may be lost while transferring, or the transferred energy cannot meet the energy for the acceptor. Energy transfer failure in this target compound is also seen in the time-resolved fluorescence spectrum.

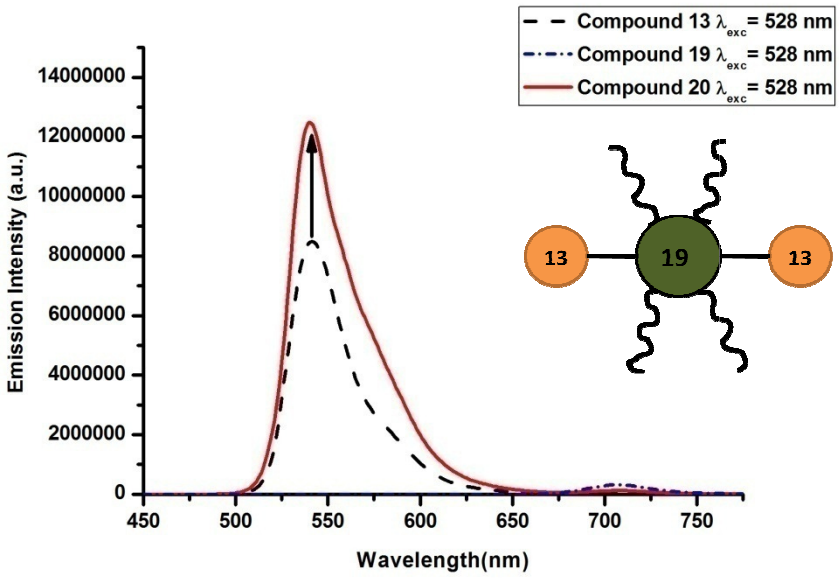

Figure 46. Normalized Emission Spectra of Donor (**13**), Acceptor (**19**) and Target (**20**)

When the solutions having the same molarities is prepared of the target **14, 17** and **20**, we observe that the emission and excitation intensity of the compounds lower respectively.

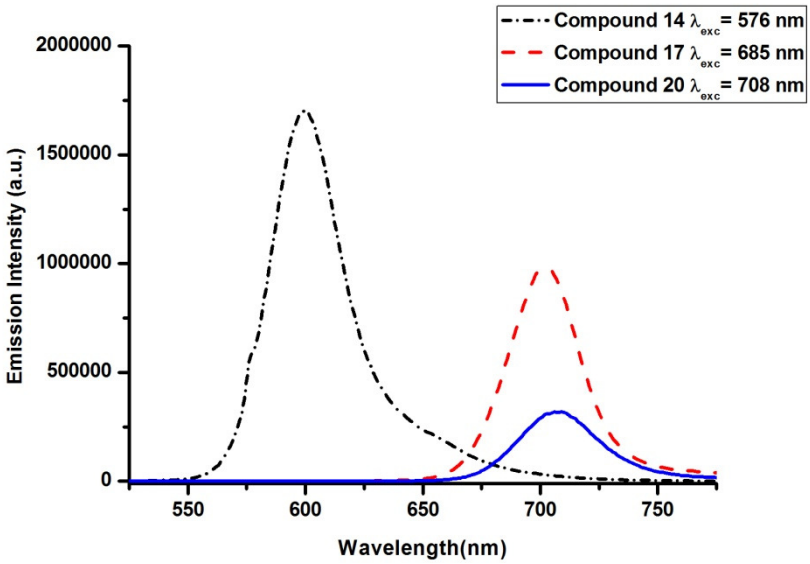

Figure 47. Normalized Emission Spectra of Target **14**, **17** and **20**

In this study, all target compounds have the same number of donor molecules, however; acceptor molecule's structure and photophysical properties alter. In the Figure 48, emission spectrum is normalized at the equal absorbance at donor wavelength to observe trends in the emission intensity. As the acceptor sites in the core increases, spectrum of the target undergoes a red shift. Distance of energy donor BODIPY increases and intensity of both emission and excitation spectrum decreases.

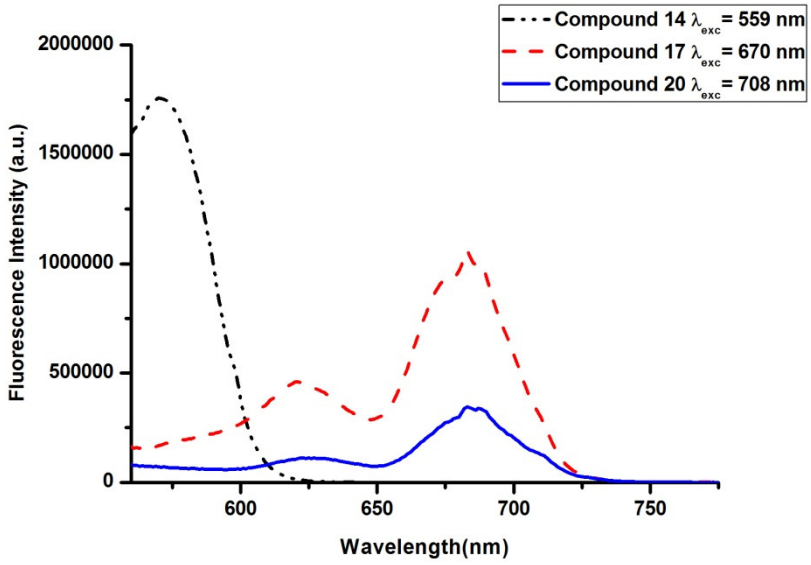

Figure 48. Normalized Excitation Spectra of Target **14**, **17** and **20**

3.4. Photophysical Data

All absorption, emission, excitation and time-resolved fluorescence are acquired in $CHCl_3$, taken from dilute stock solutions. Quantum yield and extinction coefficient calculations are performed using Rhodamine 6G in water and Cresyl Violet in methanol as reference. Absorbance of the donor, acceptor and target BODIPY dyes, and references are kept below 0.1, in order to prevent self-quenching error. The table below shows the data obtained and calculated from the references and BODIPY molecules:

Compound	λ_{abs} (nm)	ε (λ_{max}) ($M^{-1}cm^{-1}$) (nm)	λ_{ems} (nm)	Φ_F λ_{exc}(488nm)	Φ_F λ_{exc}(610nm)	τ (ns)
13	525	174.780	542	0.525	-	4.38
7	535	30.100	550	0.0358	-	-
16	661	147.460	684	-	0.131	-
19	701	226.960	725	-	0.011	-
14	528 576	24.720 12.796	599 601	0.343 0.432	-	0.33 3.64
17	528 685	133.820 164.720	702 702	0.175 0.296	-	0.09 4.14
20	529 706	73.040 75.080	706 541	0.072 0.064	-	5.81 3.73

Table 1: Photophysical Properties and Lifetimes

Extinction coefficients are calculated by using Beer-Lambert law for known concentration and pathlength;

$$A=\varepsilon*c*l \quad (2)$$

Where **A** is the absorbance, **ε** is extinction coefficient, **c** symbolizes concentration and **l** is pathlength. Pathlength is taken as 1 cm, which is the length of UV cuvette. According to results, donor and acceptor BODIPY molecules have more ability to absorb light than that of combined molecule: the target molecules. In addition, by looking the results of acceptor BODIPY dyes, we can conclude that increasing conjugation increases the extinction coefficient and shifts the spectrum to red region.

Life-time fluorescence results also indicate that there becomes an energy transfer between the target **14** and **17**. At the donor wavelength, we observe 0.33 ns and 0.09 ns for **14** and **17**, respectively. However, at the acceptor molecule wavelength, target molecules show nearly classic BODIPY life-time values. In compound **20**, the data shows that target molecule has higher life-time fluorescence in donor emission wavelength than acceptor emission wavelength, indicating poor energy transfer.

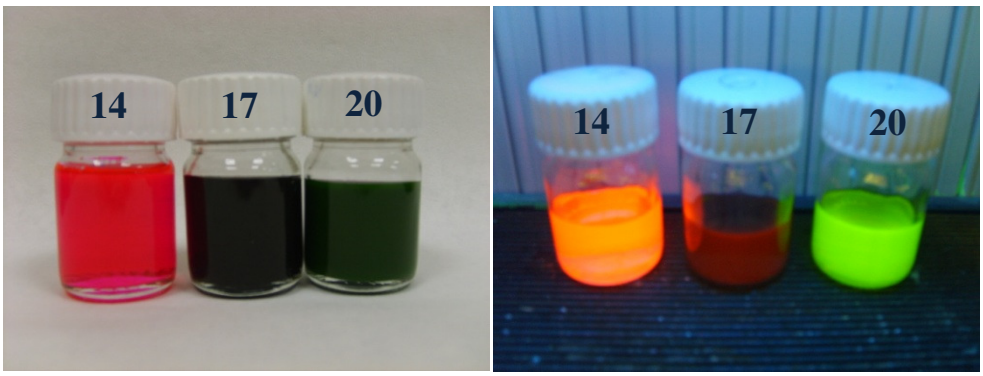

Figure 49: Solutions of target molecules under ambient (left) and under UV light (right).

CHAPTER 4

CONCLUSION

In this study, we have designed three novel BODIPY dyes and analyzed their spectroscopic properties. These molecules contain three BODIPY molecules, each having two same donor part and one acceptor core. Donor and acceptor BODIPY dyes are connected to each other by coupling reactions. Ethynyl groups attach donor and acceptor part together and maintain the conjugation. Energy transfer efficiencies of three target compounds and photophysical properties are examined.

Compound **14, 17** and **20** are designed be the target products having same donor BODIPY sides. Their acceptor core changes in the conjugation and energy transfer efficiency for each target is examined. Compound **14**, having the less conjugated structure, shows more than 80% energy transfer efficiency. **17**, on the other hand, has about 40% efficiency, since it has more conjugation. Compound **20** has the most conjugated structure and it has no ability to transfer the energy from donor to acceptor. In addition, it is observed that, increasing conjugation increases the absorption and emission maxima of wavelength, spectrum shift to red end of the visible region. The energy transfer is also proved by the life-time fluorescence spectrum of target, donor and acceptor BODIPY molecules.

In conclusion, three supramolecular targets, each containing three different BODIPY dyes are synthesized. The fact that there is indeed an energy transfer from the donor to the acceptor and the efficiency of energy transfer are shown with data acquired from spectroscopic analysis.

REFERENCES

1. Treibs, A.; Kreuzer, F. H. *Justus Liebigs Ann. Chem*. **1968**, *718*, 208

2. Haugland, R. P. *The Handbook-A guide to fluorescent probes and labeling technologies*, 10th ed.; Invitrogen Corp., **2005**.

3. (a) Coskun, A.; Akkaya, E. U. *J. Am. Chem. Soc*. **2005**, 127, 10464–10465. (b) Rurack, K.; Kollmannsberger, M.; Resch-Genger, U.; Daub, J. *J. Am. Chem. Soc*. **2000**, 122, 968–969. (c) Coskun, A.; Akkaya, E. U. *J. Am. Chem. Soc*. **2006**, 128, 14474–14475. (d) Zeng, L.; Miller, E. W.; Pralle, A.; Isacoff, E. Y.; Chang, C. J. *J. Am. Chem. Soc*. **2006**, 128, 10– 11. (e) Coskun, A.; Deniz, E.; Akkaya, E. U. *Org. Lett*. **2005**, 7, 5187– 5189. (f) Saki, N.; Dinc, T.; Akkaya, E. U. *Tetrahedron* **2006**, 62, 2721– 2725. (g) Coskun, A.; Turfan, B. T.; Akkaya, E. U. *Tetrahedron Lett*. **2003**, 44, 5649–5651. (h) Ekmekci, Z.; Yilmaz, M. D.; Akkaya, E. U. *Org. Lett*. **2008**, 10, 461–464.

4. (a) Li, F.; Yang, S. I.; Ciringh, Y. Z.; Seth, J.; Martin, C. H.; Singh, D. L.; Kim, D.; Birge, R. R.; Bocian, D. F.; Holten, D.; Lindsey, J. L. *J. Am. Chem. Soc*. **1998**, 120, 10001–10017. (b) Yilmaz, M. D.; Bozdemir, O. A.; Akkaya, E. U. *Org. Lett*. **2006**, 8, 2871–2873.

5. Rurack, K.; Kollmannsberger, M.; Daub, *J. Angew. Chem., Int. Ed*. **2001**, 40, 385–387. (b) Goze, C.; Ulrich, G.; Mallon, L. J.; Allen, B. D.; Harriman, A.; Ziessel, R. *J. Am. Chem. Soc*. **2006**, 128, 10231–10239. (c) Ziessel, R.; Goze, C.; Ulrich, G.; Cesario, M.; Retailleau, P.; Harriman, A.; Rostron, J. P. *Chem.-Eur. J*. **2005**, 11, 7366–7378. (d) Ulrich, G.; Goze, C.; Guardigli, M.; Roda, A.; Ziessel, R. *Angew. Chem., Int. Ed*. **2005**, 44, 3694–3698. (e) Goze, C.; Ulrich, G.; Ziessel, R. *Org. Lett*. **2006**, 8, 4444–4448. (f) Dost, Z.; Atilgan, S.; Akkaya, E. U. *Tetrahedron* **2006**, 62, 8484–8488. (g) Baruah, M.; Qin, W.; Vallee, R. A. L.; Beljonne, D.; Rohand, T.; Dehaen, W.; Boens, N. *Org. Lett*. **2005**, 7, 4377–4380. (h) Rohand, T.; Baruah, M.; Qin, W.; Boens, N.; Dehaen, W. *Chem. Commun*. **2006**, 266–268. (i) Rohand, T.; Qin, W.; Boens, N.; Dehaen, W. *Eur. J. Org. Chem*. **2006**, 4658–4663. (j) Gabe, Y.; Ueno, T.; Urano, Y.; Kojima, H.; Nagano, T. *Anal. Bioanal. Chem*. **2006**, 386, 621–626. (k) Li, L. L.; Han, J. Y.;

Nguyen, B.; Burgess, K. *J. Org. Chem*. **2008**, 73, 1963–1970. (l) Thivierge, C.; Bandichhor, R.; Burgess, K. *Org. Lett*. **2007**, 9, 2135–2138.

6. (a) Erhan Deniz; G. Ceyda Isbasar; O. Altan Bozdemir; Leyla T. Yildirim; Aleksander Siemiarczuk; and Engin U. Akkaya, *Org. Lett*., Vol. 10, No. 16, **2008**. (b) Dost, Z.; Atilgan, S.; Akkaya, E. U. *Tetrahedron* **2006**, 62, 8484–8488.

7. Loudet, A.; Burgess, K. *Chem. Rev*. **2007**, 107, 4891–4932.

8. Boyer J. H., Haag A. M., Sathyamoorthi G., Soong M. L., Thangaraj K., *Heteroat. Chem.*, **1993**, *4*, 39 – 49.

9. Deniz, E.; Isbasar, G. C.; Bozdemir, O. A.; Yildirim, L. T.; Siemiarczuk, A.; Akkaya, E. U., *Org. Lett*., **2008**; Vol. 10, No. 16

10. Yuichiro Ueno, Jiney Jose, Aurore Loudet, César Pérez-Bolívar, Pavel Anzenbacher, Jr., and Kevin Burgess, *J. Am. Chem. Soc.*, **2011**, *133* (1)

11. [1](a) R. W. Wagner, J. S. Lindsey, *Pure Appl. Chem*. **1996**, 68, 1373. (b) M. S. Vollmer, F. W¸rthner, F. Effenberger, P. Emele, D. U. Meyer, T. St¸mpfig, H. Port, H. C. Wolf, *Chem. Eur. J*. **1998**, 4, 260. (c) M. S. Vollmer, F. Effenberger, T. St¸mpfig, A. Hartschuh, H. Port, H. C. Wolf*, J. Org. Chem*. **1998**, 63, 5080. (d) F. Li, S. I. Yang, Y. Ciringh, J. Seth, C. H. Martin, D. L. Singh, D. Kim, R. R. Birge, D. F. Bocian, D. Holten, J. S. Lindsey, *J. Am. Chem. Soc*. **1998**, 120, 10 001. (e) R. W. Wagner, J. Seth, S. I. Yang, D. Kim, D. F. Bocian, D. Holten, J. S. Lindsey*, J. Org. Chem*. **1998**, 63, 5042.

12. (a) Chi-Wai Wan, Armin Burghart, Jiong Chen, Fredrik Bergstrˆm, Lennart B. Johansson, Matthew F. Wolford, Taeg GyumKim, Michael R. Topp, Robin M. Hochstrasser, and Kevin Burgess, *Chem. Eur. J*. **2003**, 9, 4430 ± 4441. (b) M. Deniz Yilmaz, O. Altan Bozdemir, Engin U. Akkaya, *Org. Lett*., Vol. 8, No. 13, **2006**. (c) Chang Yeon Lee, Omar K. Farha, Bong Jin Hong, Amy A. Sarjeant, SonBinh T. Nguyen, and Joseph T. Hupp, *J. Am. Chem. Soc*. **2011**, 133, 15858–15861. (d) Anthony Harriman, Guillaume Izzet, and Raymond Ziessel, *J. AM. CHEM. SOC*. **2006**, 128, 10868-10875. (e) O. Altan Bozdemir, Yusuf Cakmak, Fazli Sozmen, Tugba Ozdemir, Aleksander Siemiarczuk, Engin U. Akkaya, *Chem. Eur. J.* **2010**, 16, 6346 – 6351.

13. Förster, Th. *"Zwischenmolekulare Energiewanderung und Fluoreszenz". Annalen der Physik* **1948**. **437**: 55–75.

14. Anthony Harriman, Guillaume Izzet, and Raymond Ziessel, *J. AM. CHEM. SOC*. **2006**, 128, 10868-10875

15. Joseph R. Lakowicz, *"Principles of Fluorescence Spectroscopy", Plenum Publishing Corporation, 2nd edition*, **1999**

16. M. Deniz Yilmaz, O. Altan Bozdemir, Engin U. Akkaya, *Org. Lett*., Vol. 8, No. 13, **2006**.

17. F. H. *Cocks in Energy Demand and Climate Change, WileyVCH*, Weinheim, **2009**.

18. O. Altan Bozdemir, Sundus Erbas-Cakmak, O. Oner Ekiz, Aykutlu Dana, and Engin U. Akkaya, *Angew. Chem. Int. Ed*. **2011**, 50, 10907 –10912

19. Ozlem S.; Akkaya E. U. *J. Am. Chem. Soc.,* **2009**, 131, 48.

20. Montcourrier, P.; Mangeat, P. H.; Valembois, C.; Salazar, G.; Sahuquet, A.; Duperray, C.; Rochefort, H. *J. Cell Sci.* **1994**, 107, 2381–2391.

21. V. P. Ananikov, D. G. Musaev, K. Morokuma, *"Theoretical Insight into the C-C Coupling Reactions of the Vinyl, Phenyl, Ethynyl, and Methyl Complexes of Palladium and Platinum" Organometallics* **2005**, 24, 715.

22. Meijere A., Diederich F., *Metal catalyzed cross coupling, Volume 1, Wiley-VCH, Wienheim*, **2004**

23. Chao Liu, Hua Zhang, Wei Shi, and Aiwen Lei *Chem. Rev.*, **2011**, *111* (3), pp 1780–1824.

24. *Palladium-Catalyzed Cross-Coupling Reactions of Organoboron Compounds* Norio. Miyaura, Akira. Suzuki *Chem. Rev*., **1995**, 95 (7), pp 2457–2483.

25. *Selected Patented Cross-Coupling Reaction Technologies*Jean-Pierre Corbet and Gérard Mignani *Chem. Rev*., 2006, 106 (7), pp 2651–2710 2006

26. Justin M. Chalker , Charlotte S. C. Wood andBenjamin G. Davis, *J. Am. Chem. Soc.*, 2009, *131* (45)

27. Sonogashira, K.; Tohda, Y.; Hagihara, N., *Tetrahedron Lett.* **1975**, **16**: 4467–4470

28. Chinchilla, R.: Najera, C., *Chem. Soc. Rev.* **2011**, **40**: 5084–5121

29. Sonogashira, K. *J. Organomet. Chem.* **2002**, 653: 46–49

30. Yin, L.; Liebscher, J.*"Carbon-Carbon Coupling Reactions Catalyzed by Heterogeneous Palladium Catalysts*",*Chem. Rev.* **2006**, **107**: 133–173

31. Dudnik, A.; Gevorgyan, V., *Angewandte Chemie (International ed. in English),* **2010***,* **49** (12).

32. Bohm, V. P. W.; Herrmann, W. A., *Eur. J. Org. Chem.* **2000**, **200**: 3679–3681

33. Yin, L.; Liebscher, J. ,*Chem. Rev.* **2006**, **107**: 133–173

34. Amatore, C.; Jutand, A., *Acc. Chem. Res.* **2000**, **33**, 314–321.

35. Corona, C.; Bryant, B. K.; Arterburn, J. B. *Org. Lett*. **2006**, 8, 1883

36. Hong, B.-C.; Nimje, R. Y. Curr. *Org. Chem*. **2006**, 10, 2191.

37. Mujahidin, Didin; Doye, Sven. *European Journal of Organic Chemistry* **2005** (13): 2689–2693

38. Fodale V, Santamaria LB. *Eur J Anaesthesiol, **2002,*** **19** (7): 466–73

39. Mongin O., Gossauer A., *Tetrahedron Lett.*, **1996**, *37*, 3825.

40. Turro, N.J. *Modern Molecular Photochemistry*, University Science Books, Sausalito, **1991.**

41. Andrews, D.L. *Chemical Physics* ,**1989**, **135** (2): 195

42. Lakowicz, J.R. *Principles of Fluorescence Spectroscopy*, 2nd ed., Kluwer/Plenum, New York, **1999**

43. Yasutaka Kurishita [†], Takahiro Kohira [†], Akio Ojida*[‡], and Itaru Hamachi, *J. Am. Chem. Soc.*, **2010**, *132* (38), pp 13290–13299

44. Jason M. Serin , Darryl W. Brousmiche , and Jean M. J. Fréchet, *J. Am. Chem. Soc.*, **2002**, *124* (40), pp 11848–11849

45. Azov, V.A.; Schlegel, A.; Diederich, F. *Angew. Chem., Int. Ed.,* **2005**, 44, 4635.

46. Turro, N.J., *Modern Molecular Photochemsitry*, University Science Books, Sausalito, **1991**

47. Yusuf Cakmak and Engin U. Akkaya, *Org. Lett.*, **2009**, *11* (1), pp 85–88

48. Rakeshwar Bandichhor , Anca D. Petrescu , Aude Vespa , Ann B. Kier , Friedhelm Schroeder , Kevin Burgess **,** *J. Am. Chem. Soc.*, **2006**, *128* (33), pp 10688–10689

49. O. Altan Bozdemir, Yusuf Cakmak, Fazli Sozmen, Tugba Ozdemir, Aleksander Siemiarczuk, Engin U. Akkaya, *Chem. Eur. J.* **2010**, 16, 6346 – 6351.

50. Lakowicz, J.R. *Principles of Fluorescence Spectroscopy*, Kluwer Acadamic, Plenum Publishers, **1999**.

APPENDIX A

NMR SPECTRA

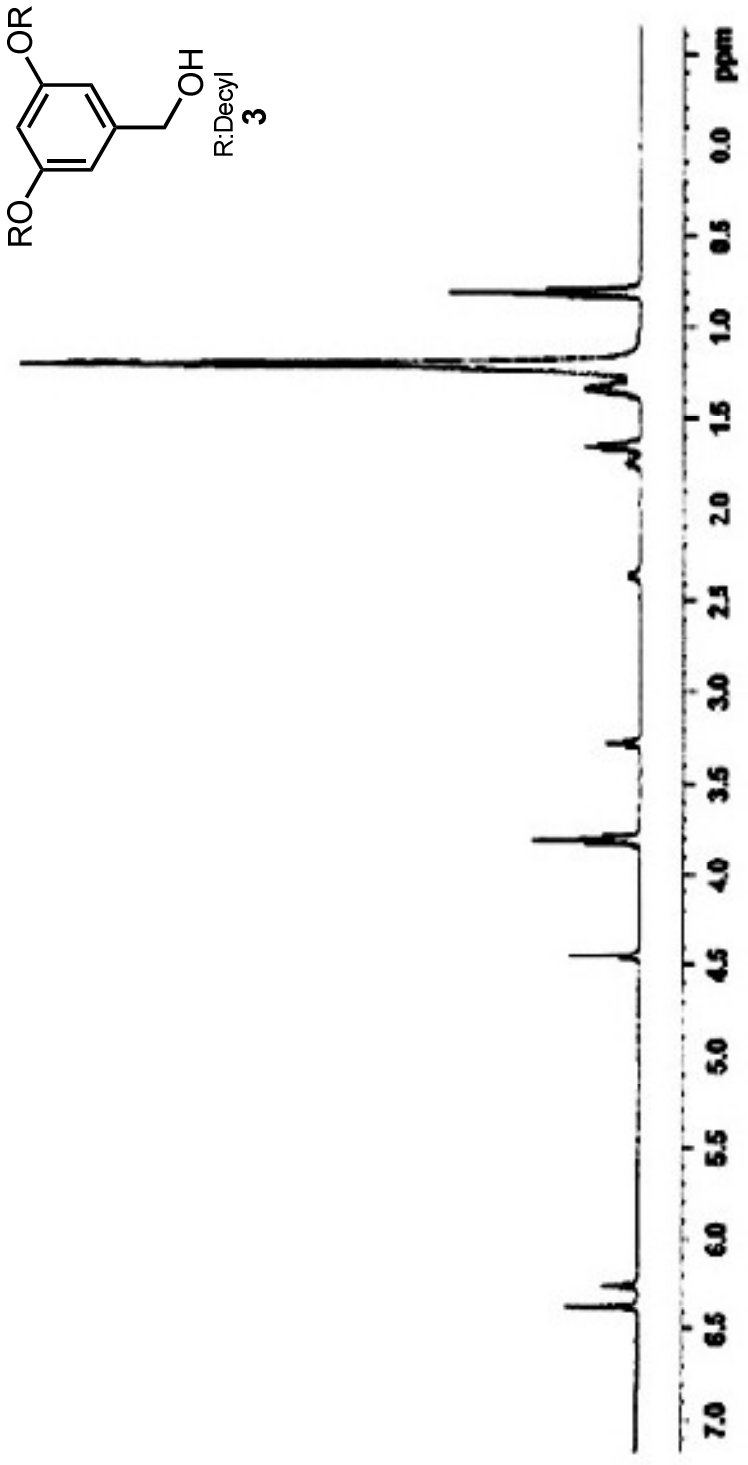

Figure 50. ^{1}H NMR spectrum of Compound **3**

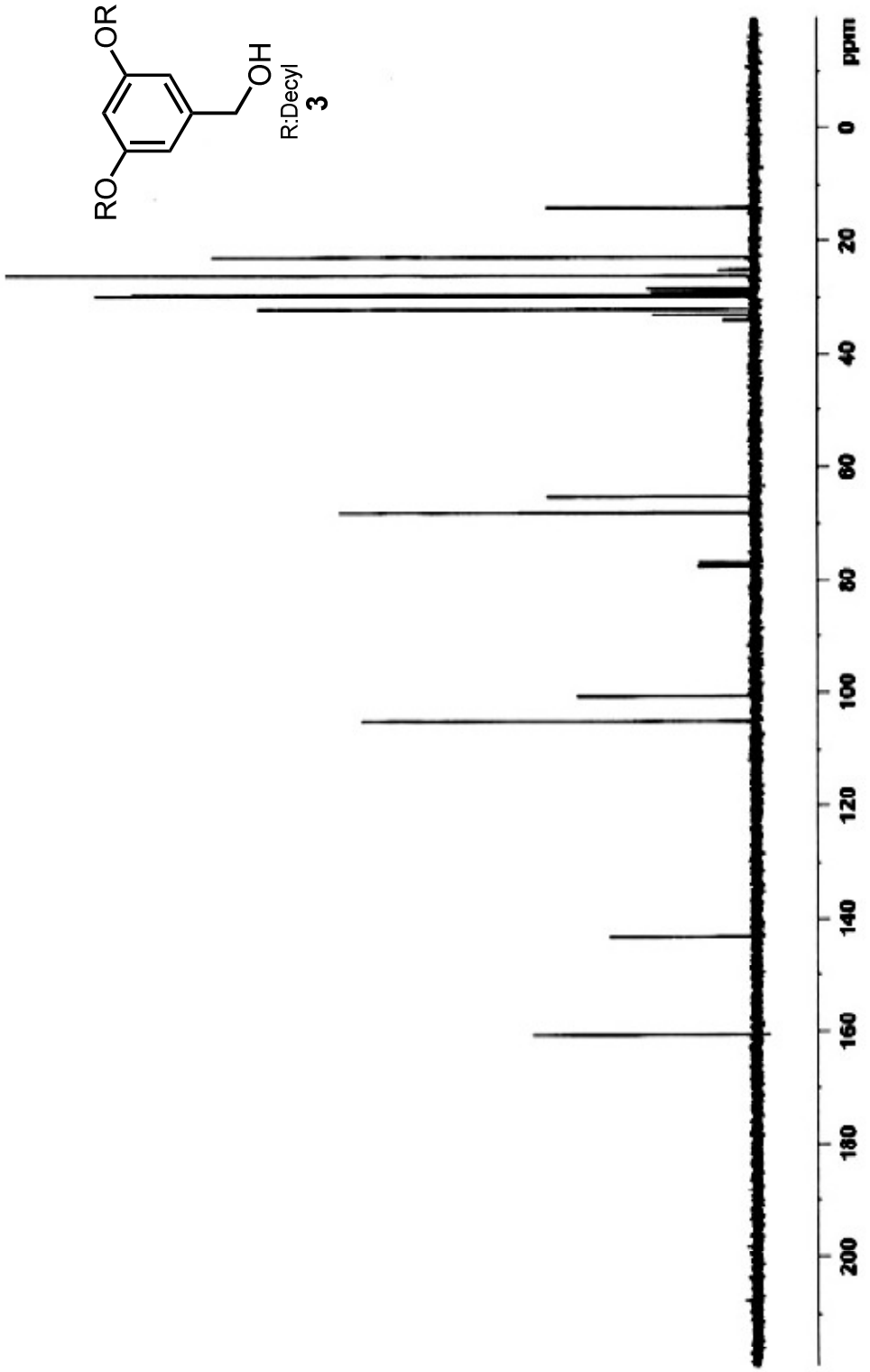

Figure 51. ^{13}C NMR spectrum of Compound **3**

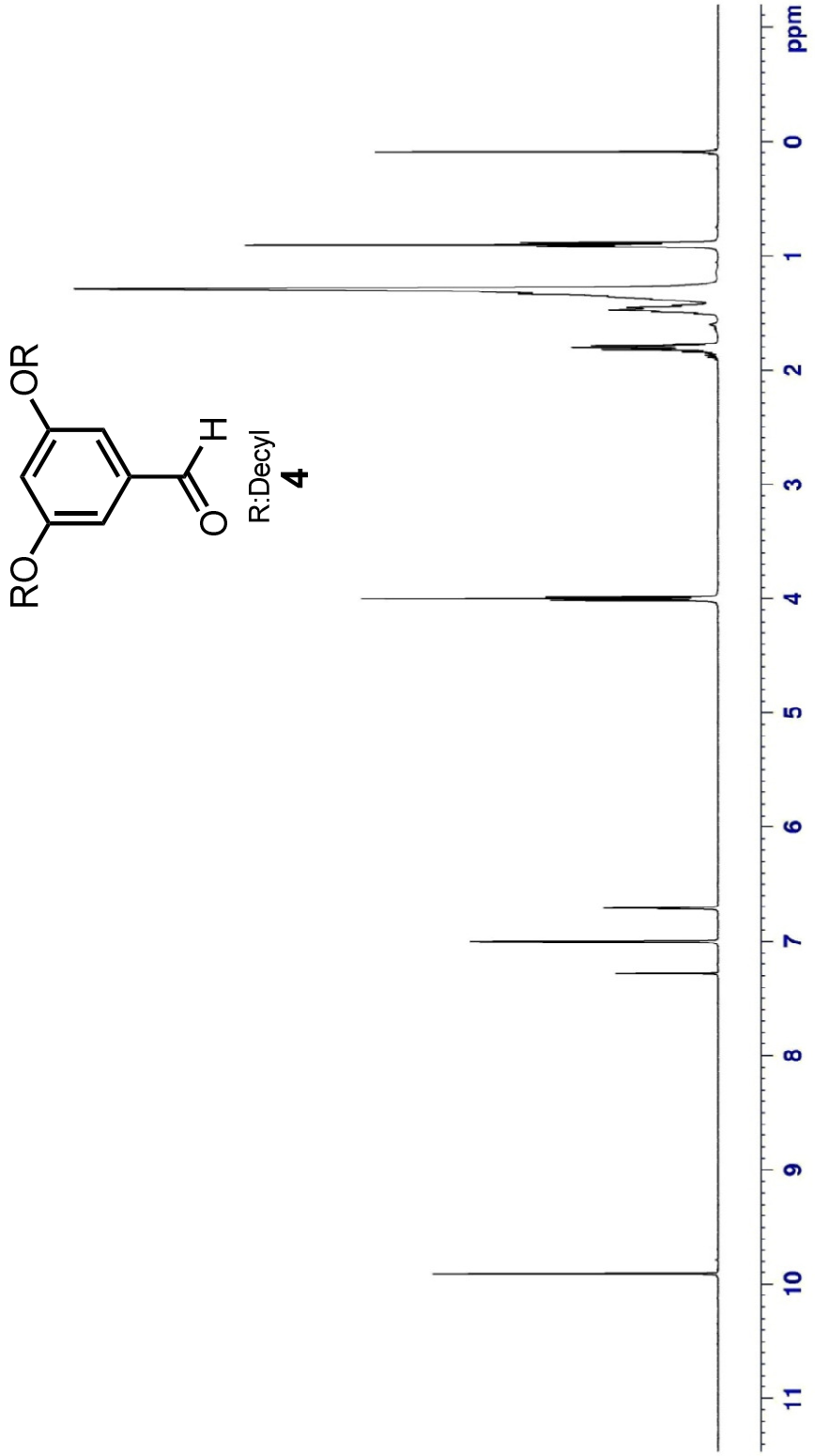

Figure 52. ^{1}H NMR spectrum of Compound **4**

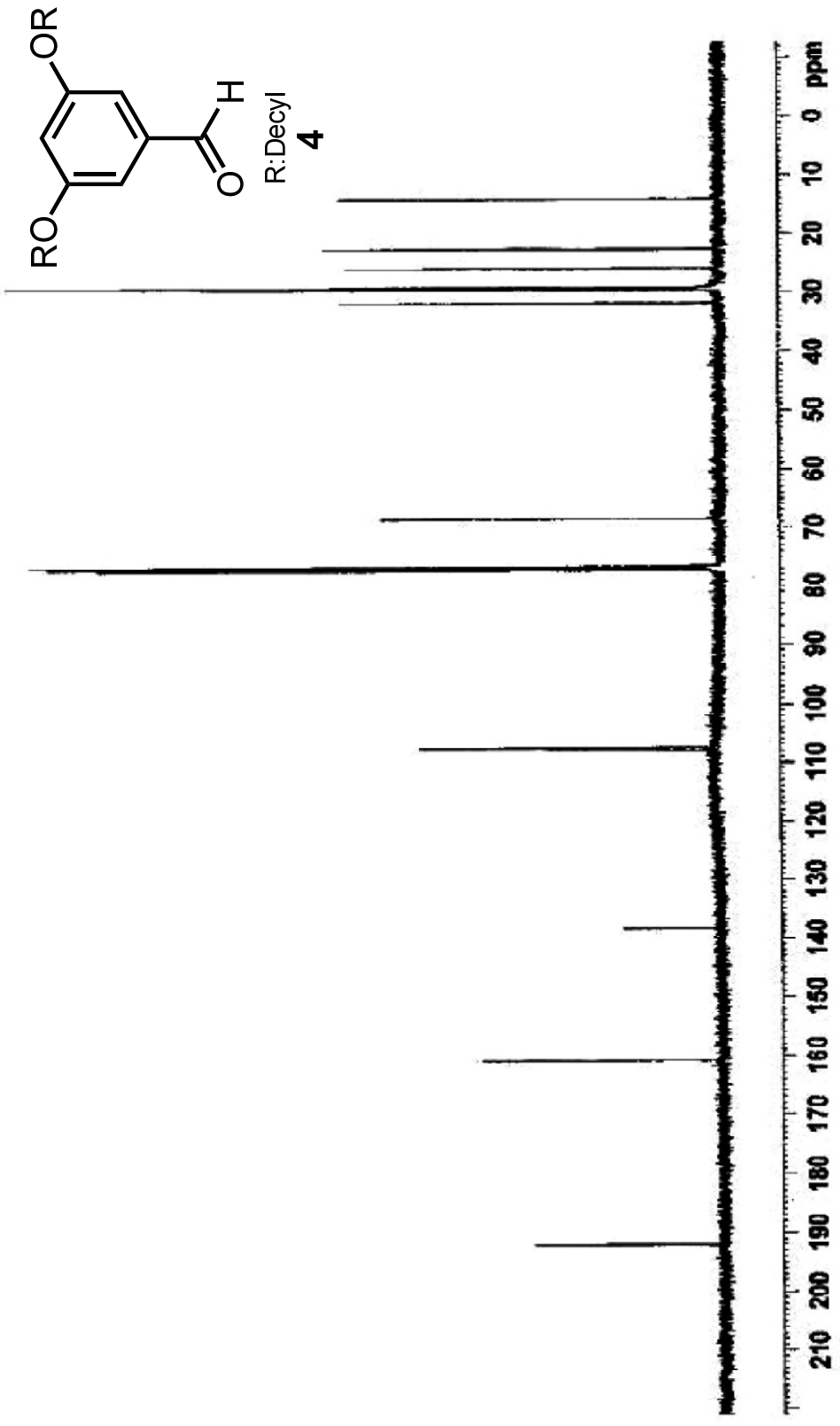

Figure 53. ^{13}C NMR spectrum of Compound **4**

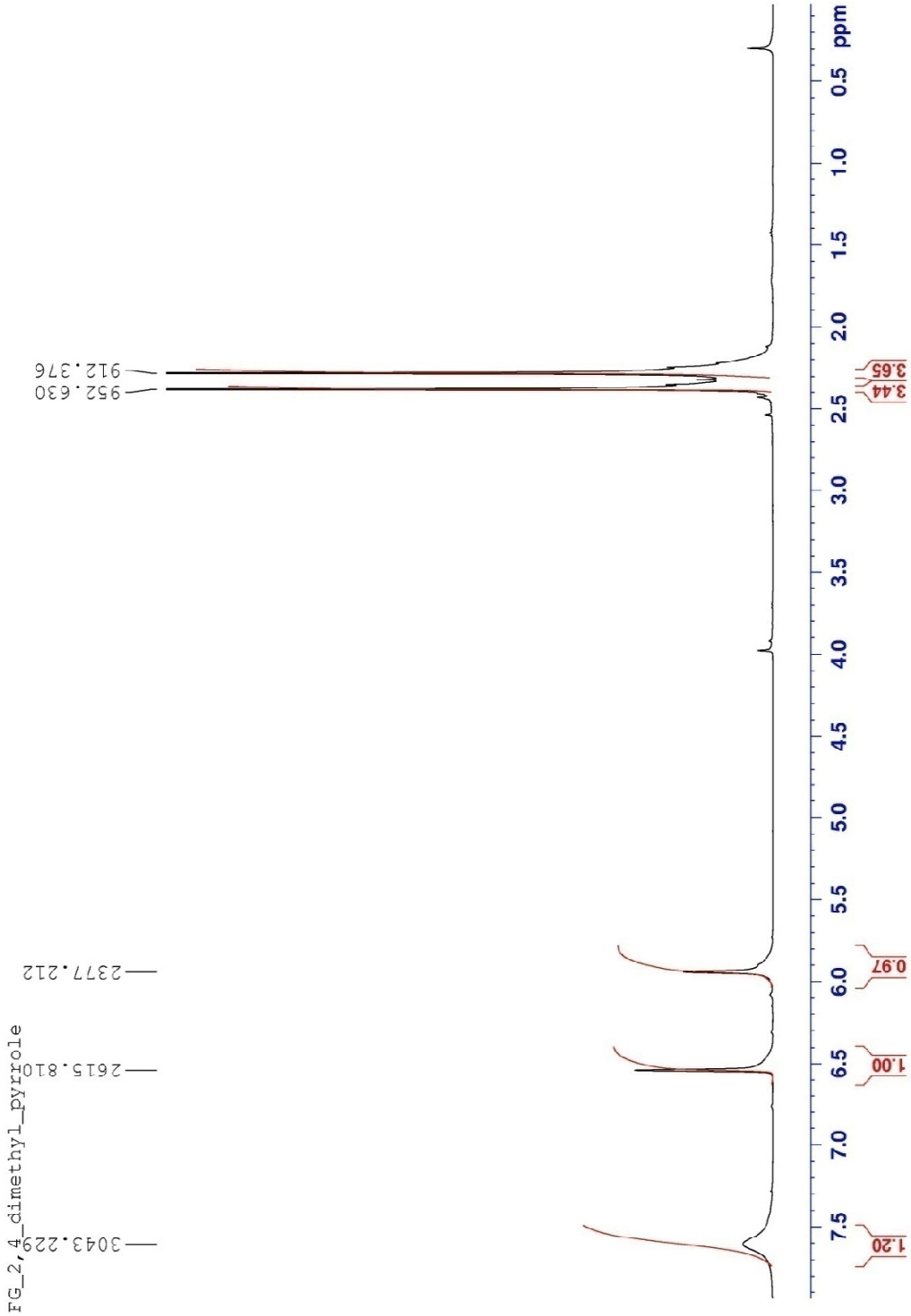

Figure 54. [1]H NMR spectrum of Compound **5**

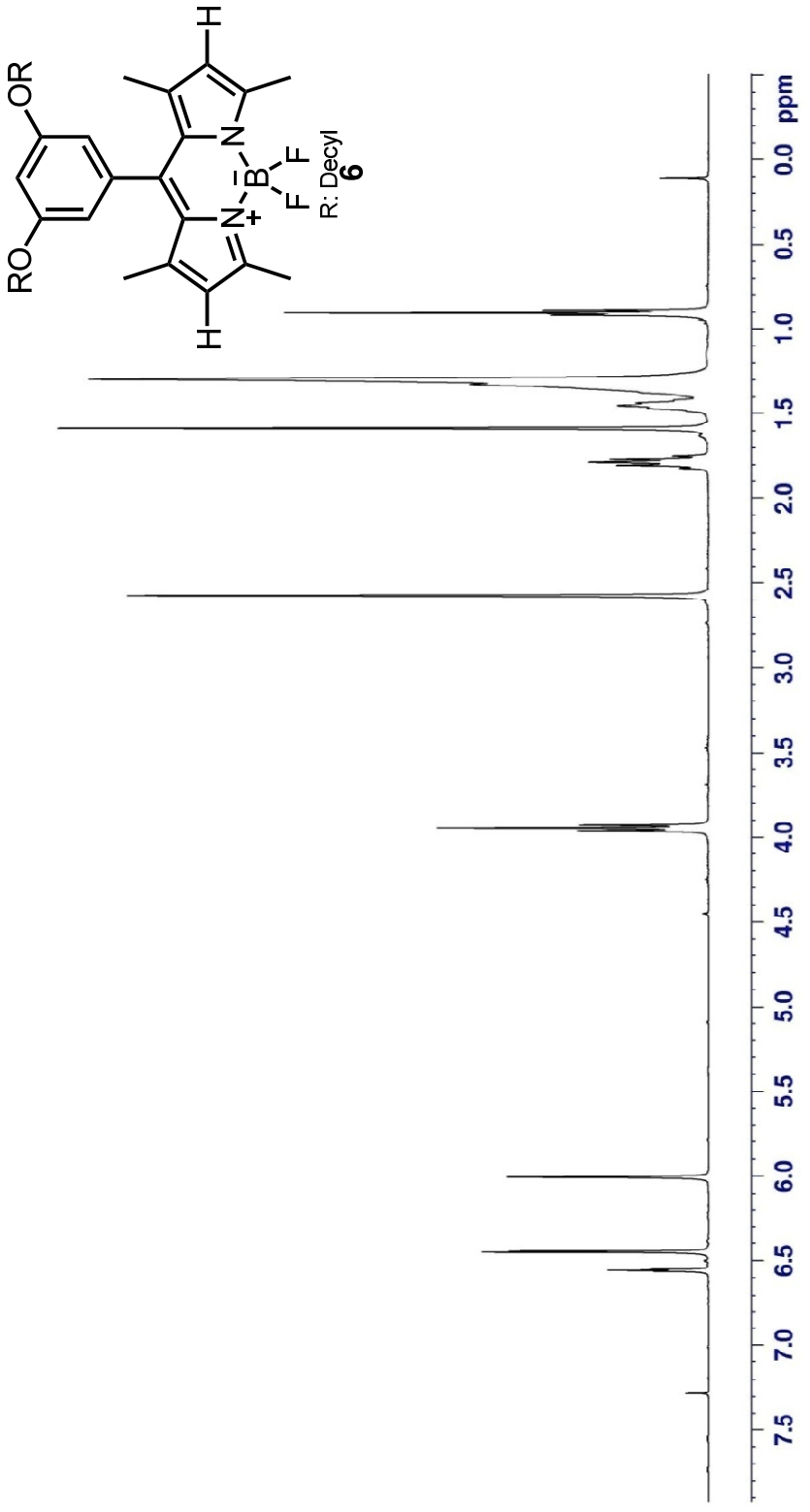

Figure 55. ^{1}H NMR spectrum of Compound **6**

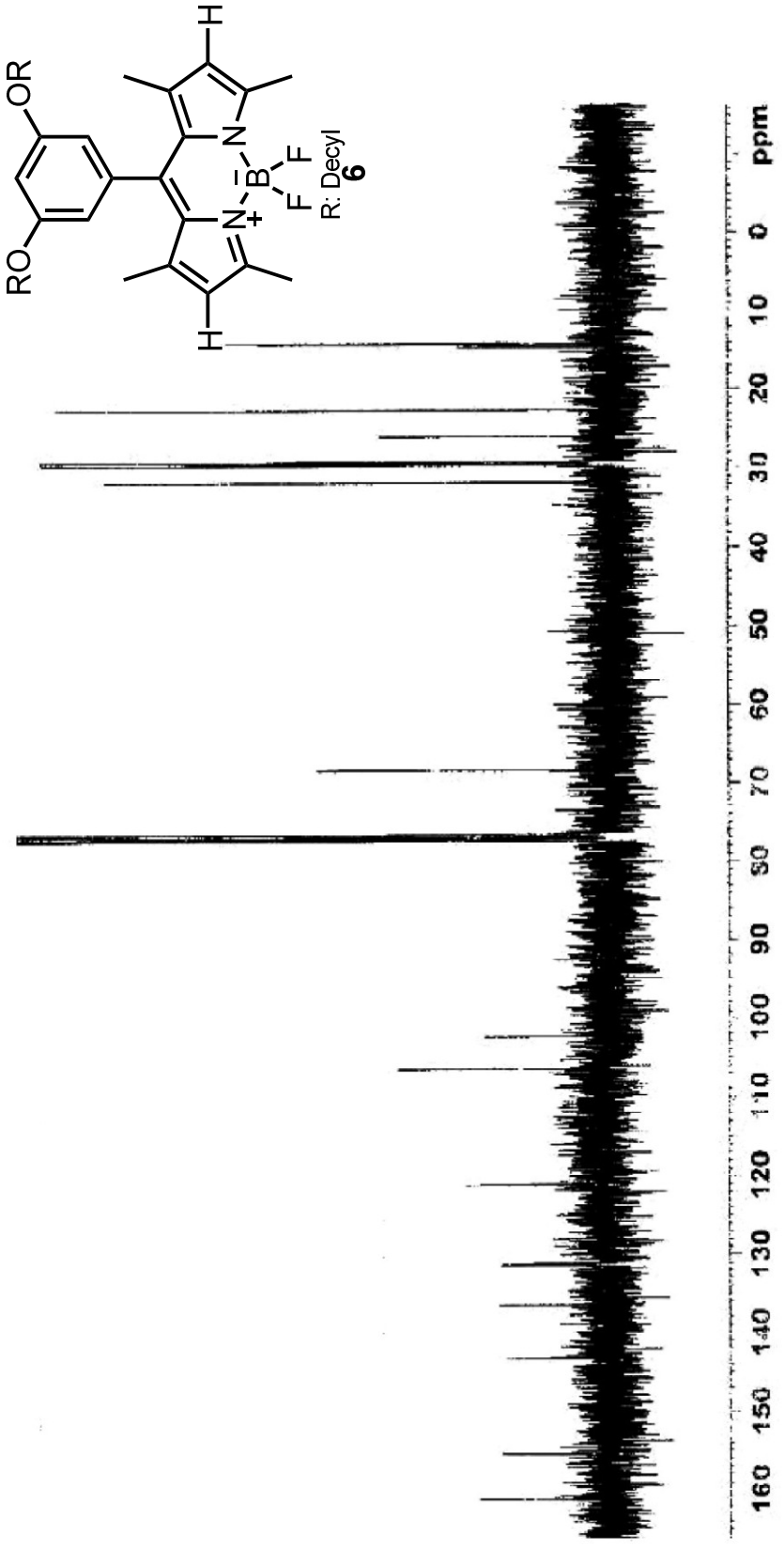

Figure 56. ^{13}C NMR spectrum of Compound **6**

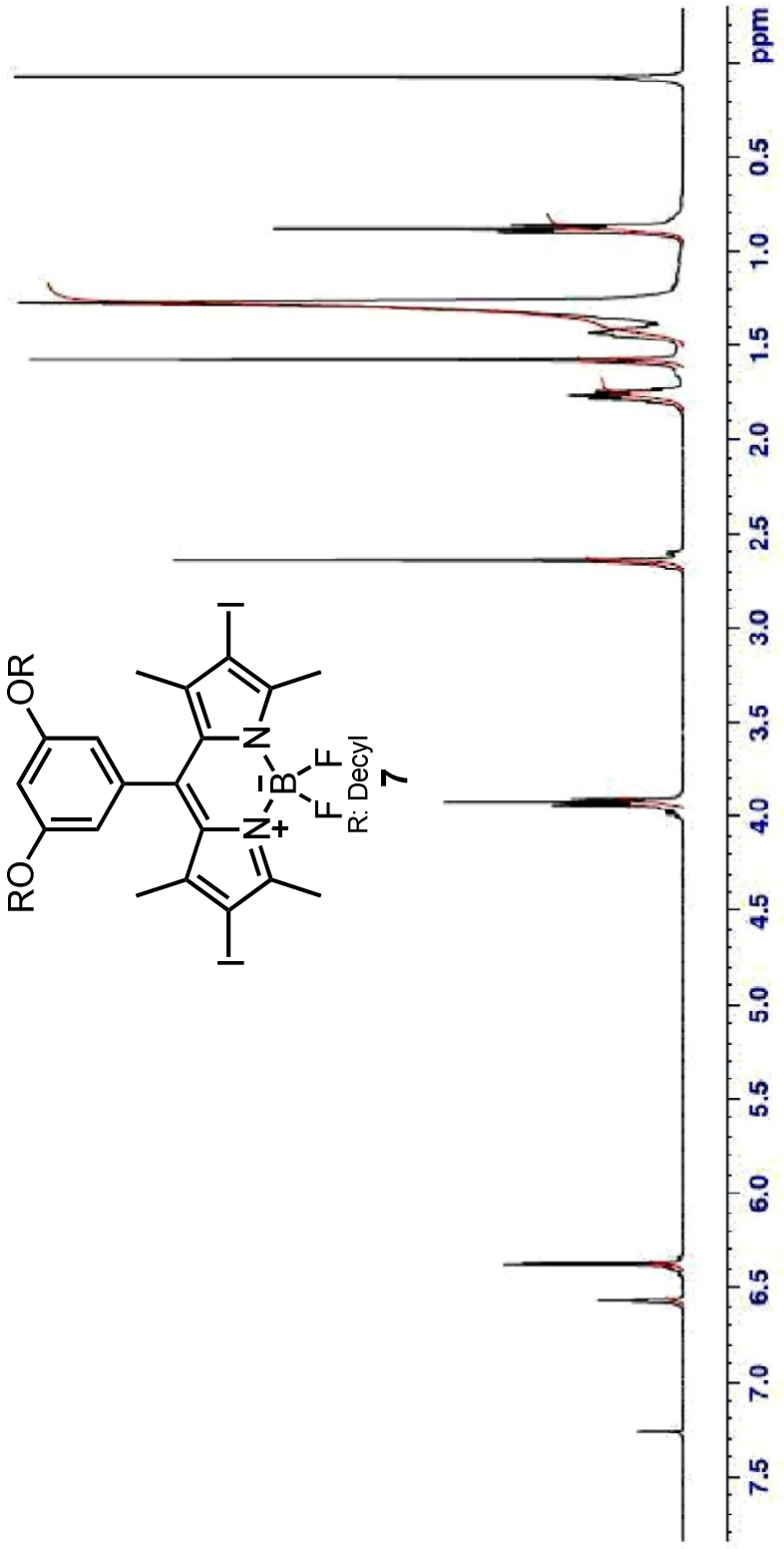

Figure 57. ^{1}H NMR spectrum of Compound **7**

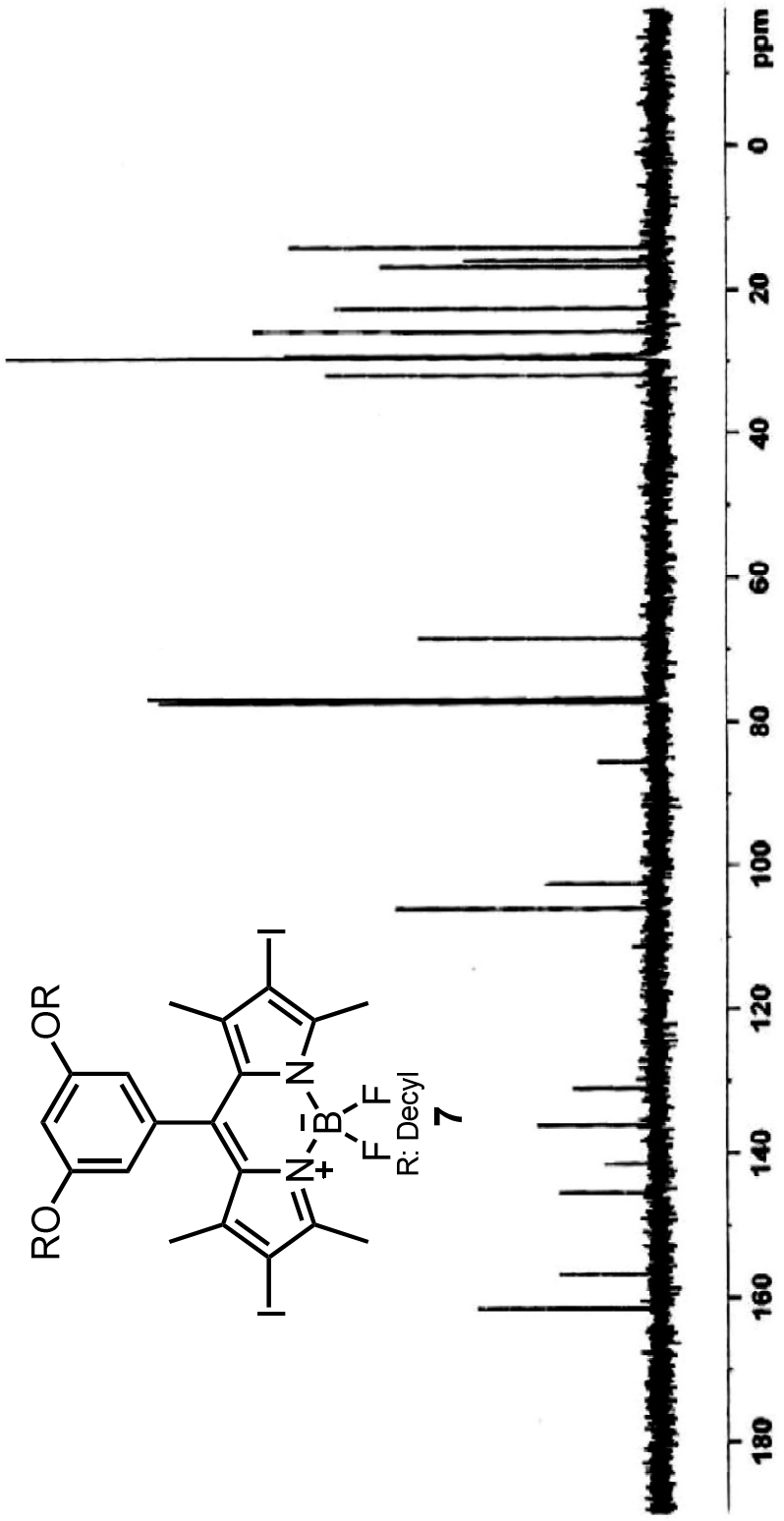

Figure 58. ^{13}C NMR spectrum of Compound **7**

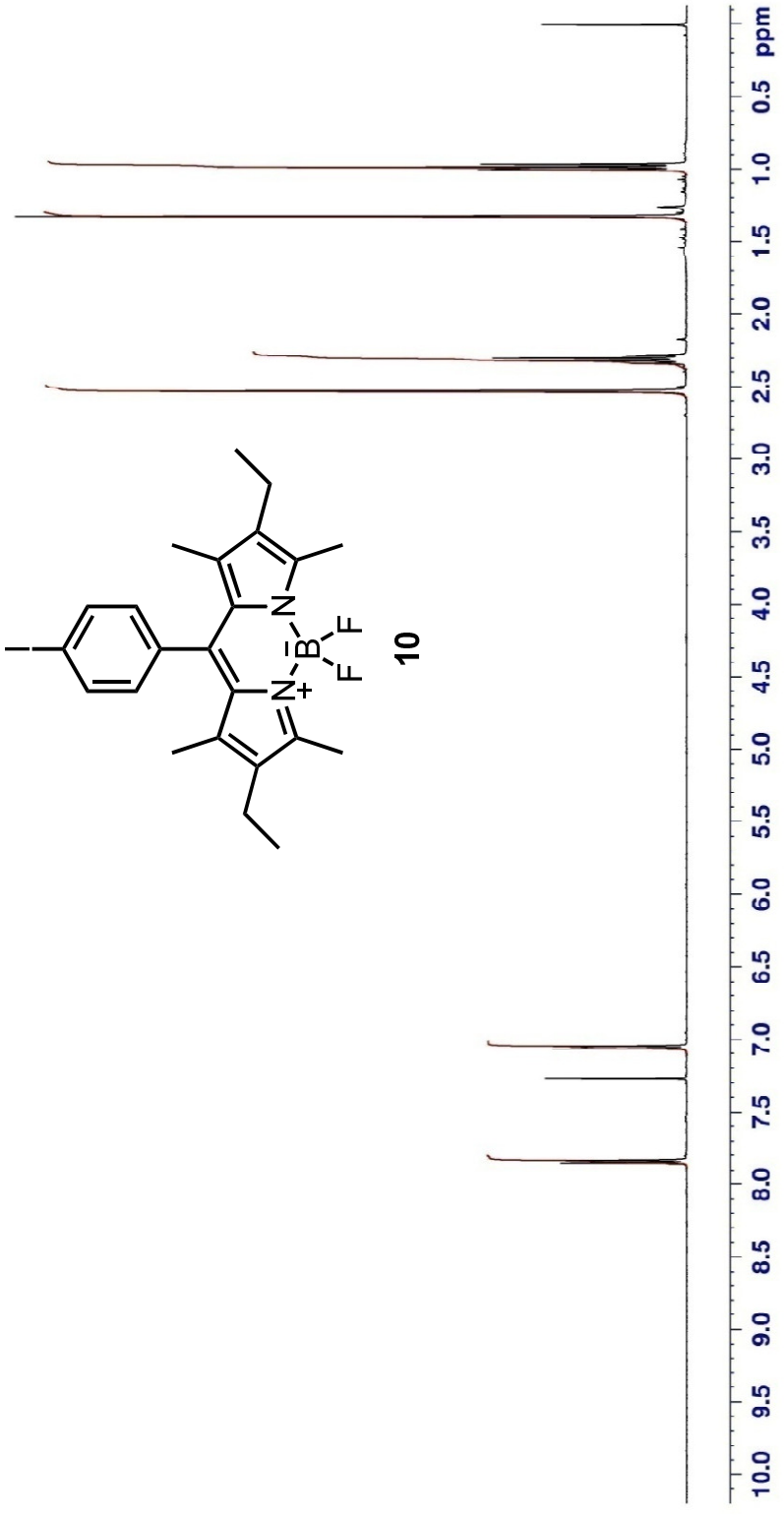

Figure 59. ^{1}H NMR spectrum of Compound **10**

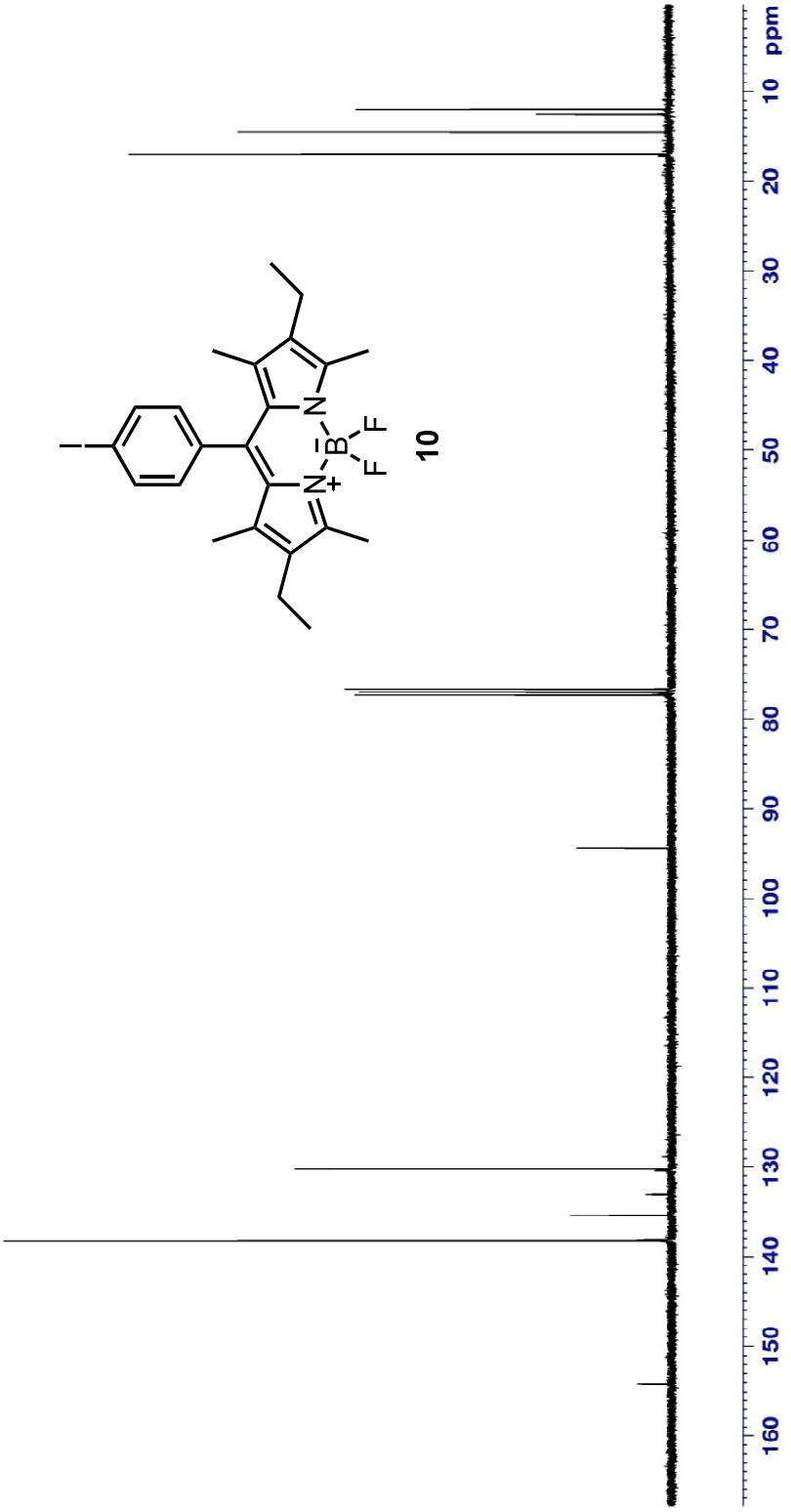

Figure 60. ^{13}C NMR spectrum of Compound **10**

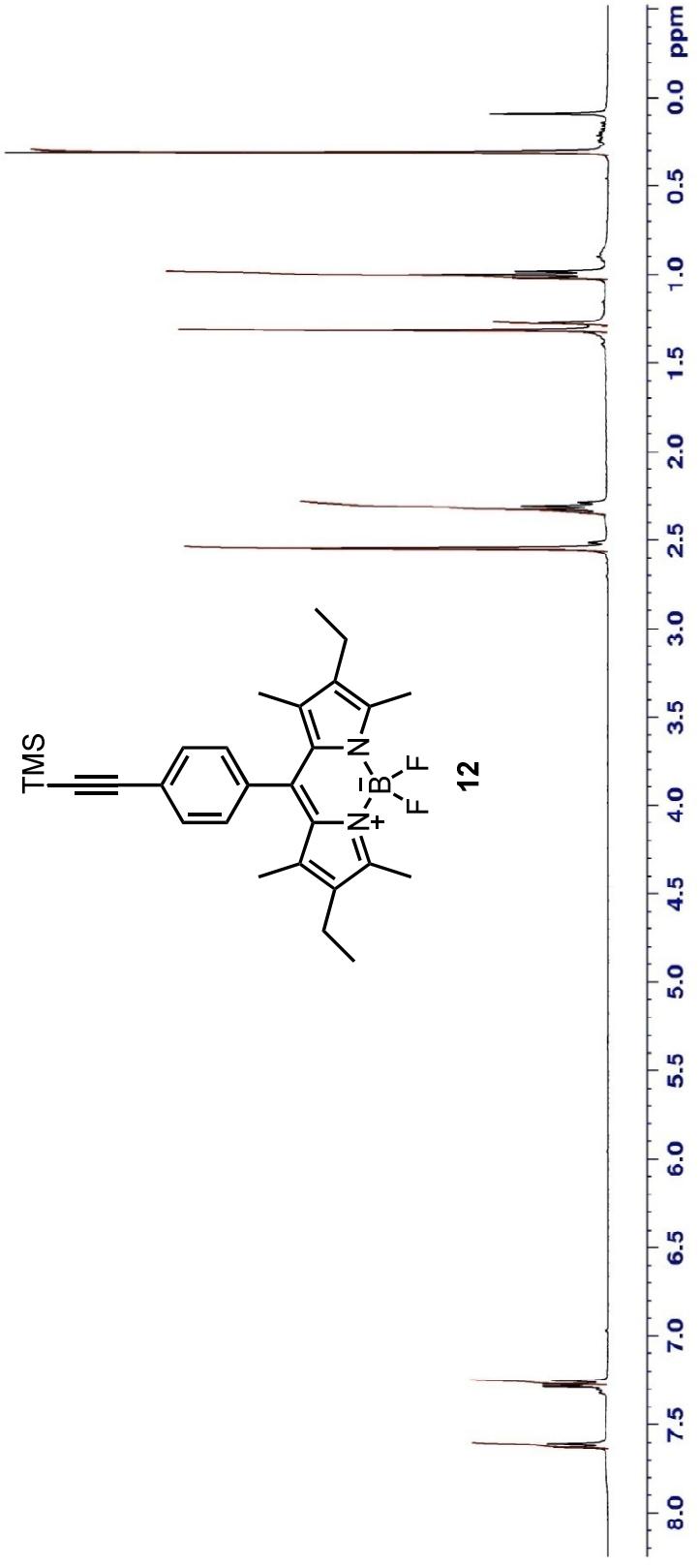

Figure 61. [1]H NMR spectrum of Compound **12**

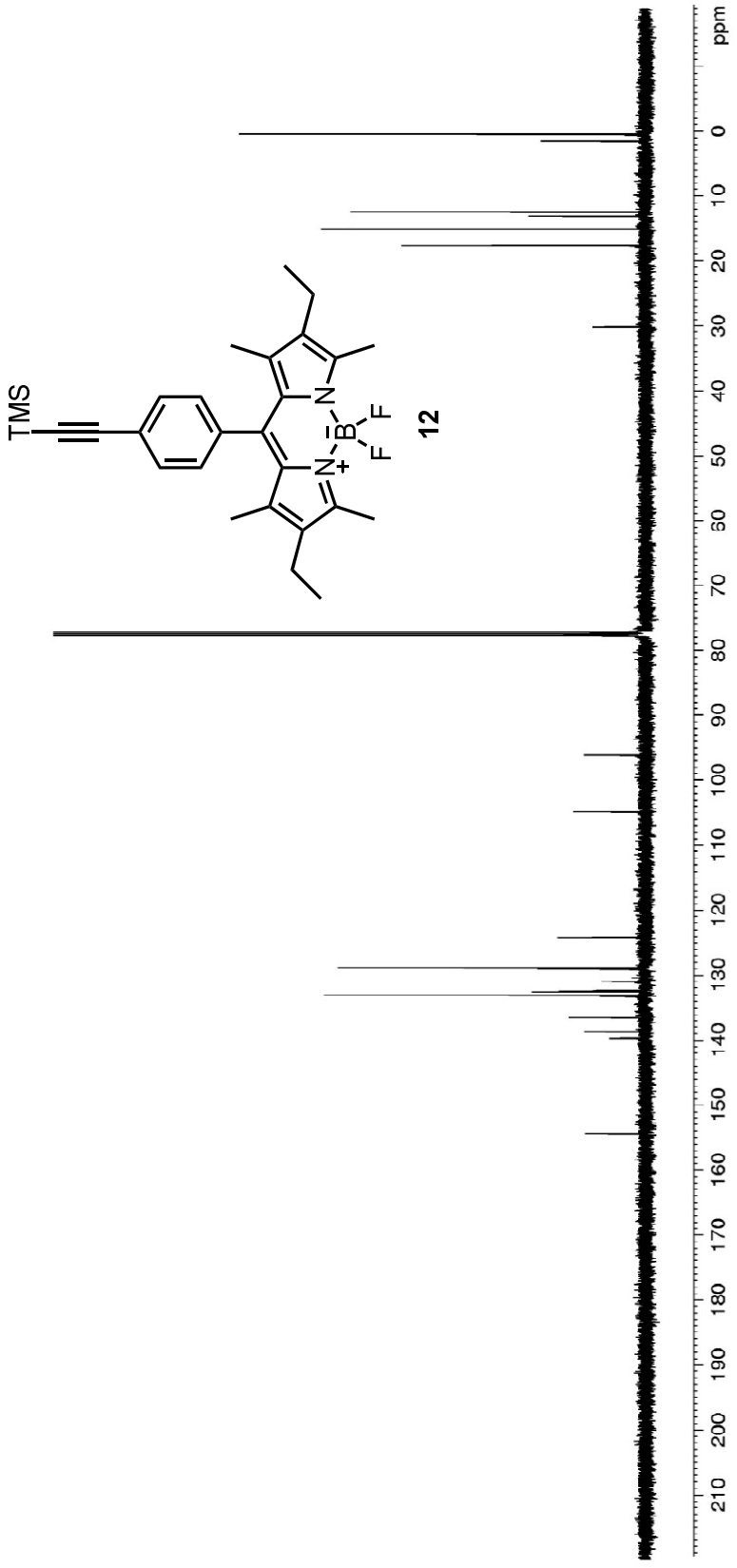

Figure 62. ^{13}C NMR spectrum of Compound **12**

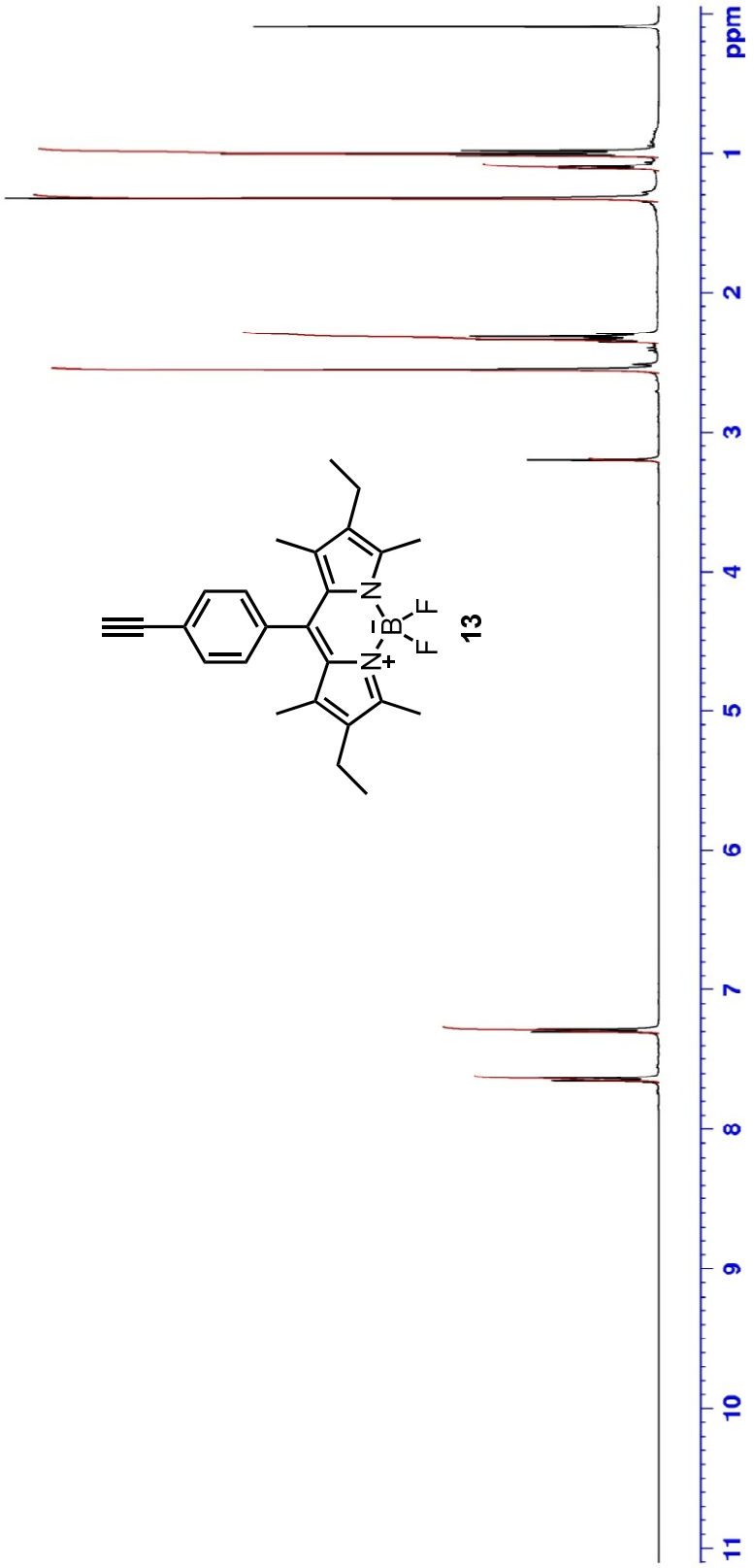

Figure 63. ^{1}H NMR spectrum of Compound **13**

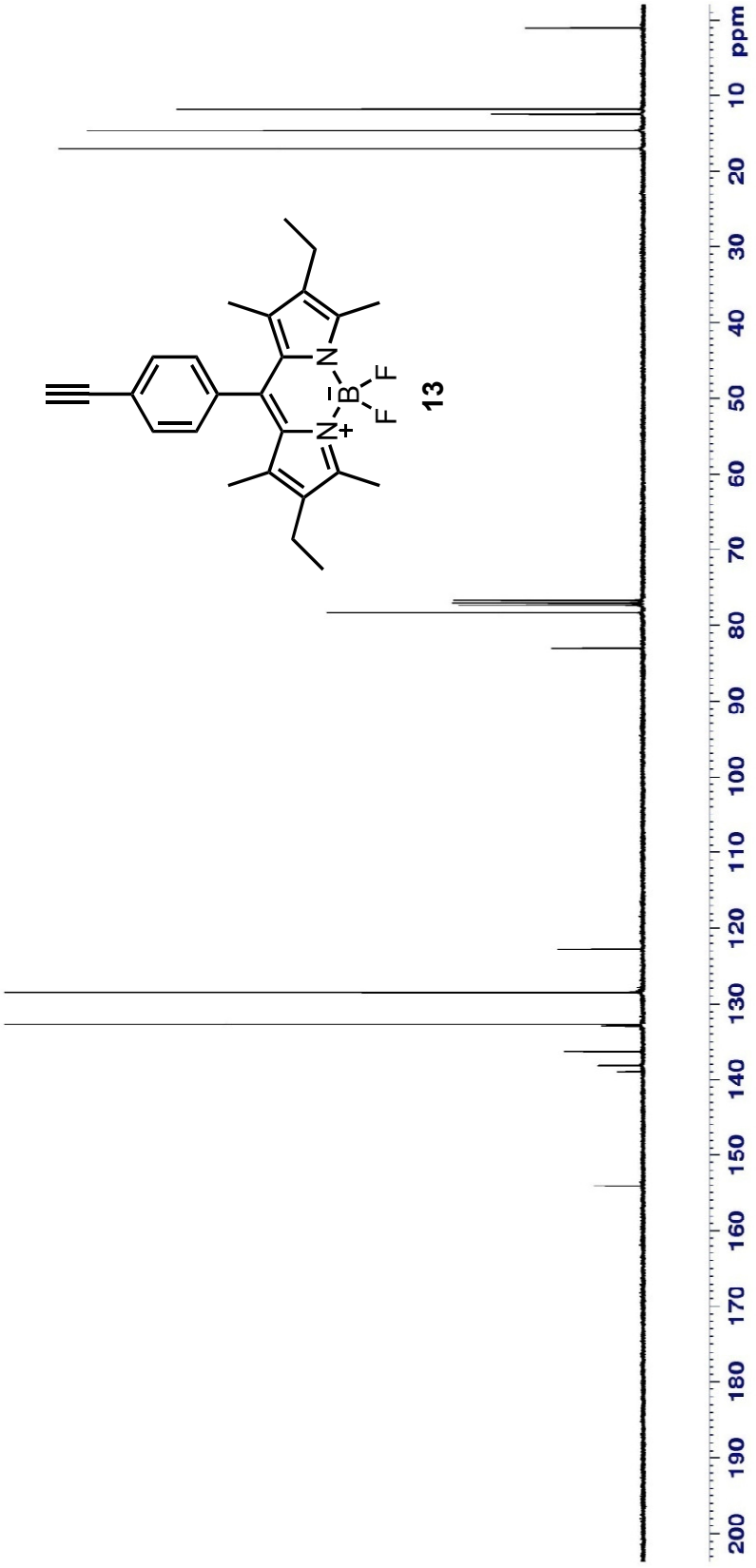

Figure 64. ^{13}C NMR spectrum of Compound **13**

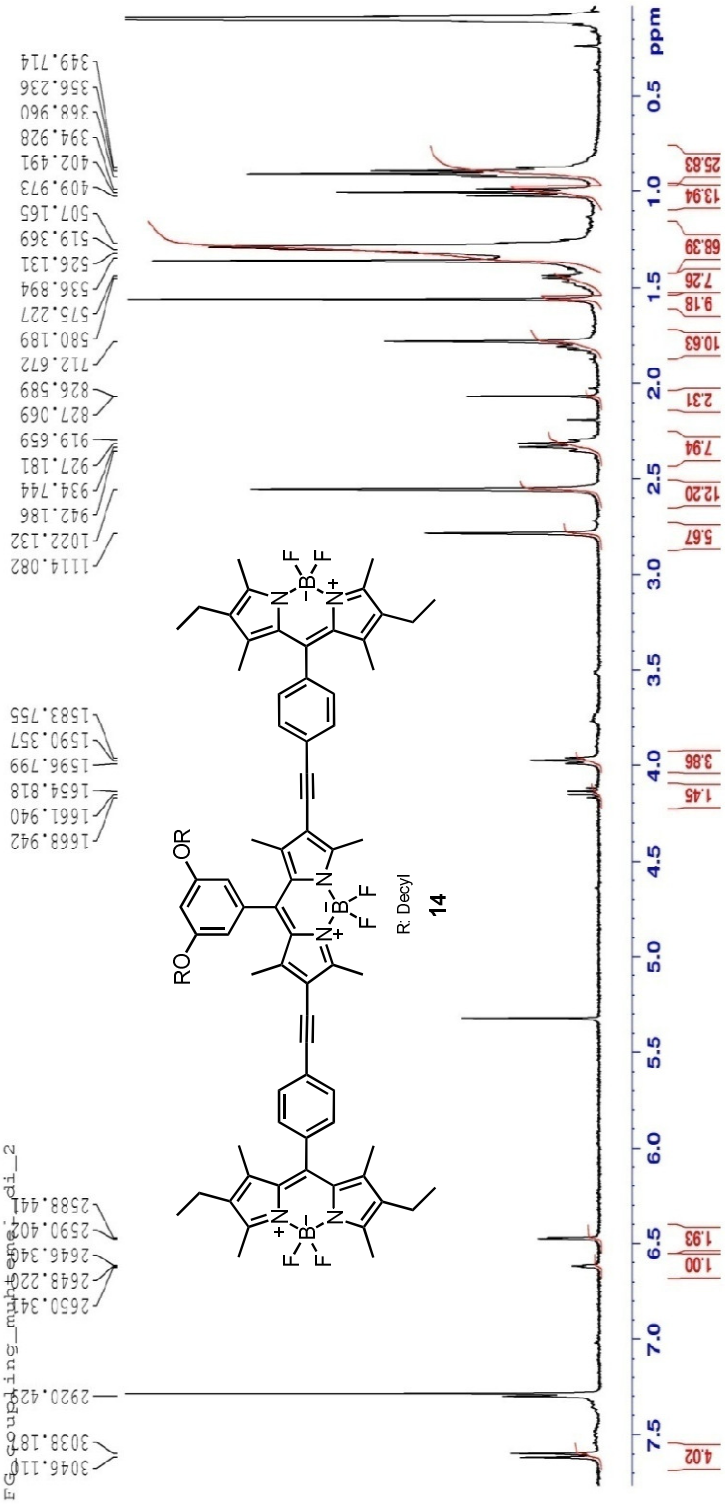

Figure 65. ^{1}H NMR spectrum of Compound **14**

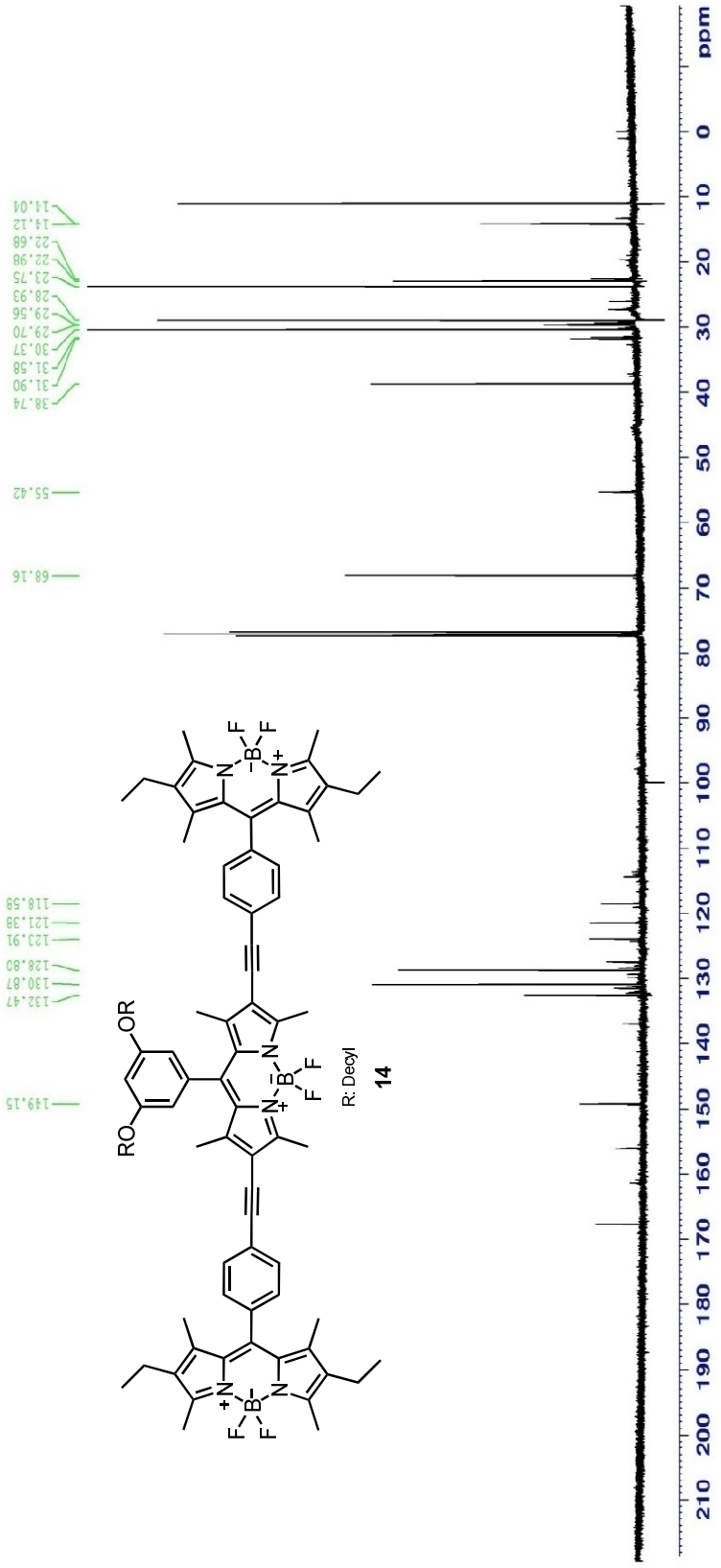

Figure 66. ^{13}C NMR spectrum of Compound **14**

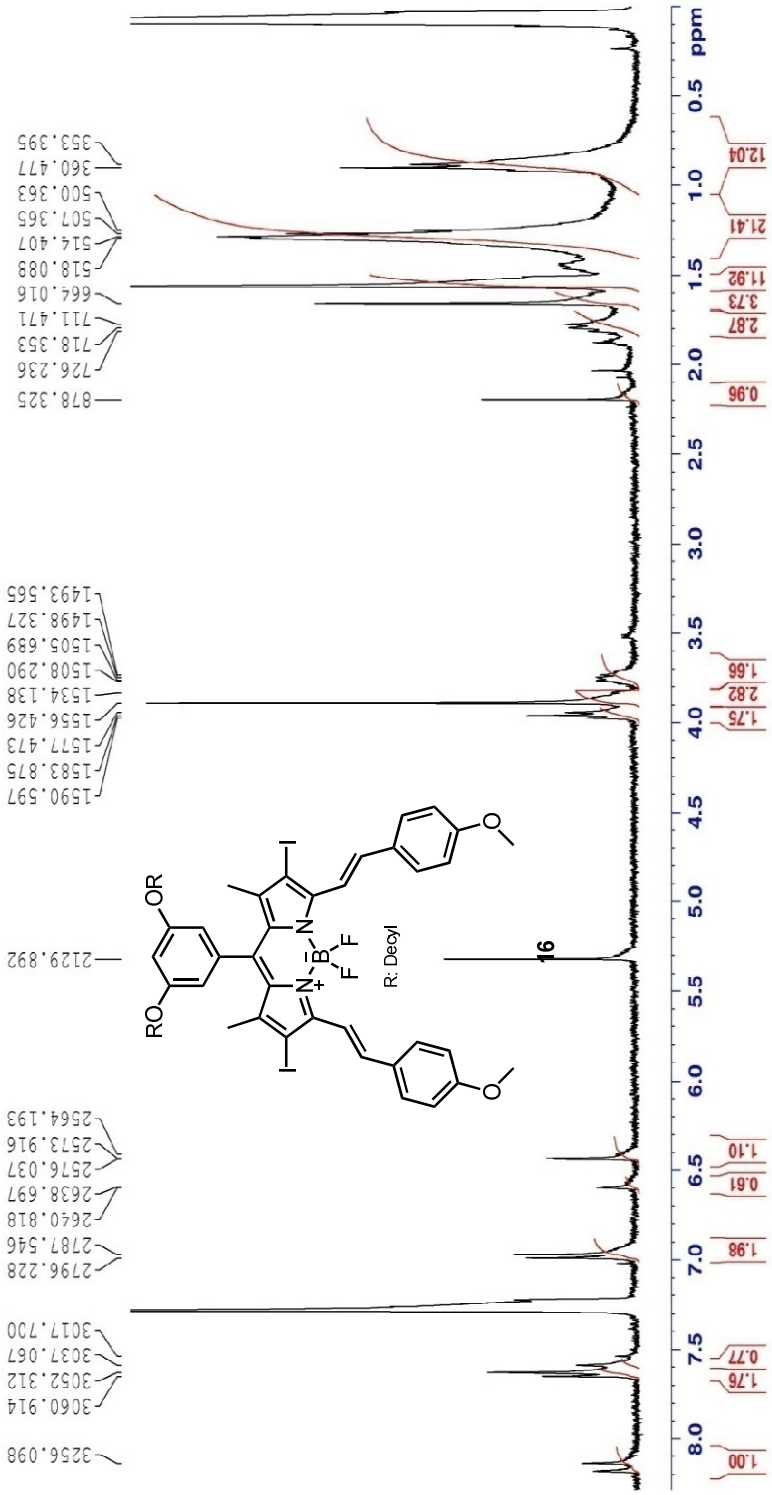

Figure 67. [1]H NMR spectrum of Compound **16**

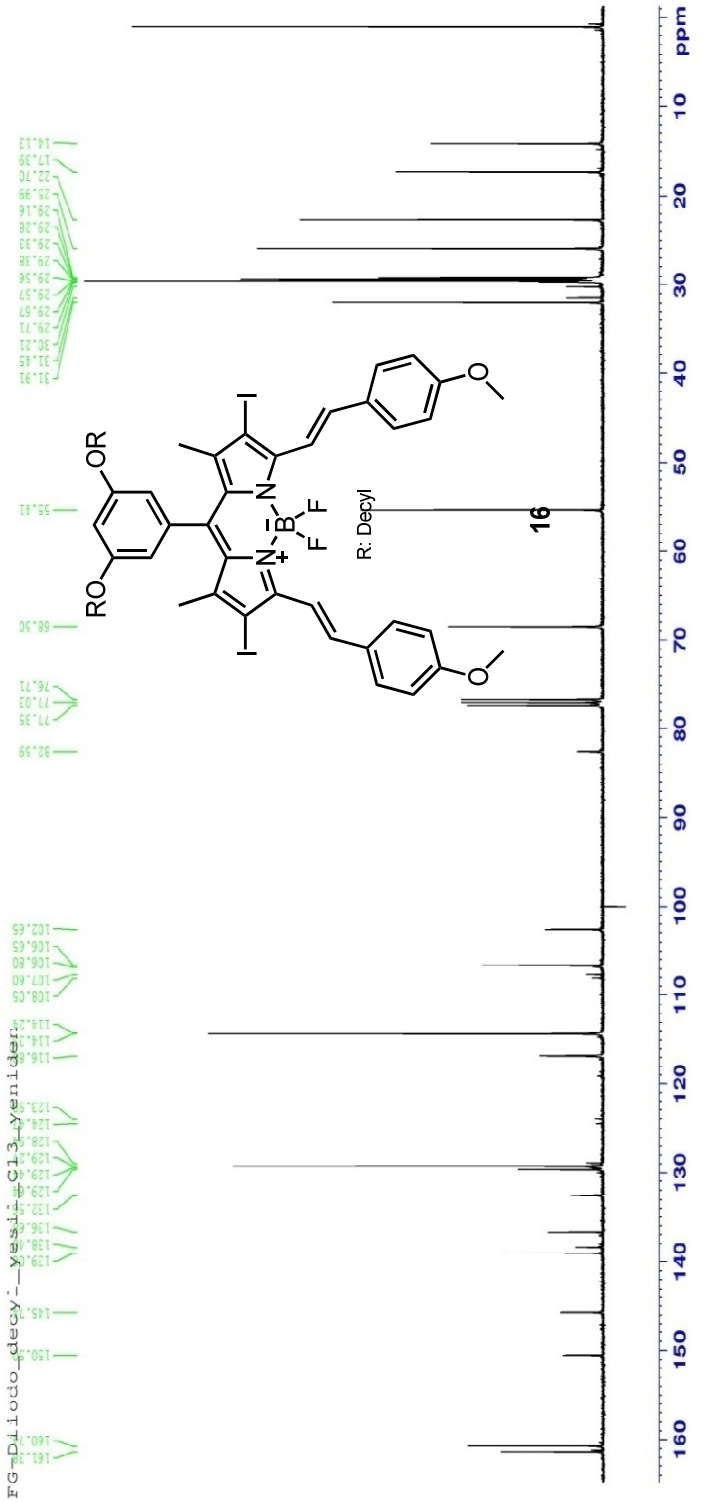

Figure 68. ^{13}C NMR spectrum of Compound **16**

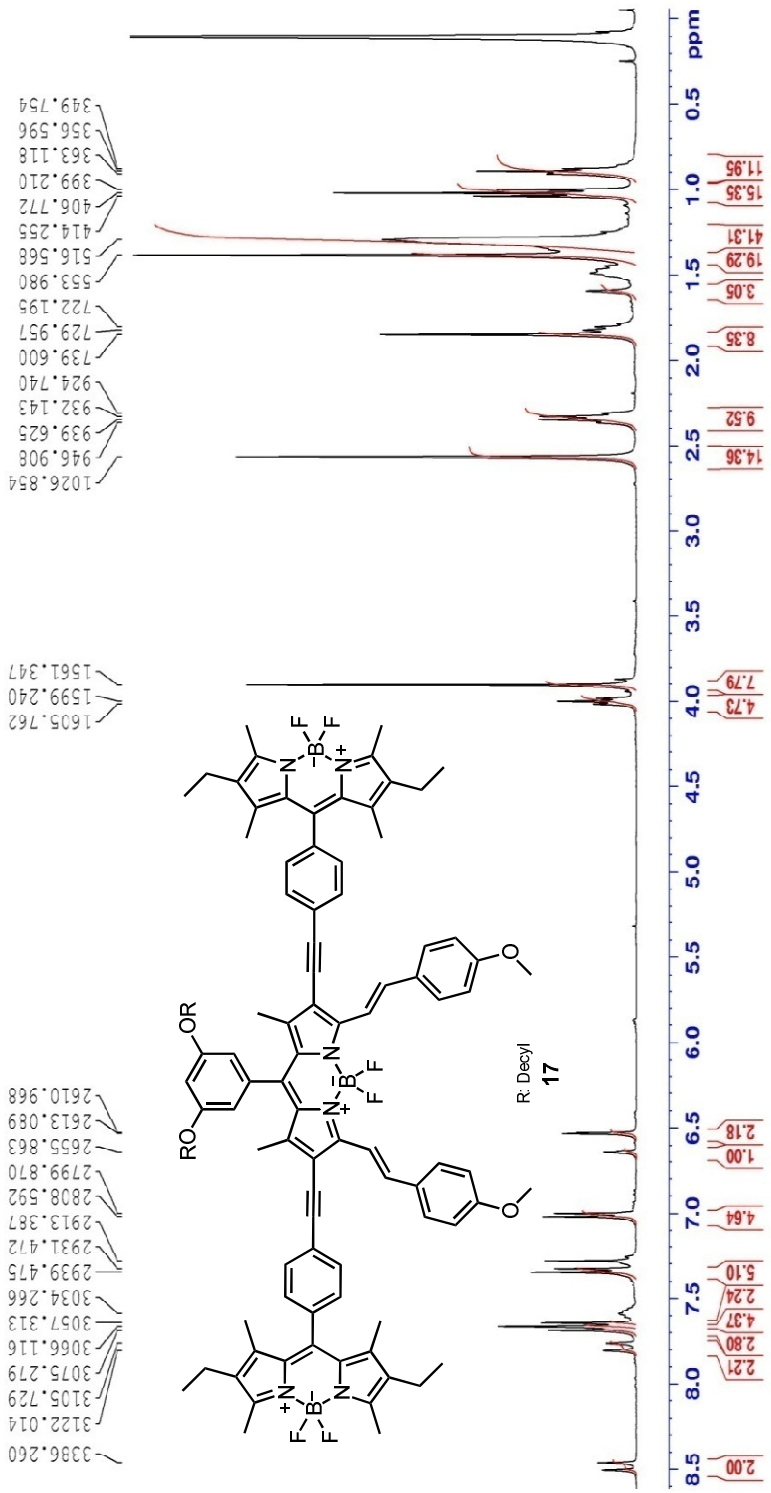

Figure 69. ^{1}H NMR spectrum of Compound **17**

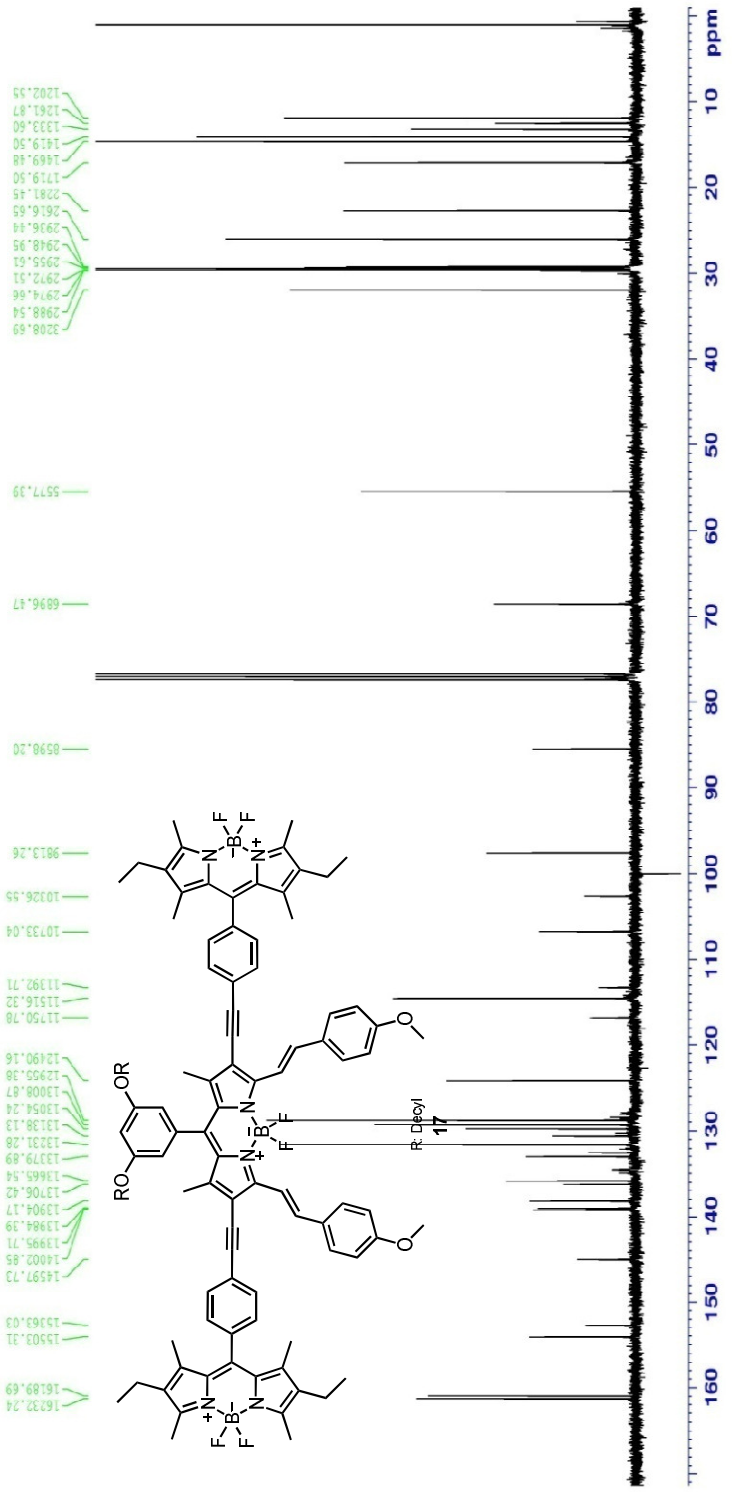

Figure 70. ^{13}C NMR spectrum of Compound **17**

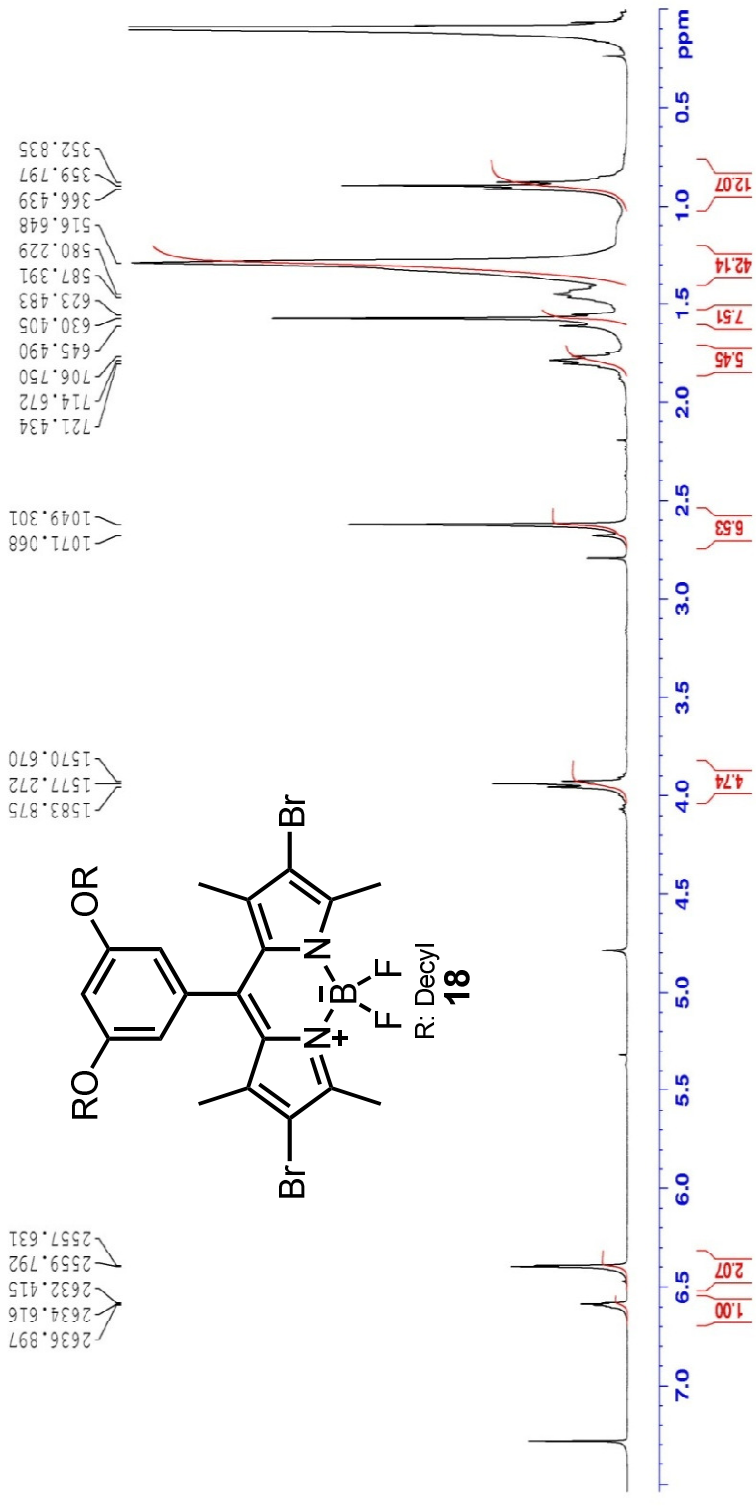

Figure 71. ^{1}H NMR spectrum of Compound **18**

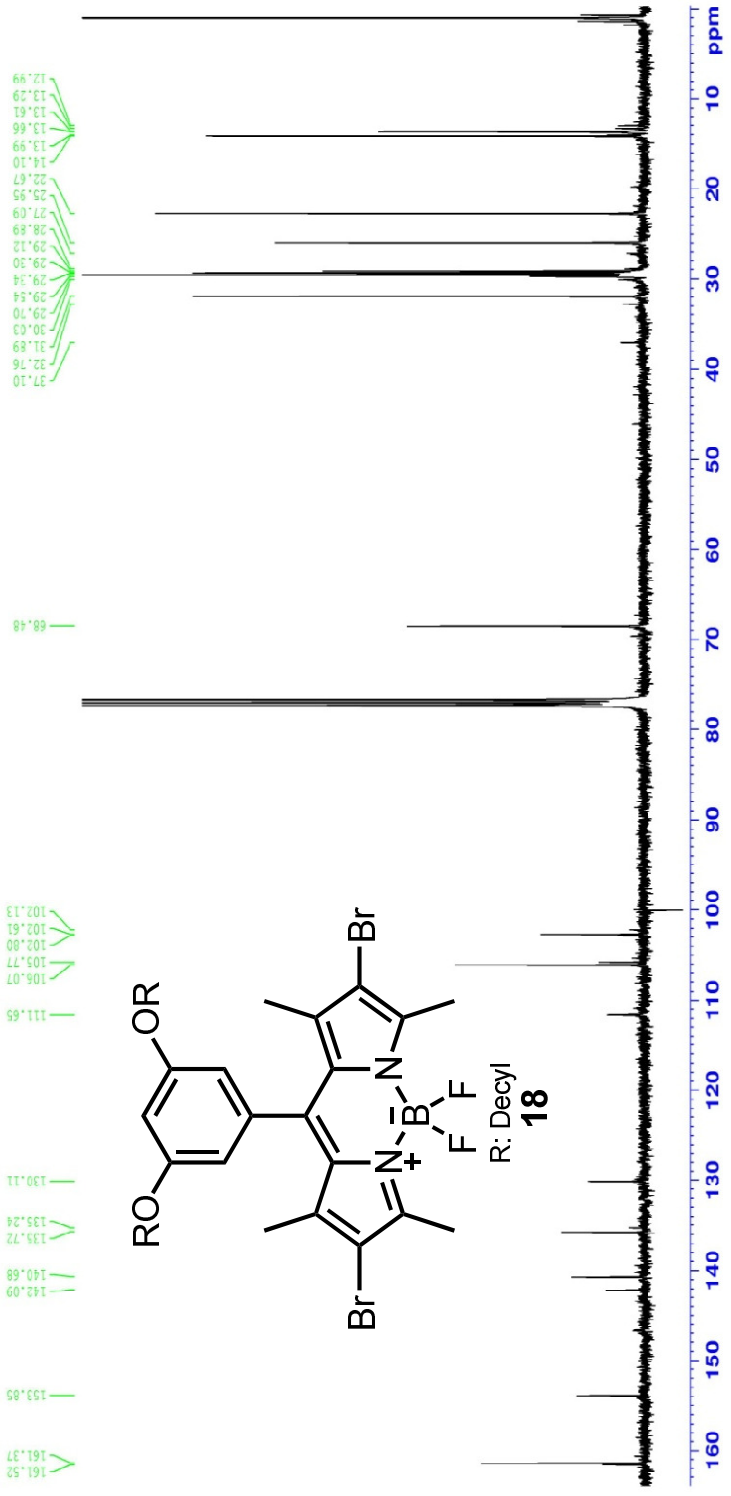

Figure 72. ^{13}C NMR spectrum of Compound **18**

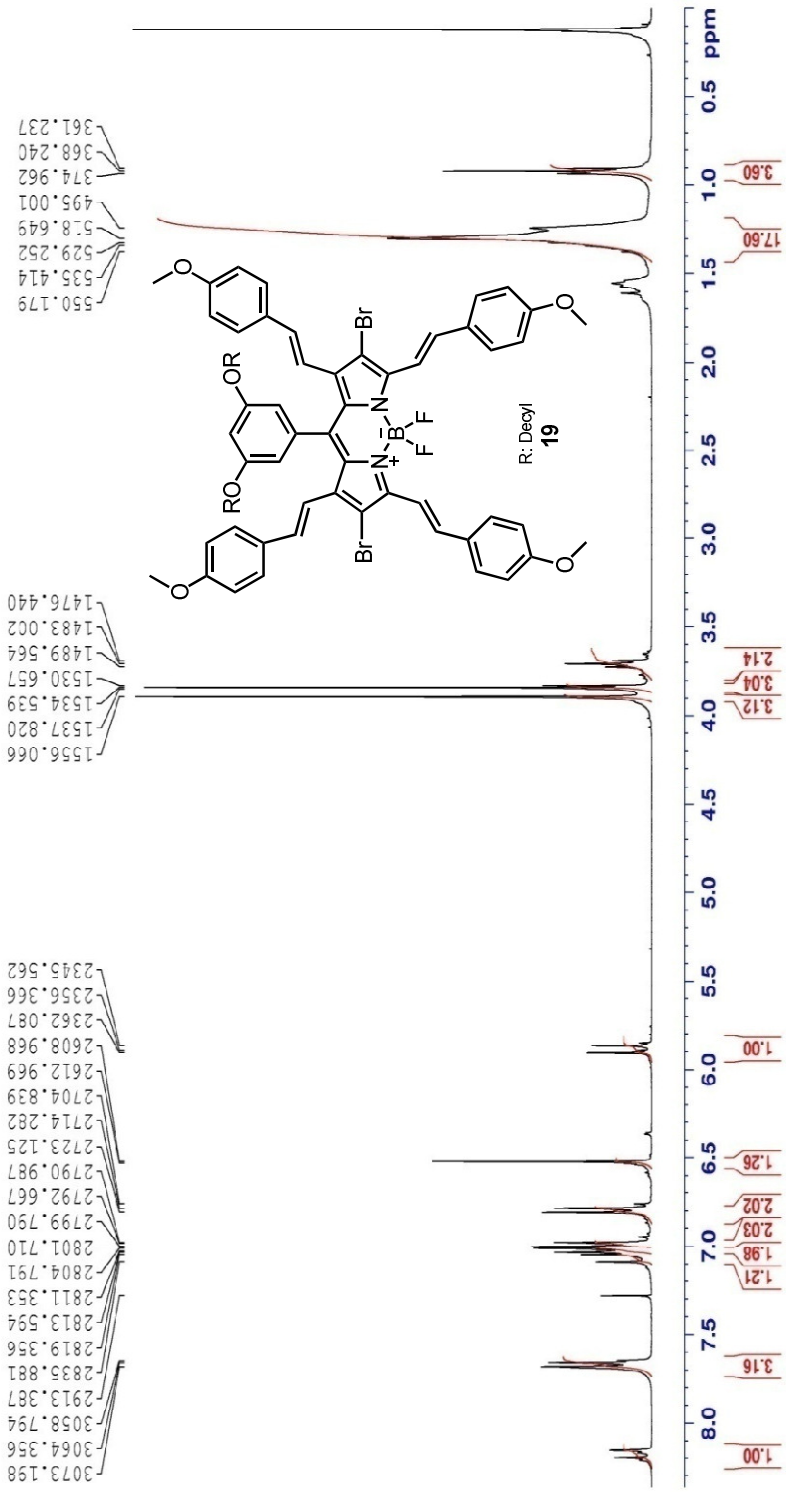

Figure 73. ^{1}H NMR spectrum of Compound **19**

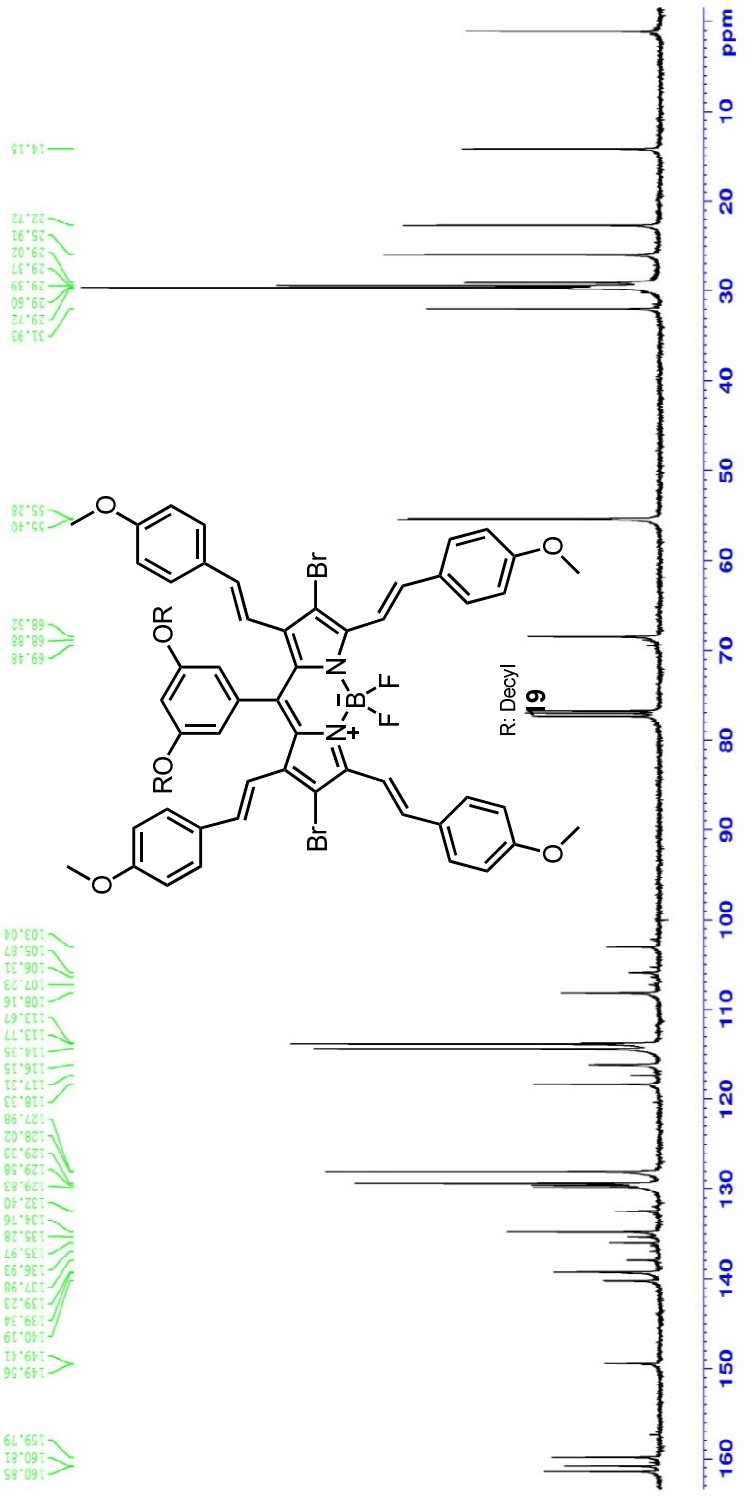

Figure 74. ^{13}C NMR spectrum of Compound **19**

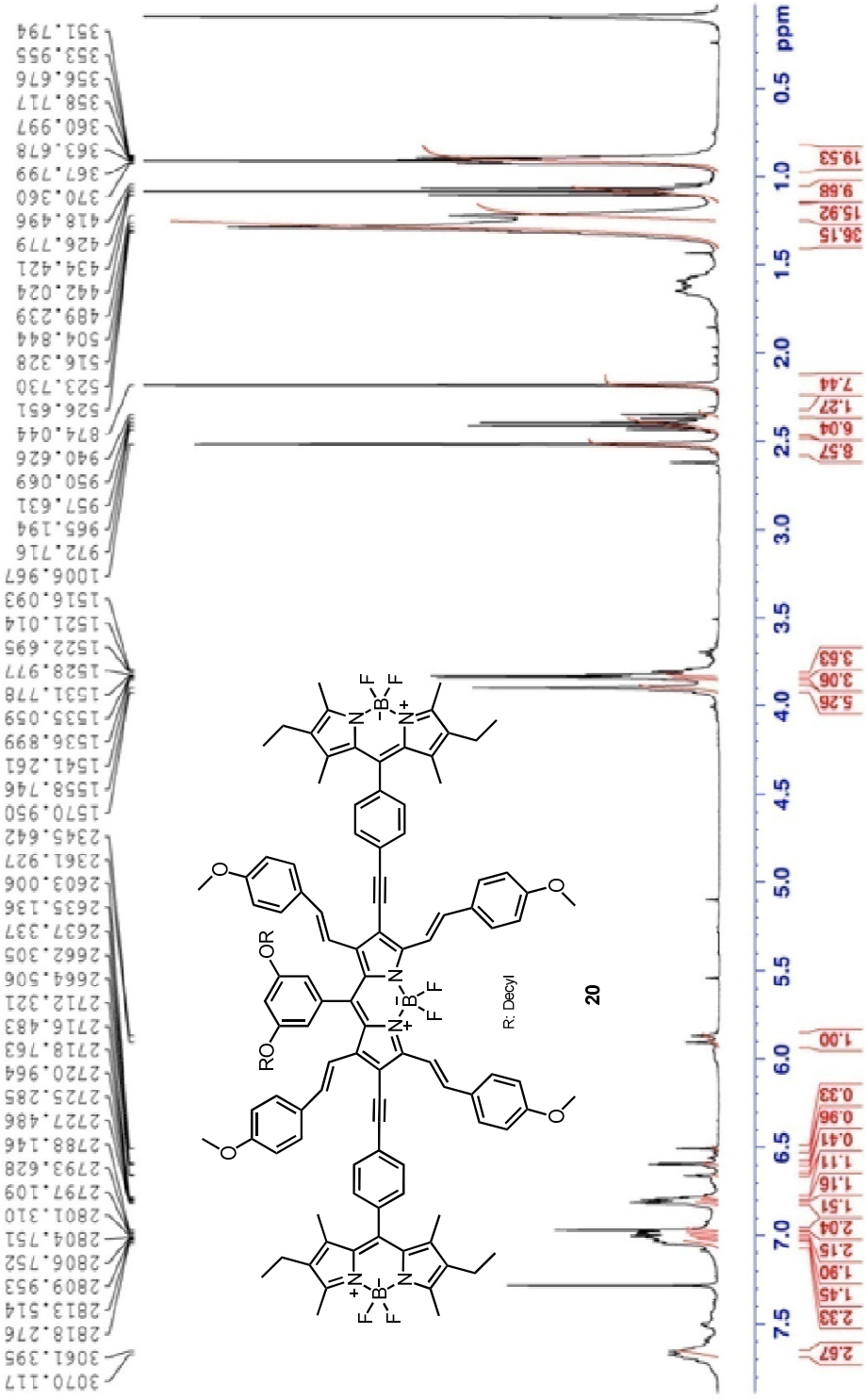

Figure 75. ^{1}H NMR spectrum of Compound **20**

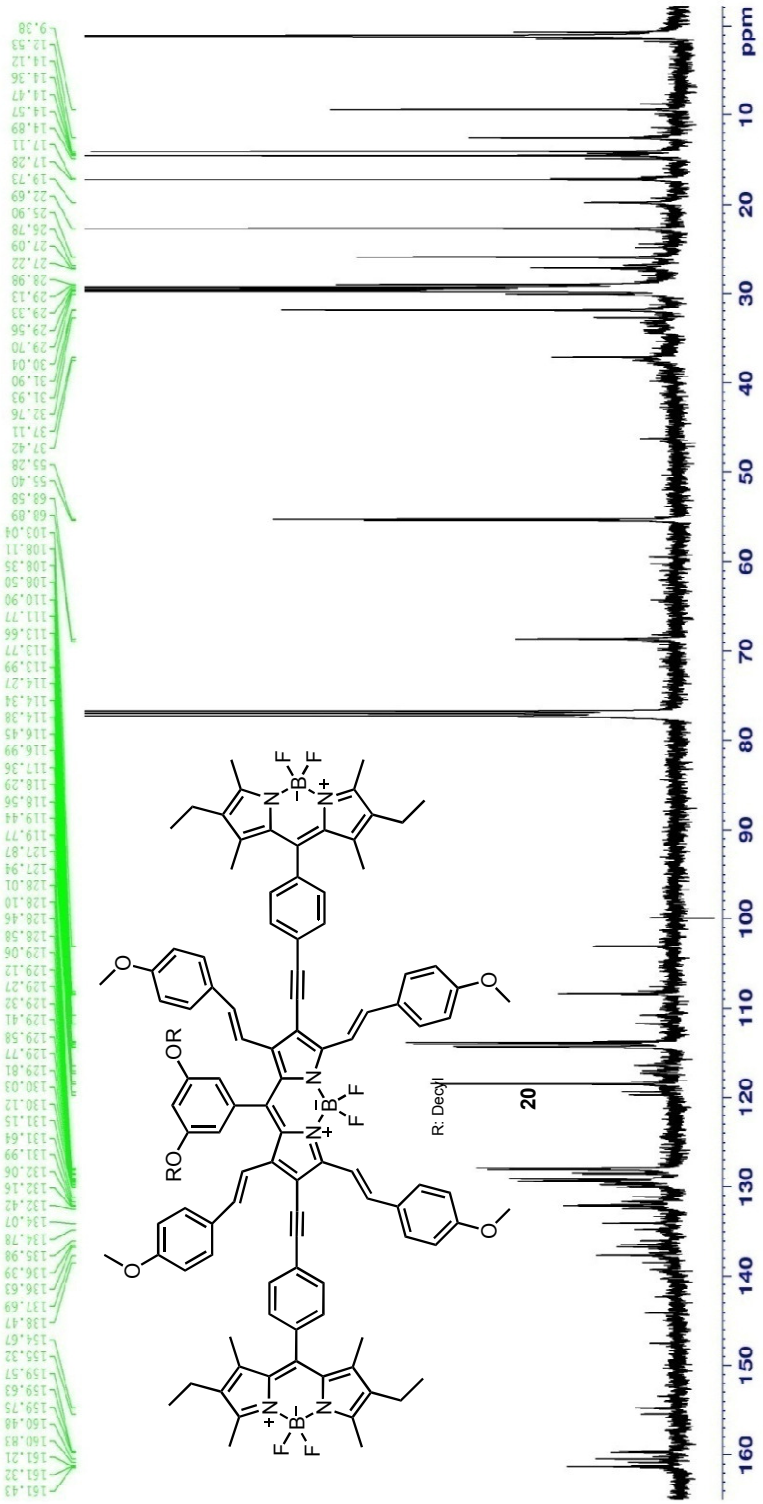

Figure 76. ^{13}C NMR spectrum of Compound **20**.

APPENDIX B

MASS SPECTRA

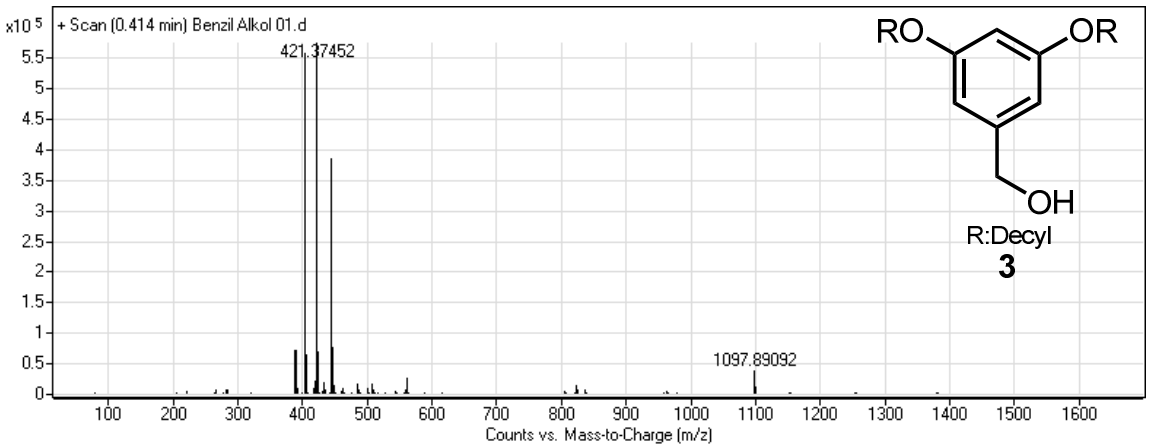

Figure 77. ESI-HRMS of Compound **3**

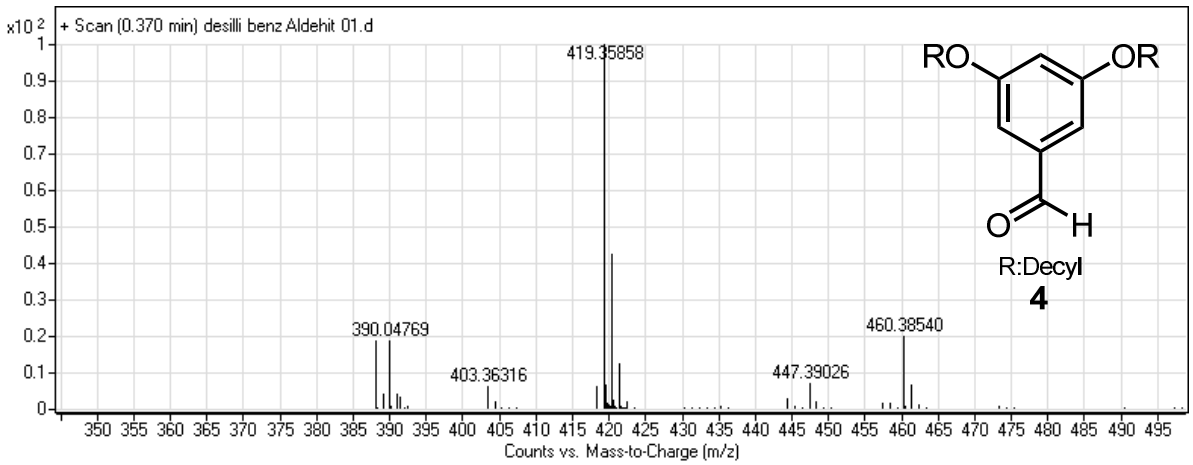

Figure 78. ESI-HRMS of Compound **4**

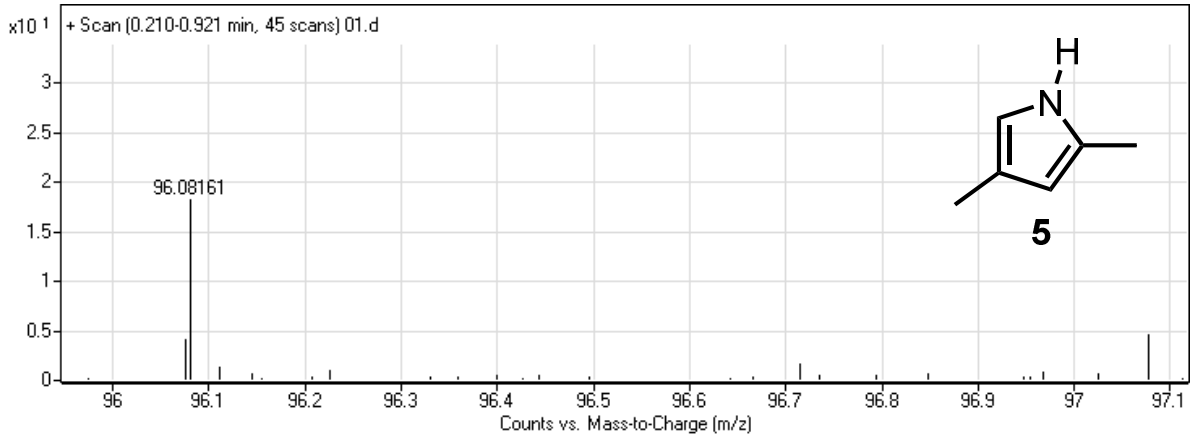

Figure 79. ESI-HRMS of Compound **5**

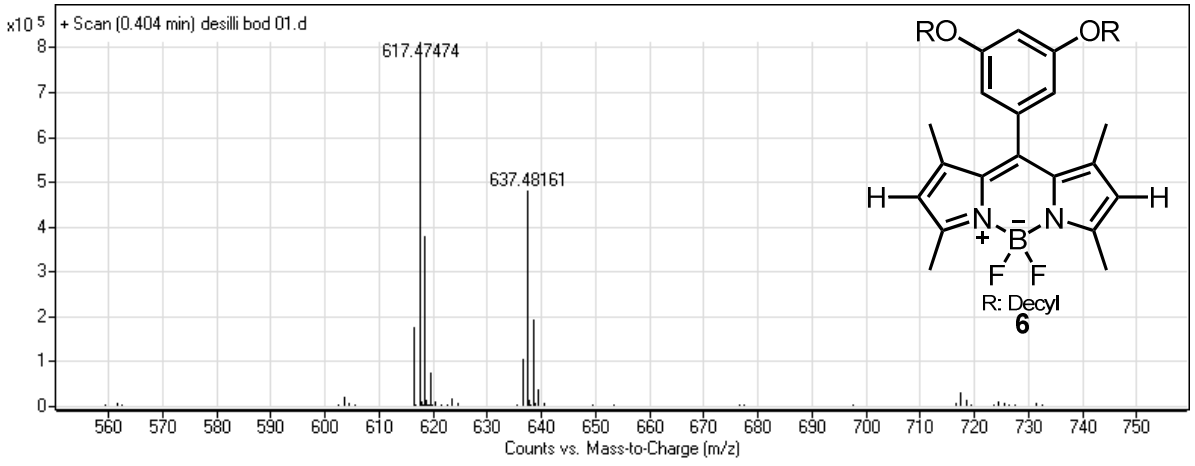

Figure 80. ESI-HRMS of Compound **6**

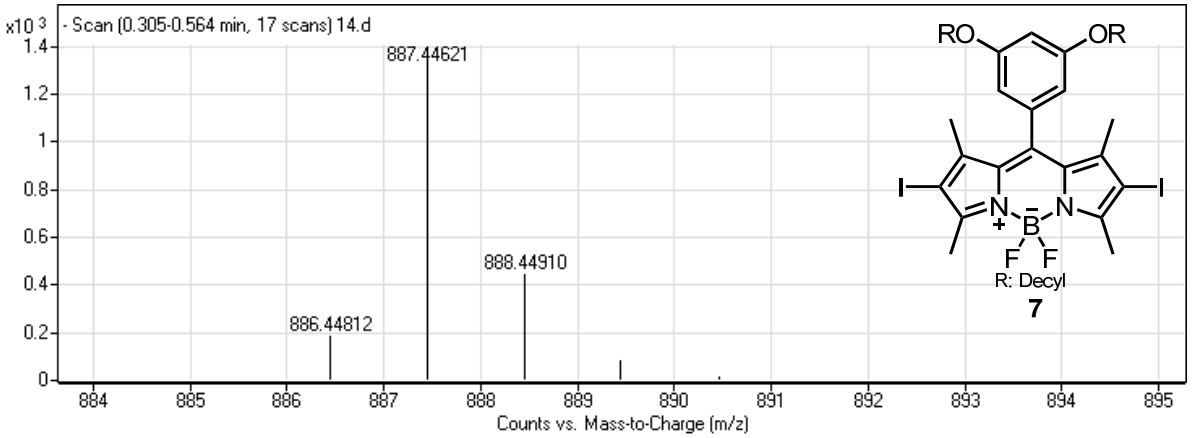

Figure 81. ESI-HRMS of Compound **7**

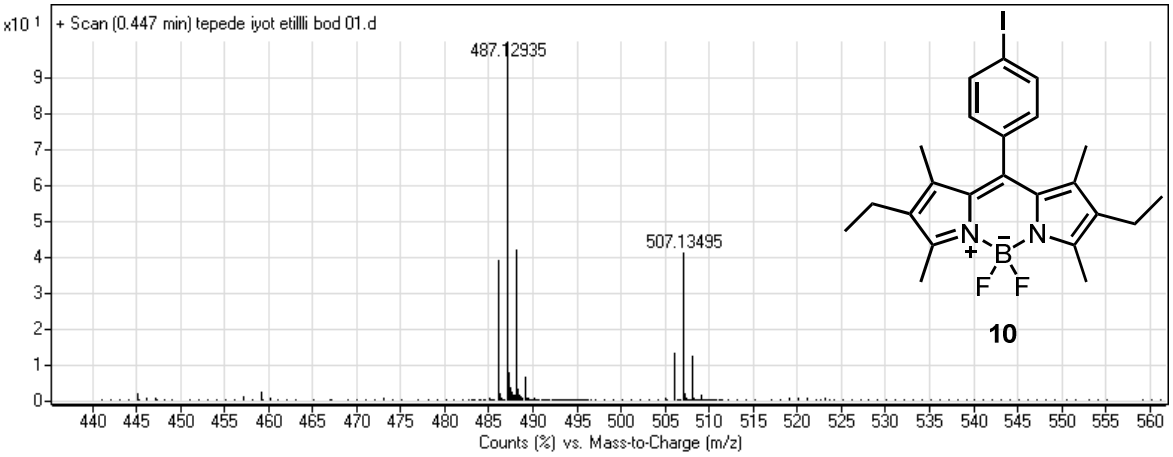

Figure 82. ESI-HRMS of Compound **10**

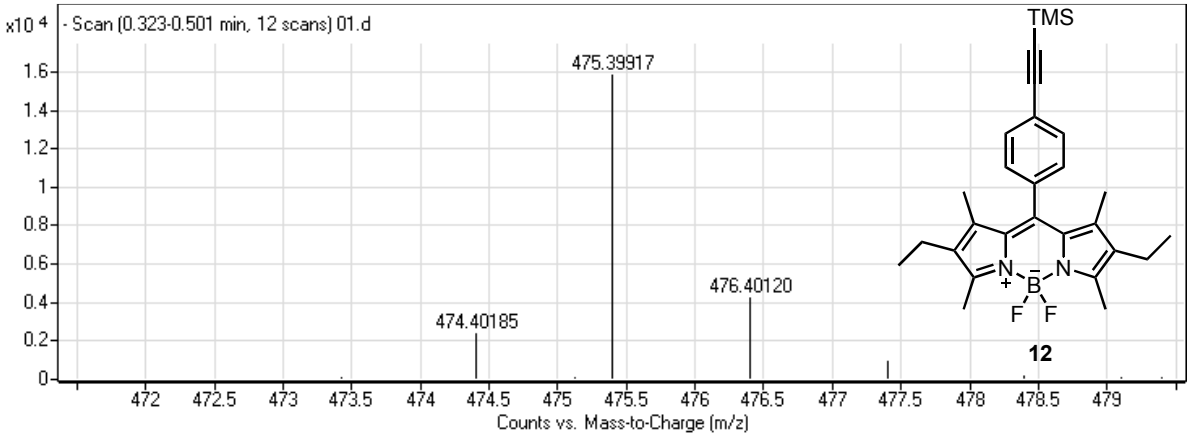

Figure 83. ESI-HRMS of Compound **12**

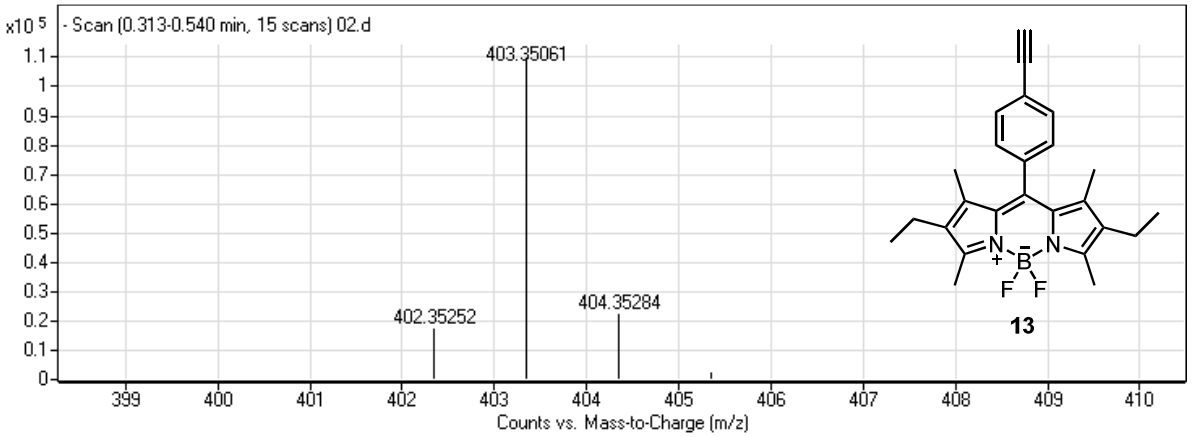

Figure 84. ESI-HRMS of Compound **13**

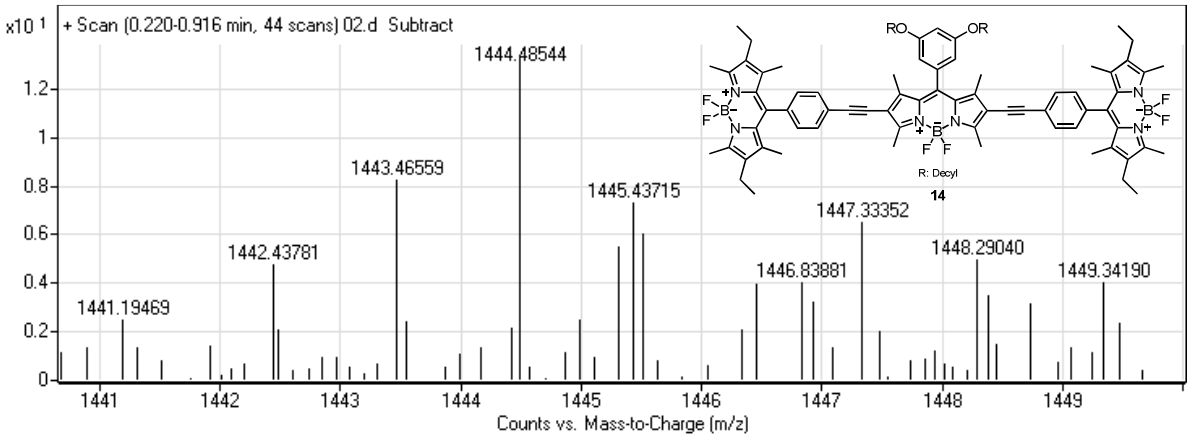

Figure 85. ESI-HRMS of Compound **14**

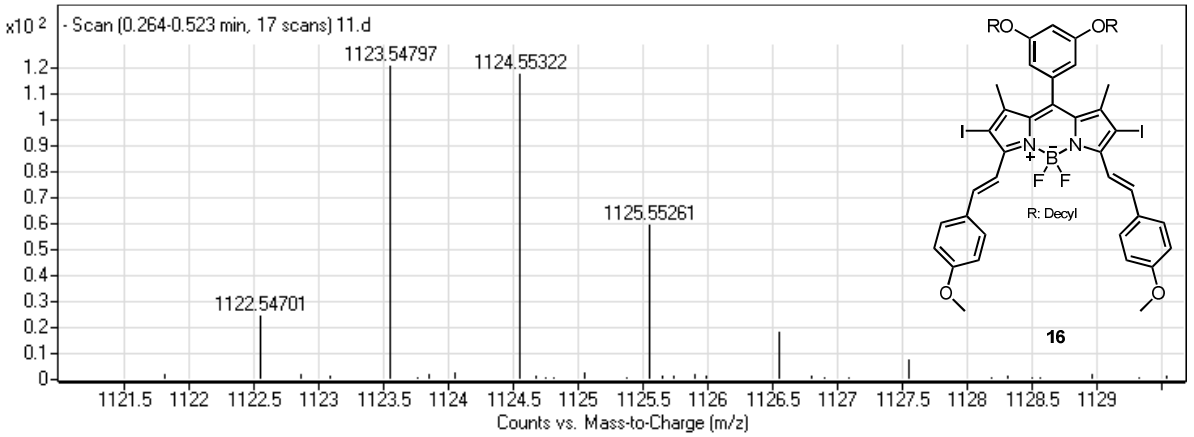

Figure 86. ESI-HRMS of Compound **16**

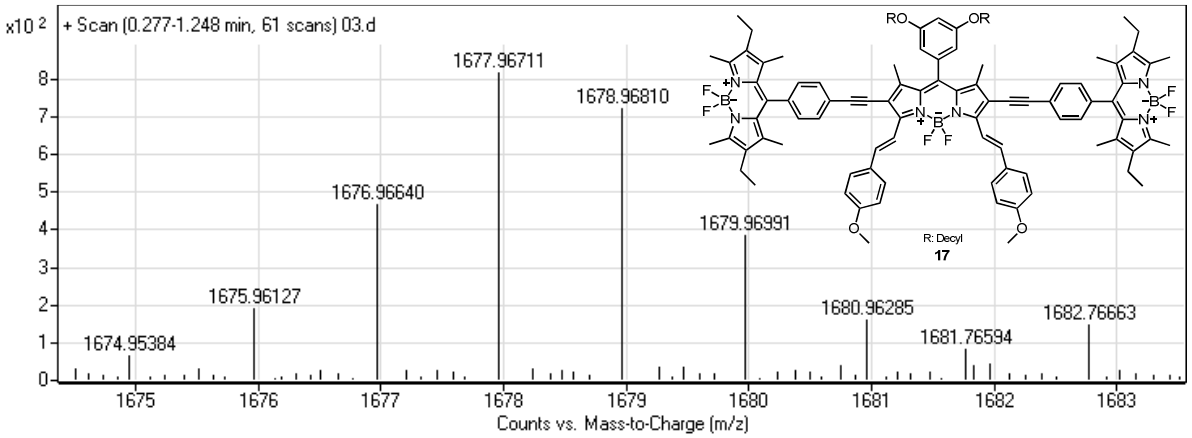

Figure 87. ESI-HRMS of Compound **17**

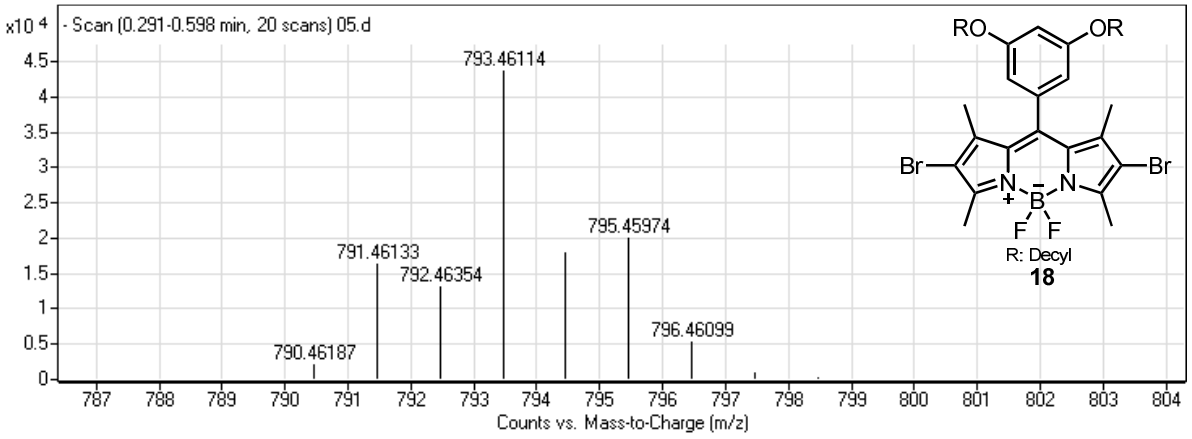

Figure 88. ESI-HRMS of Compound **18**

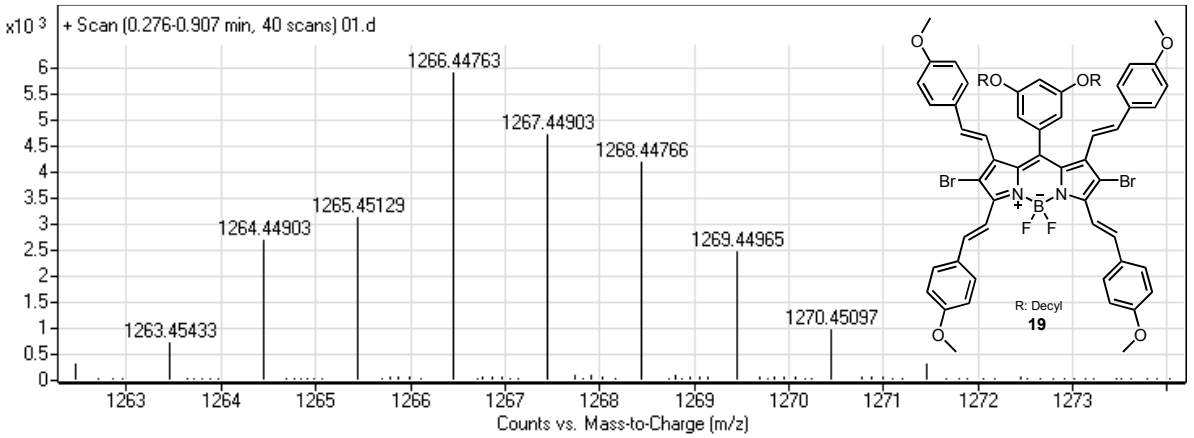

Figure 89. ESI-HRMS of Compound **19**

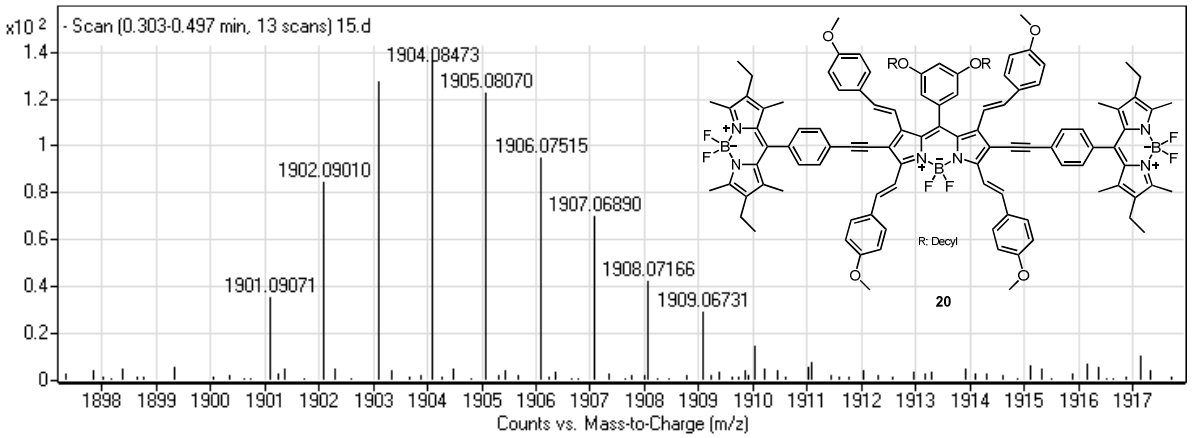

Figure 90. ESI-HRMS of Compound **20**